The Synthesis of Water-Soluble Analogues of $Pt_2(\mu_2\text{-}S)_2(PPh_3)_4$

A thesis

submitted in partial fulfilment

of the requirements for the degree

of

Masters of Science in Chemistry

at

The University of Waikato

by

Ryan Bradley Sutton

THE UNIVERSITY OF
WAIKATO
Te Whare Wānanga o Waikato

2019

Abstract

Platinum has a very rich chemistry with sulfur, and this field has been extensively studied. Of particular interest are complexes containing the $\{Pt_2(\mu_2\text{-}S)_2\}$ core, comprising two platinum atoms with μ_2-sulfurs bridging through a flexible hinge. These complexes can act as potent metalloligands (through the two sulfurs) toward a wide range of transition metal and other centres, allowing for the synthesis of complexes with trinuclear mixed-metal cores $\{Pt_2(\mu_3\text{-}S)_2M\}$ (M = heterometal). The $\{Pt_2(\mu_2\text{-}S)_2\}$ core is also highly nucleophilic and alkylated by the mildest of reagents. The ancillary ligands coordinated to the $\{Pt_2(\mu_2\text{-}S)_2\}$ core are primarily triphenylphosphine (PPh_3), resulting in the complexes being significantly insoluble in water, preventing any forms of bioactivity or biphasic catalysis from being assessed.

This research project has widened the scope of $\{Pt_2(\mu_2\text{-}S)_2\}$ complexes *via* the synthesis of the new water-soluble complexes $Pt_2(\mu_2\text{-}S)_2(PTA)_4$, $[Pt_2(\mu_3\text{-}S)_2(PTA)_4Rh(cod)]Cl$, and $[Pt_3(\mu_3\text{-}S)_2(PTA)_6]^{2+}$ (PTA = 1,3,5-triaza-7-phosphaadamantane, cod = 1,5-cyclooctadiene) that were characterised by electrospray ionisation mass spectrometry (ESI-MS) and phosphorus-31 nuclear magnetic resonance spectroscopy ($^{31}P\{^1H\}$ NMR). The complex $[Pt_3(\mu_3\text{-}S)_2(PTA)_6]^{2+}$ was synthesised during the research into the use of a sulfide exchange column as an alternative source of sulfide for the synthesis of $Pt_2(\mu_2\text{-}S)_2(PTA)_4$.

The water-soluble phosphine ligands tris(2-carboxyethyl)phosphine (TCEP) and monosulfonated triphenylphosphine $[TPPMS]^-$ were determined to be unsuitable ligands for complexes of the general form $Pt_2(\mu_2\text{-}S)_2(L)_4$ (L = TCEP, $[TPPMS]^-$). During these attempted syntheses the complex $Pt_2(\mu_2\text{-}S)_2(cod)_2$ was successfully produced and characterised with ESI-MS, ^1H NMR, ^1H-^1H COSY, and ^{13}C-^1H HSQC (Proton nuclear magnetic resonance spectroscopy, Correlation Spectroscopy, Heteronuclear Single Quantum Coherence).

The use of thioacetamide ($CH_2C(S)NH_2$) as an alternative source of sulfide in the synthesis of $Pt_2(\mu_2\text{-}S)_2(PPh_3)_4$ was found to be a poor substitute for the well established $Na_2S{\cdot}9H_2O$. The reaction does result in $[Pt(CH_3C(S)NH)(PPh_3)_2]^+$, subsequently isolated as the BPh_4^- salt, $[Pt(CH_3C(S)NH)(PPh_3)_2](BPh_4)$ and was characterised by ESI-MS and $^{31}P\{^1H\}$ NMR. The X-ray crystal structure of the by-product *trans*-$Pt(SC(O)CH_3)_2(PPh_3)_2$ was obtained.

Acknowledgements

I will start by thanking my supervisor Prof. Bill Henderson, for the support and guidance along with spell checking that he kindly provided through the time of my research and writing of this thesis.

I would like to thank Ryland G. Fortney-Zirker for providing necessary starting materials that were used in several reactions, alongside Jenny Stockdill, Annie Barker, and Karla Watson, for giving me glassware and chemicals when our lab frequently lacked them.

Thanks also to Associate Prof. Graham Saunders for solving the X-ray crystal structure.

Special thanks goes to Ingrid Lindeman and Hayden Thomas for generously spell checking my writings.

Finally I want to thank all the friends and family that offered support.

Table of Contents

List of Figures

List of Tables

List of Abbreviations

ESI	Electrospray Ionisation
ESI-MS	Electrospray Ionisation Mass Spectrometry
ICP MS	Inductively Coupled Plasma Mass Spectrometry
TOF	Time Of Flight
NMR	Nuclear Magnetic Resonance
^{1}H NMR	Proton Nuclear Magnetic Resonance
^{31}P{^{1}H} NMR	Phosphorus-31 Nuclear Magnetic Resonance
UV/Visable	Ultraviolet Visible Spectroscopy
CSD	Cambridge Structural Database
m/z	mass-to-charge ratio (ESI-MS)
CEV	Capillary Exit Voltage
s	singlet (NMR)
d	doublet (NMR)
m	multiplet (NMR)
MHz	Mega Hertz
Hz	Hertz
J	coupling constant (in Hz)
ppm	parts-per-million
^{1}H-^{1}H COSY	Correlation Spectroscopy
^{13}C-^{1}H HSQ	Heteronuclear Single Quantum Coherence
PTA	1,3,5-triaza-7-phosphaadamantane
PTA=O	1,3,5-triaza-7-phosphaadamantane oxide
PTA=S	1,3,5-triaza-7-phosphaadamantane sulfide
dppp	1,3-bis(diphenylphosphino)propane
dppe	1,2-bis(diphenylphosphino)ethane
dppm	1,1-bis(diphenylphosphino)methane
dppf	1,1'-bis(diphenylphosphino)ferrocene
bipy	2,2'-bipyridine
Pyr	pyridine
PMe_2Ph	dimethylphenylphosphine
PMe_3	trimethylphosphine
Me	methyl

^{n}Bu	butyl group
PPh_3	triphenylphosphine
Ph	phenyl
PPh_3=S	triphenylphosphine sulfide
PPh_3=O	triphenylphosphine oxide
$PPh(C_6H_5OMe)_2$	bis(4-methoxyphenyl)phenylphosphine
$AsPh_3$	triphenylarsine
TPPMS	monosulfonated triphenylphosphine
TPPMS=S	monosulfonated triphenylphosphine sulfide
TPPMS=O	monosulfonated triphenylphosphine oxide
TPPTS	trisulfonated triphenylphosphine
TCEP	tris(2-carboxyethyl)phosphine
cod	1,5-cyclooctadiene
$CH_3C(S)NH_2$	thioacetamide
D_2O	deuterated water
DMSO	dimethyl sulfoxide
DMSO-d_6	deuterated dimethyl sulfoxide
$CDCl_3$	deuterated chloroform
MeOH	methanol
EtOH	ethanol
CH_2Cl_2	dichloromethane
DMF	dimethylformamide
THPC	tetrakis(hydroxymethyl)phosphonium chloride
mL	millilitre
mmol	millimole
mg	milligram
mm	millimetre
h	hours

Chapter 1:
Review of the Phosphine Ligated $\{Pt_2(\mu_2\text{-}S)_2\}$ Core, and Introduction to the Research Undertaken

1.1 Introduction to the $\{Pt_2(\mu_2\text{-}S)_2\}$ Core

Platinum(II) is a soft Lewis acid and therefore has a higher affinity for π-bonding ligands (R_3P, R_2S, CN^-, NO_2^-) and heavier halogens, and shows a low affinity for hard ligands (F^-,O).[1] In particular platinum has a high affinity towards sulfur donor ligands (SO_2, RS^-, S_n^{2-}) with the polysulfide dianions producing complexes such as $[Pt(S_5)_2]^{2-}$ and $[Pt_4S_4]^{4+}$.[1] This variety allows for the formation of the μ_2-sulfide bridging aggregate $\{Pt_2(\mu_2\text{-}S)_2\}$, this four-membered ring system exists as part of a larger complex, supported and stabilised by various ligands.

The $\{Pt_2(\mu_2\text{-}S)_2\}$ core is most commonly synthesised in the metathesis reaction between *cis*-$PtCl_2L_2$ and $Na_2S{\cdot}9H_2O$,[2] where L = a suitable ligand, the most common phosphine ligand used is triphenylphosphine (PPh_3). The use of triphenylphosphine results in the preparation of $Pt_2(\mu_2\text{-}S)_2(PPh_3)_4$, which has a rich and extensive chemistry that has been thoroughly reviewed previously.[3–5] This chemistry will be briefly covered here before moving to the primary focus, the various phosphine and arsine ligands that have been researched in combination with the $\{Pt_2(\mu_2\text{-}S)_2\}$ core.

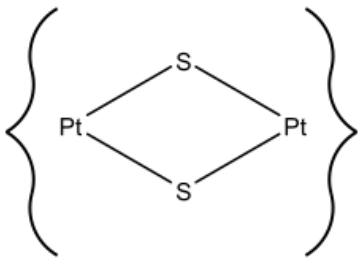

Figure 1: Diagram of the $\{Pt_2(\mu_2\text{-}S)_2\}$ core. Ligands not illustrated.

The $\{Pt_2(\mu_2\text{-}S)_2\}$ core is comprised of two μ_2-sulfurs bridging to the platinum atoms producing a four-membered ring (Figure 1), allowing the μ_2-sulfurs to act as a hinged bridge between the platinum atoms with a variable dihedral angle (the angle between the two PtS_2 planes). Within $Pt_2(\mu_2\text{-}S)_2(PPh_3)_4$ the platinum atoms are in their normal square-planar geometry. The hinge angle orientation is

not static and is affected by several factors. Investigations into $\{M_2(\mu_2\text{-}S)_2\}$ complexes have led to the determination that weak metal-metal interactions can occur in d^8 metals in this ring system. The hinge angle is dependent on a few key features; the acuteness increases along with the diffuseness of the metal orbitals taking part, therefore increasing down the group. The σ-donor ability and steric bulk of the terminal ligands have influence over the hinge angle as well. A complex that lacks sufficient steric hindrance and has four good σ-donor ligands bonded to the metal centres, results in a $\{Pt_2(\mu_2\text{-}S)_2\}$ core with a dihedral angle that will prefer a bent structure, in contrast to ligands that are poor σ-donors, which tend to form planar complexes.[3]

Terminal ligands with two or more bulky groups, such as PPh_3, will form complexes that are more planar. Furthermore the more electronegative the atoms of the hinge are (moving up the group), the tendency to form planar structures is increased e.g. S^{2-} to O^{2-}.[6]

1.1.1 The $\{Pt_2(\mu_2\text{-}S)_2\}$ Core's Behaviour as a Metalloligand

The $\{Pt_2(\mu_2\text{-}S)_2\}$ core is capable of acting as a metalloligand towards various metal centres, through strong bonding interactions from the μ_2-sulfur bridges which act as strong electron donors. The aforementioned highly flexible hinge angle accompanied with variable ligand orientation benefits the $\{Pt_2(\mu_2\text{-}S)_2\}$ core in this ability. The $\{Pt_2(\mu_2\text{-}S)_2\}$ core is an applicable metalloligand to a large swath of main group and transition metal centres with their accompanying ligands, as it is readily available to coordinate to the heterometal forming a $\{Pt_2(\mu_3\text{-}S)_2M\}$ centred complex (M = heterometal) as shown in Figure 1.1.

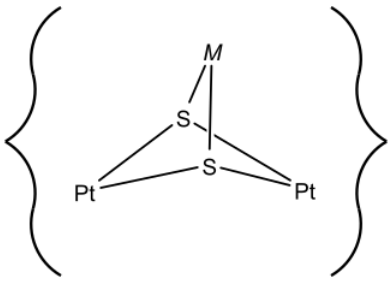

Figure 1.1: Diagram of the $\{Pt_2(\mu_3\text{-}S)_2M\}$ core. Ligands not illustrated.

The heterometal aggregate complexes produced from the use of $\{Pt_2(\mu_2\text{-}S)_2\}$ as a metalloligand provides the capability for the aggregates to be quite varied; this encompasses complexes where the heterometal in question maintains a low

coordination number; the steric bulk of the PPh_3 ligands helps achieve this. The complexes of the form $[Pt_2(\mu_3\text{-}S)_2(PPh_3)_4(ML)]^{2+}$, (ML = $Ru(\eta^6\text{-p-cymene})$ or $Rh(\eta^5\text{-}C_5Me_5)$) have the heterometal maintaining a five-coordinate geometry.[7] Complexes of this type have the potential to possess interesting chemistry due to the proximity of the d^6 and d^8 metal centres, such as demonstrating catalytic ability.[8]

The application of the $\{Pt_2(\mu_2\text{-}S)_2\}$ core as a metalloligand allows it to be used as a precursor to generate larger $\{Pt_2(\mu_3\text{-}S)_2M\}$ nuclearity aggregates. An example of this is the interaction of the $\{Pt_2(\mu_2\text{-}S)_2\}$ core with the silver complex $AgCl(PPh_3)$ resulting in the first aggregate complex containing a metal sulfur core of $\{Pt_2(\mu_3\text{-}S)_2Ag\}$, followed by an increase to $\{Pt_2(\mu_2\text{-}S)_2Ag_2\}$, with a final reaction step to the $\{(Pt_2(\mu_3\text{-}S)_2)_2Ag_2\}$ core (Figure 1.2).[9] The phosphine ligand in this platinum sulfide silver aggregate is the commonly used PPh_3.[9] This demonstrates a stepwise reaction that allows the $\{Pt_2(\mu_2\text{-}S)_2\}$ core to build larger nuclearity aggregates through its highly versatile sulfur bridges.

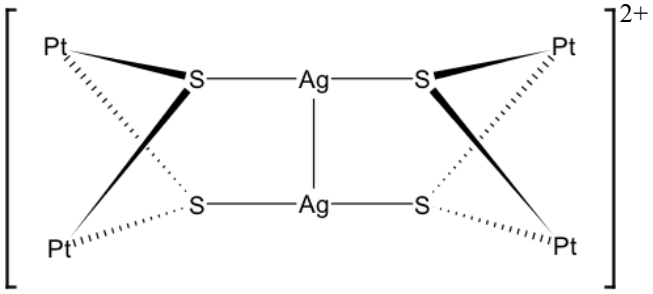

Figure 1.2: Diagram of $\{(Pt_2(\mu_3\text{-}S)_2)_2Ag_2\}$ aggregate. PPh_3 ligands have been excluded.

The $\{Pt_2(\mu_2\text{-}S)_2\}$ core, when implemented as a metalloligand, can also be used in the stabilisation of heterometals in higher oxidation states, an ability provided by the μ_2-sulfur bridges because of their strong electron donor characteristics. This has been observed in adducts of vanadium(V),[10] iron(III), [10] and cobalt(III)[11,12] specifically the complexes $[Pt_2(\mu_3\text{-}S_2)(PPh_3)_4VO(OMe)_2]^+$ and $[Pt_2(\mu_3\text{-}S_2)(PPh_3)_4(MQ_2)]^+$, (M = Co, Fe. Q = 8-hydroxyquinoline anion).

1.1.2 Alkylation of the $\{Pt_2(\mu_2\text{-}S)_2\}$ Cores

The $\{Pt_2(\mu_2\text{-}S)_2\}$ core is able to undergo alkylation with the mildest of organic electrophiles, such as CH_2Cl_2 among many others,[13–15] through mono or

dialkylation, which can convert the μ_2-sulfide bridges to μ_2-thiolates. The monoalkylation can occur with reactions of alkyl chlorides, bromides, along with long chain alkyl iodides. With the implementation of these reagents a large number of derivatives have been produced in the form of $[Pt_2(\mu_2\text{-}S)(\mu_2\text{-}SR)(PPh_3)_4]^+$ where the R group can include functional groups such as amide, ester, ketone, guanidine, hydrazone, semicarbazone, thiosemicarbazone, nitrile, oxime, urea, and thiourea (Figure 1.3).[13–15] Arylation of the μ_2-sulfur is also possible through reactions with Ph_2IBr.[16]

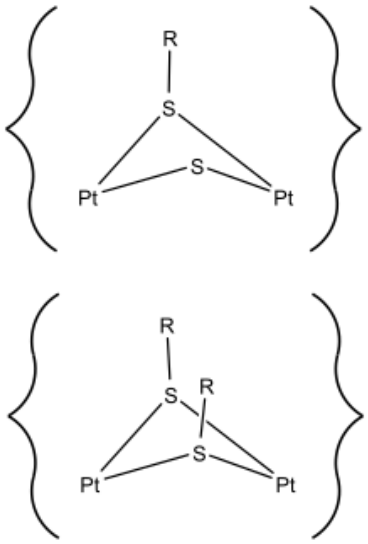

Figure 1.3: Diagram of mono and dialkylation of the $\{Pt_2(\mu_2\text{-}S)_2\}$ core.

The dialkylation of the $\{Pt_2(\mu_2\text{-}S)_2\}$ core is also possible and has been studied. This requires a stronger alkylating agent to achieve $[Pt_2(\mu_2\text{-}SR)_2(PPh_3)_4]^{2+}$ complexes (Figure 1.3). The reagents required for this are short-chain alkyl iodides, alkyl sulfates, along with some activated alkyl bromides.[14,17] The dialkylation of the $\{Pt_2(\mu_2\text{-}S)_2\}$ core can be promoted by the selection of the phosphine ligands. A phosphine that has a larger electron donating ability encourages the dialkylation, whereas the inverse is true for weak electron donors, which discourage dialkylation.[14]

The dimethylation of the $\{Pt_2(\mu_2\text{-}S)_2\}$core can be readily achieved with Me_2SO_4, along with the monomethylation of previously alkylated complexes.[18,19] This reactant is advantageous as it also generates a poorly nucleophilic anion ($MeSO_4^-$) which is beneficial as it does not promote the dissociation of PPh_3 ligands that can occur in the reaction with alkyl halides.[20,21] This is in contrast to reactions where MeI is used as the alkylating agent, which highlights an example of the secondary reactions that occur with alkyl halides. Successful methylation produces I^-, which is a sufficiently strong enough nucleophile to allow for the anion to substitute for PPh_3 giving the product $[Pt_2(\mu_2\text{-}SMe)_2(PPh_3)_3I]^+$.[19,22]

Dialkylation of both μ_2-sulfurs resulting in a bidentate bridging alkyl chain between the two sulfurs has also been established, and an example of this is the reaction of $Pt_2(\mu_2\text{-}S)_2(PPh_3)_4$ and $ClCH_2CH_2Cl$ giving the product; $[Pt_2(\mu_2\text{-}SCH_2CH_2S)_2(PPh_3)_4]^{2+}$.[21]

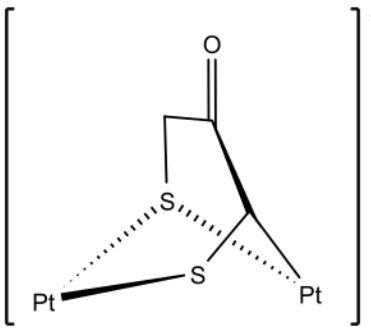

Figure 1.4: Diagram of the (C-S-Pt-S-Pt) ring system. formed from a dialkylation side reaction.

A second form of side reaction has been observed after the dialkylation of the complex $Pt_2(\mu_2\text{-}S)_2(PPh_3)_4$, with 1,3-dichloroacetone in the presence of base. It involves the loss of the SCH_2 activated proton *via* a base and the subsequent insertion of the CH group into the $\{Pt_2(\mu_2\text{-}S)_2\}$ ring, resulting in the creation of the five-membered (C-S-Pt-S-Pt) ring seen in Figure 1.4.[5,19]

These alkylation routes have allowed for a wide range of derivatives of $Pt_2(\mu_2\text{-}S)_2(PPh_3)_4$ to be produced. Even with monoalkylation occurring and therefore decreasing the electron density of the available μ_2-sulfide, the thiolate complexes are still able to act as a metalloligand towards several heterometal centres. The cationic complexes have the general form of $[Pt_2(\mu_2\text{-}SR)(\mu_3\text{-}S(ML))(PPh_3)_4]^{2+}$, (ML = $AuPPh_3$, HgPh, HgFc (ferrocenyl) and R = ^nBu, CH_2Ph).[23]

1.1.3 Ligand Exchange Reactions

The ability for monoplatinum halide complexes (PtX_2L_2) (X = halide. L = ligand) to have selective ligand exchange upon the reaction with $Pt_2(\mu_2\text{-}S)_2(PPh_3)_4$ is dependant on the ligands that are implemented and thire individual properties e.g. chelating or kinetically non-labile groups such as cod or PPh_3, remain bonded to the platinum. The halide, commonly a chloride, is removed and replaced with the sulfide bonding interaction with $Pt_2(\mu_2\text{-}S)_2(PPh_3)_4$ resulting in a triplatinum complex of the general form $Pt_3(\mu_3\text{-}S)_2(PPh_3)_4(L)_2$ (L = ligand).[24]

In the opposite circumstance where the halide, alkyl, or aryl ligands used are the more kinetically non-labile groups a phosphine can be lost, this is demonstrated by the reactions of *trans*-$PtHCl(PPh_3)_2$, which results in the removal of a PPh_3 and

Cl^- group, whereas in reactions with $Pt_2(\mu_2\text{-}S)_2(PPh_3)_4$, the result is a triplatinum complex that lacks a second PPh_3 ligand on the third platinum $[Pt_3(\mu_3\text{-}S)_2(PPh_3)_5H]^+$.[25] Where the ligands implemented have an increased lability over the halide, the halide remains bonded to the platinum and the ligand is replaced. This is observed in the reaction between $PtCl_2(SOMe_2)_2$ and $Pt_2(\mu_2\text{-}S)_2(PPh_3)_4$ resulting in the loss of one chloride and a $SOMe_2$ group in the formation of the triplatinum complex $[Pt_3(\mu_3\text{-}S)_2(PPh_3)_4Cl(SOMe_2)]^+$.[24]

The research undertaken here has taken advantage of the ligand exchange reactions of *cis*-$PtCl_2L_2$ and $Pt_2(\mu_2\text{-}S)_2(PPh_3)_4$ complexes. Attempts to replace the common insoluble phosphine ligand PPh_3 with the water-soluble phosphine 1,3,5-triaza-7-phosphaadamantane (PTA), monosulfonated triphenylphosphine $[TPPMS]^-$, and tris(2-carboxyethyl)phosphine (TCEP) have been made.

1.1.4 The Use of Electrospray Ionisation Mass Spectrometry

An aspect that this research will take full advantage of is the behaviour of the $Pt_2(\mu_2\text{-}S)_2(L)_4$ complex in ESI-MS. The electrospray ionisation technique is one of the softer methods available for mass spectral ionisation, making it very useful for the analysis of complexes that may be labile or thermally sensitive. This encompasses the $Pt_2(\mu_2\text{-}S)_2(L)_4$ coordination complexes.

Ion fragmentation can be induced while using ESI with the increase of the capillary exit and skimmer cone voltages. The variability of the acceleration voltages allows the electrospray to alter how hard or soft the technique is for the sample. The application of this technique means that a sample can be analysed through a range of voltages allowing for observations of fragmentation to be obtained and therefore leading to further incite in to the complex under investigation, as its fragment ions may hold important information.

The detector paired with the ion source is equally as important; for this application a time-of-flight (TOF) mass analyser is used as it provides accurate data along with having a large upper mass limit. This makes ESI-TOF a desirable ionisation technique and mass analyser for $Pt_2(\mu_2\text{-}S)_2(L)_4$ coordination complexes,

the technique allows for the assessment of the viability of reactions that are midway through to completion or on a very small scale. Samples can easily be removed from the reaction vessel and quickly analysed.

1.2 The Phosphine Ligands of the $\{Pt_2(\mu_2\text{-}S)_2\}$ Core

The ligand most commonly bonded to the $\{Pt_2(\mu_2\text{-}S)_2\}$ core is triphenylphosphine, which is desirable as it is a low cost solid, that is air stable.[26,27] In turn the platinum complexes produced are air stable solids as well.[2] However, this bulky phosphine ligand is not the only phosphine used in combination with the $\{Pt_2(\mu_2\text{-}S)_2\}$ core, several others have been successfully characterised in the general forms $Pt_2(\mu_2\text{-}S)_2(L)_4$ and $Pt_2(\mu_2\text{-}S)_2(L')_2$ (L = the phosphines PMe_2Ph, dppy),[28,29] and (L' = dppp, dppe, dppf, diop which are bidentate chelating phosphines).[30–33]

The flexibility of the $\{Pt_2(\mu_2\text{-}S)_2\}$ core hinge angle has been mentioned previously, this is measured by the dihedral angle between the two platinum sulfur planes. The exact ligand implemented directly affects this angle. These are shown in Table 1 for a variety of previously characterised complexes.

Table 1: Dihedral angle of $Pt_2(\mu_2\text{-}S)_2(L)_4$ complexes.

Complex	Dihedral angle	Ref
$Pt_2(\mu_2\text{-}S)_2(dppp)_2$	134.8°	[30]
$Pt_2(\mu_2\text{-}S)_2(dppe)_2$	140.2°	[31]
$Pt_2(\mu_2\text{-}S)_2(dppy)_4$	180°	[29]
$Pt_2(\mu_2\text{-}S)_2(PMe_2Ph)_4$	121°	[28]

1.2.1 The Phosphine Ligands, dppp and dppe

The ligand dppp is a bidentate chelating phosphine, comprised of two diphenylphosphines that are linked through the phosphorus by a $(CH_2)_3$ bridge in the form $Ph_2P(CH_2)_3PPh_2$ (Figure 1.5).

An aspect of the dppp ligand is that it results in an increase in the nucleophilicity for the $\{Pt_2(\mu_2\text{-}S)_2\}$ core, when compared to the phosphine dppe ($Ph_2P(CH_2)_2PPh_2$), an analogue of dppp (Figure 1.5). As a ligand dppp is more efficiently able to donate the lone pair of electrons on the two phosphorus atoms.

The bite angle of dppp is less restricted and therefore is closer to that of two separate phosphines, whereas dppe has more restriction due to its shorter ethylene bridge.[30]

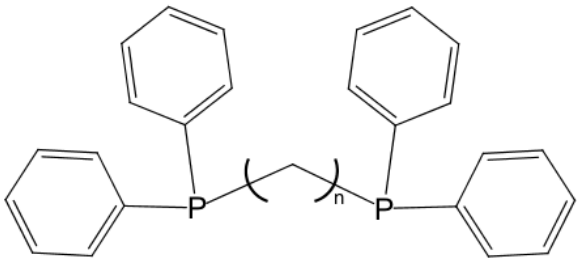

Figure 1.5: Diagram of dppe where n = 2 $(CH_2)_2$ and dppp where n = 3 $(CH_2)_3$.

From this increased nucleophilicity, $Pt_2(\mu_2\text{-}S)_2(dppp)_2$ reactions with dichloromethane proceed at a faster rate then reactions with $Pt_2(\mu_2\text{-}S)_2(dppe)_2$. The reactions yield slightly different products as the longer methylene bridge in dppp allows the bidentate ligand a greater range of flexibility than its counterpart. For both dppp and dppe the reaction results in the formation of $PtL(S_2CH_2)$ and $PtLCl_2$ (L = dppp, dppe). In the complex that contains dppp, the reaction product $Pt(dppp)(S_2CH_2)$ is intially formed, then goes on to react further to produce $[Pt_2(\mu_2\text{-}S)_2(dppp)_2(CH_2SCH_2)]Cl_2$.[30]

Something that is common in all of the $\{Pt_2(\mu_2\text{-}S)_2\}$ complexes containing phosphine ligands is the ability of the hinge to fold around itself. This is perhaps best described by the exceedingly prevalent analogy of the $\{Pt_2(\mu_2\text{-}S)_2\}$ core having a butterfly structure. Where the platinum atoms and their accompanying phosphine ligands are the wings of the butterfly, and the folding action is comparable to the wings fluttering. This inversion of the hinge angle is afforded by the low energy difference between the bent and planar geometries in the range of 4-8 kcal/mol,[6,34] meaning the planar geometry can act as an intermediate between the two bent forms Figure 1.6.

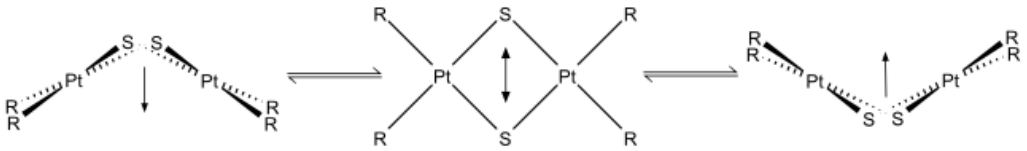

Figure 1.6: Diagram depicting $Pt_2(\mu_2\text{-}S)_2(R)_4$ ring inversions.

The ^{13}C NMR spectra of the $Pt_2(\mu_2\text{-}S)_2(L)_2$ complexes, (L = dppp, dppe) demonstrates the equivalence of all the phenyl rings, which is not expected for these bidentate ligands. This indicates at room temperature in solution there is sufficient energy for the transition between the bent geometry and its inverted form occurring faster then the NMR time scale, so the phenyl rings appear equivalent. The X-ray crystal structures of these complexes show the bent inequivalent geometry that is expected for the phenyl rings of the ligands that is not observed in the ^{13}C NMR.[30,31]

A comparable ligand to the ones mentioned here is the phosphine dppm. It bears similarities to dppp and dppe, only differing in the length of the bridging methylene group. The bridging group consists of only one methylene between the two PPh_2 groups, and therefore this is the most constrained bidentate phosphine of this type having the tightest P-Pt-P bite angle.[35]

This ligand has not been documented in the literature to form $Pt_2(\mu_2\text{-}S)_2(dppm)_2$. However it has been implemented in the formation of complexes with organochalcogenide bridging groups $\{Pt_2(\mu_2\text{-}XR)_2\}$ (XR = SPr, SPh, SePh, or C_6H_4Me-p),[36] along with the formation of the tri platinum $Pt_3(\mu_3\text{-}XR)_2(dppm)_2$ complexes.[37]

The analogous iodo bridged complex $Pt_2(\mu_2\text{-}I)_2(dppm)_2$ has been shown to exist,[38] the analogous chloro and bromo complexes lack the $\{Pt_2(\mu_2\text{-}X)_2\}$ ring system, opting for a Pt-Pt bonded centre with dppm bridging the metal-metal bond with the halogen each acting as a terminal ligand on each platinum. [39,40]

1.2.2 The Phosphine Ligand, dppy

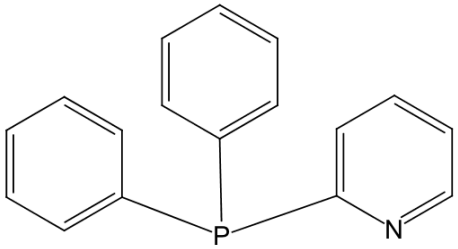

Figure 1.7: Diagram of the ligand dppy.

The use of the ligand dppy (Figure 1.7) which only differs from PPh_3 in that one of the phenyl rings is replaced with a pyridine which results in a subtstantial change to the hinge bending of the $\{Pt_2(\mu_2\text{-}S)_2\}$ core, and

therefore the complex $Pt_2(\mu_2\text{-}S)_2(dppy)_4$ has a completely flat square-planar geometry (Table 1). From this it can be concluded that it will not participate in the hinge angle inversion that occurs in the $\{Pt_2(\mu_2\text{-}S)_2\}$ cores of analogous complexes.

The $Pt_2(\mu_2\text{-}S)_2(dppy)_4$ does react with CH_2Cl_2 in a similar way to the other $\{Pt_2(\mu_2\text{-}S)_2\}$ cores mentioned, with the reaction resulting in the dissolution of the platinum sulfur ring as most do, along with formation of $Pt(dppy)_2Cl_2$ alongside $(dppy)Pt(\mu_2\text{-}S)_2CH_2$. The $Pt(\mu_2\text{-}S)_2CH_2$ core is square-planar with minor distortions.[29]

The $Pt_2(\mu_2\text{-}S)_2(dppy)_4$ complex has also been implemented in the assembly of heteropolymetallic sandwich structures. The dppy ligand makes this viable as the nitrogen of the pyridyl group is suitable for cross metal bridging, allowing dppy to function as a normal terminal tertiary phosphine ligand or bidentate ligand depending on the complex formed. This is demonstrated by a triangular silver unit sandwich between two $\{Pt_2(\mu_2\text{-}S)_2\}$ cores in Figure 1.8, with S-Ag bonding occurring and weak Pt-Ag and Ag-Ag interactions. The silver atoms without S-Ag-S bonding are bound through the bidentate action of the dppy from the platinum it sits above or below. [41,42]

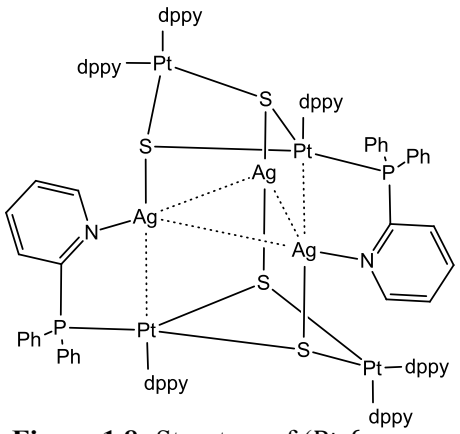

Figure 1.8: Structure of $(Pt_2(\mu_2\text{-}S)_2(dppy)_4)_2\,Ag_3$.

In a slightly altered synthesis of this platinum silver sandwich complex using a different silver starting material, a different Pt-dppy-Ag bridge complex is suspected to form. A single $Pt_2(\mu_2\text{-}S)_2(dppy)_4$ having Ag-dppm-Ag bridges between the two sulfurs, with each silver having a single bidentate dppy bound to it, providing three-coordinate silver.[41,42]

The luminescent properties of these two complexes have shown low absorption bands at 400 nm along with long lived luminescence at 560-660 nm, the low absorption bands are similar to that of the starting material.[29] The emission band at 560 nm could arise from the Ag_3/Ag-S or possibly the Pt-Ag; other silver thiocarbamates have shown similar low-temperature emissions.[43]

The low oxidation state palladium complexes of a similar structure have also been synthesised.[44] The structure differs in that the triangular silver unit is replaced with a triangular palladium unit sandwich between the two $Pt_2(\mu_2\text{-}S)_2(dppy)_4$ present, similar to that of Figure 1.8. The two dppy ligands of the platinum below or above a palladium are bonded to it through both of the pyridines not just the one. However there is no active Pt-Pd bond, the atoms are just in close proximity.[44]

Two side products are made from this synthesis, the first is similar to the silver reaction where a Pd-dppm-Pd bridges the sulfurs in $Pt_2(\mu_2\text{-}S)_2(dppy)_4$ with a pyridine of a ligand binding to each palladium, whereas the second side product is the common $\{Pt_2(\mu_3\text{-}S)_2M\}$ core with the palladium starting material.

For these sandwich complexes the versatility of the pyridyl-containing phosphine ligand is required for their construction, as other common phosphine ligands mentioned e.g. PPh_3, dppe, dppp, will only result in the formation of the common tri-metallic centres $\{Pt_2(\mu_3\text{-}S)_2M\}$. The pyridyl-containing phosphine ligands are necessary because the mono/bidentate bonding modes provide a needed electron source to the triangular palladiums for stabilisation. If these were not present to provide the electron density, other groups would be necessary, as in Murahashi's complex $(Pd_3(paracyclophane)_2(CH_3CN)_3)(BAr^F{}_4)_2$ ($BAr^F{}_4$ = B{3,5-$(CF_3)_2C_6H_3\}_4$),[45] which implements RCN ligands for this use. The dppy ligands that are not utilised in the stabilisation of the M_3 (M = Pd, Ag) barrel shaped metal centre provide shielding to the complex, the pyridyls of these ligands have yet unexplored uses as Lewis base precursors as some remain unbound in the $(Pt_2(\mu_2\text{-}S)_2(M_3)(dppy)_4$ (M = Ag, Pd) complexes.

1.2.3 The Phosphine Ligand, PMe_2Ph

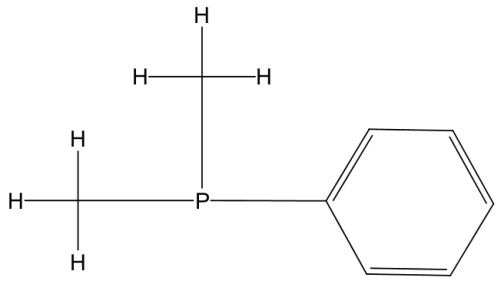

Figure 1.9: Diagram of PMe_2Ph.

The use of PMe_2Ph as a ligand (Figure 1.9), results in the $\{Pt_2(\mu_2\text{-}S)_2\}$ core having a bent hinge angle of 121° (Table 1); this is the largest bend of the complexes containing a platinum sulfur core discussed so far, excluding the core inversions of the butterfly structure. This ligand also has the least amount of steric bulk, being comprised of a phenyl ring and two methyl groups all bonded to a phosphorus. This lack of steric hindrance around the platinum sulfur core is a contributing factor to its bent geometry, as it has been found that terminal phosphine ligands that only have one or no bulky groups e.g Ph prefer bent structures.[6] The platinum-platinum distance of this bent structure is at least 3.10 Å providing no significant evidence that there is metal-metal bonding occurring through the bent core. [28]

First synthesised from the reaction of *cis*-$PtCl_2(PMe_2Ph)_2$ and sodium sulfide,[46] $Pt_2(\mu_2\text{-}S)_2(PMe_2Ph)_4$ will readily go on to react with *cis*-$PtCl_2(PMe_2Ph)_2$ and the arsine analogue *cis*-$PtCl_2(AsMe_2Ph)_2$ to form the $\{Pt_2(\mu_3\text{-}S)_2M\}$ centred complex.

Other trinuclear metal cores of the general form $Pt_2(\mu_3\text{-}S)_2(L)_4(MR)$ have been achieved with PMe_2Ph acting as the terminal phosphine ligand, where the coordinated group can be $M(C_6F_5)_2$ (M = Ni, Pd, Pt). Upon addition of the coordinating group $Pt(C_6F_5)_2$, the hinge angle becomes more acute, changing to 115° from the original 121°.[47] The platinum-platinum distance remains around 3.10 Å therefore no formal metal-metal bonding is occurring.

1.2.4 The Phosphine Ligand, diop

A phosphine ligand that has yet to be covered here is that of diop (Figure 1.10); this is a bidentate phosphine ligand that is able to coordinate to a platinum atom of the $\{Pt_2(\mu_2\text{-}S)_2\}$ core forming a seven-membered ring. It is a chiral phosphine due to the chiral carbons located in the centre of the ligand, and has been used in a platinum-tin catalyst for an asymmetric hydroformylation reaction.[33]

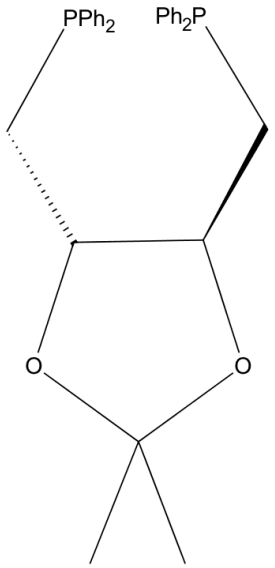

Figure: 1.10: Diagram of diop.

This ligand has also been explored while bonded to the $\{Pt_2(\mu_2\text{-}S)_2\}$ core, in the complex $[Pt_2(\mu_3\text{-}S)_2(diop)_2Rh(cod)]Cl$ as it was investigated for the potential catalytic properties in the hydrosilylation and hydrogenation reactions with acetophenone with diphenylsilane, and ketopantolactone respectively.[48] However these reactions were not completely successful; in the hydrosilylation reaction it was found the removal of the cod did not occur as readily as was needed for a catalytic procedure, with the complex being observed to undergo decomposition in both hydrosilylation and hydrogenation reactions.[48]

1.2.5 The Phosphine Ligand, dppf

The ferrocene-containing ligand, dppf, bears similarities to the class of "dpp" phosphines that have previously been mentioned here (Figure 1.5). It is two PPh_2 groups that are joined not by an alkyl chain but a ferrocene group, with each of the phosphorus atoms bonding to a carbon of the cyclopentadienyl rings of the ferrocene group (Figure 1.11).

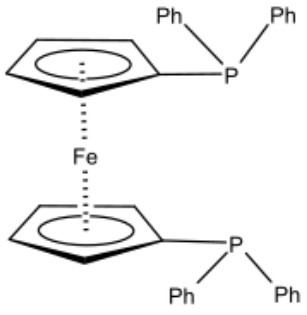

Figure 1.11: Diagram of dppf.

The presence of the iron atom within the centre of the ligand can provide flexibility that other phosphines don't have. Ferrocene is completely capable of undergoing a one-electron oxidation; these reversible redox properties do not affect the structure of the ferrocene by any large extent or result in fragmentation of the framework.[49] While dppf is acting as a ligand it has been shown to confer some of its electroactivity to the complex that it is bonded to, alterations of the oxidation state of the iron have the capacity to alter the electron density of the metal centre. As a ligand dppf has been implemented in the catalyst $PdCl_2(dppf)$ which is used in the cross coupling of

Grignard reagents and in the monoalkylation and arylation of dichlorobenzenes, along with finding a use as a catalyst in several other reactions.[49]

As a ligand, dppf has been shown to have a wide range over which the P-M-P (M = suitable metal) angle can operate and still act successfully as a bidentate ligand; the complex $[Pt_2(\mu_3\text{-}S)_2(dppf)_2Tl](PF_6)$ is in the lower end of the range with the P-Pt-P angle of 97.5°. The range of the bite angle extends over 93.6° seen in *fac*-$[Re(CO)_3(dppf)]Cl$,[50] up to a large bite angle 117.8° found in $Cu_2(\mu\text{-}NO_3)_2(dppf)_2$.[51]

The complex $PdCl_2(dppf)$ can have the ferrocene undergo its reversible one-electron oxidation, along with an irreversible one-electron reduction occurring on the palladium. While the ligand is bound to the palladium the oxidation of the ferrocene group becomes thermodynamically unfavourable making it difficult. This is also true for the analogous platinum complex $PtCl_2(dppf)$. Both the platinum and palladium complexes offer an increase in the kinetic stability of the oxidation product as well.[49]

Starting from $PtCl_2(dppf)$, the complex $Pt_2(\mu_2\text{-}S)_2(dppf)_2$ has been successfully synthesised,[32] *via* the same mechanism as most $\{Pt(\mu_2\text{-}S)_2\}$ centred complexes are prepared, through a reaction with $Na_2S{\cdot}9H_2O$.[2] The dppf complex, as for all μ_2-S bridging platinums centres the complex has a nucleophilicity great enough to rapidly undergo a nucleophilic attack with chlorinated solvents e.g. CH_2Cl_2. The reactions first yield mono, then dialkylated complexes, before complete degradation occurs generating the starting material $PtCl_2(dppf)$, along with $Pt(SCH_2Cl)_2(dppf)$. A possible near-catalytic cycle has been proposed for these reactions, as it does regenerate the starting material along with the chloromethanethiolato complex.[32]

The complex $Pt_2(\mu_2\text{-}S)_2(dppf)_2$ has been used as a heterometallic ligand in the coordination to non-platinum metal centres through the μ_2-S bridges which $\{Pt_2(\mu_2\text{-}S)_2\}$ complexes are known for. This has been accomplished using thallium in the general form $[Pt_2(\mu_3\text{-}S)_2(dppf)_2Tl](X)$ ($X = NO_3$, PF_6), in an attempt to construct an electroactive heteropolymetallic complex. The ligand dppf was chosen for this as the commonly implemented phosphine PPh_3, alongside the

platinum(II) in the $\{Pt_2(\mu_2\text{-}S)_2\}$ core, does not demonstrate great redox potential. Whereas the ligand dppf does, and therefore can possibly contribute this to the greater complex. Thallium was selected for its high redox ability and how it can be bound to the $\{Pt_2(\mu_2\text{-}S)_2\}$ while remaining unsaturated.[52]

The crystal structure of $[Pt_2(\mu_3\text{-}S)_2(dppf)_2Tl](PF_6)$ has been determined,[52] this revealed that the dppf ligand does not differ greatly from the PPh_3 analogues in bond lengths, resulting from the similarity of steric and electronic effects between the ligands.[52] The heteropolymetallic centre of the complex is also relatively unaltered having similar bonding parameters regardless of the phosphine ligands attached. This subsequently allows for the alteration of the redox potential of the heteropolymetallic centre *via* the ligands, without disturbing the core structure of the complex as it still can provide a vacant site available on the heterometal.[52]

The crystal structure of the $[Pt_2(\mu_3\text{-}S)_2(dppf)_2Tl](PF_6)$ shows that the Pt and Tl are held in the structure with close contact but at non-bonding distances of 3.389Å. This is sufficient to result in strong Pt-Tl spin-spin coupling $^2J_{Pt\text{-}Tl}$ observed in the ^{195}Pt NMR even without a direct metal-metal bonding interaction occurring.[52] As the metals separation is just outside the expected range for a Pt-Tl bonding interaction,[53] along with the observed $^2J_{Pt\text{-}Tl}$ coupling being weaker in $[Pt_2(\mu_3\text{-}S)_2(dppf)_2Tl](PF_6)$ then in complexes where Pt-Tl direct bonding is suggested.[52,53]

The redox activity of the complex $[Pt_2(\mu_3\text{-}S)_2(dppf)_2Tl](PF_6)$ was investigated using cyclovoltametric measurements. This reveals the oxidation of the thallium as an irreversible anodic peak and was shown in the cyclic voltammogram at +0.32 V, matching the same irreversible anodic peak that occurs in the PPh_3 analogue. The two analogues differ as the dppf complex has a single pair of redox waves present at +0.89 V resulting from both ligands each undergoing a one-electron oxidation simultaneously with minimal charge transfer communication occurring between the ligands.[52]

1.3 The Arsine Ligand Derivatives of the $\{Pt_2(\mu_2\text{-}S)_2\}$ Core

There is a large focus on both mono/bidentate terminal phosphine ligands when it comes to the $\{Pt_2(\mu_2\text{-}S)_2\}$ centred complexes, although the selection of ligands is not limited to these. A small amount of research has been done into the arsine analogues of pre-established phosphine ligands. The arsine ligands differ in comparison to their phosphine counterparts while bound in $\{Pt_2(\mu_2\text{-}S)_2\}$ centred complexes, as they possess a poorer electron donating ability. This results in an alteration of the sulfide bridges, decreasing their reactivity towards alkylating agents. The arsine ligands also come with an increased lability over the phosphine analogues.

This can be exemplified with the complex $Pt_2(\mu_2\text{-}S)_2(AsPh_3)_4$. The synthesis method is the same used for the phosphine analogue.[2] The reaction proceeds slower giving a lower final yield, the lability of the triphenylarsine ligand is suspected to be responsible for this, when comparing to the same reaction for triphenylphosphine.[54] Analysis of $Pt_2(\mu_2\text{-}S)_2(AsPh_3)_4$ *via* ESI-MS shows the protonated ion $[M+H]^+$ in lower intensities when compared to the phosphine analogues. This is due to the poorer electron donating arsine ligands resulting in a less electron-rich sulfide bridge, subsequently decreasing the protonation of the complex.[54]

The triphenylarsine analogue continues to differ from its phosphine counterpart, when it comes to the alkylation chemistry of the complexes. Monoalkylated $Pt_2(\mu_2\text{-}S)_2(AsPh_3)_4$ in the form of $[Pt_2(\mu_2\text{-}S)(\mu_2\text{-}SCH_2C_6H_4Br)(AsPh_3)_4]^+$ has been shown to be unstable in a solution of CH_2Cl_2, whereas monoalkylated $Pt_2(\mu_2\text{-}S)_2(PPh_3)_4$ complexes do not degrade over the same time.

Further evidence of the arsine ligated complexes lacking stability upon alkylation comes from the attempts at dialkylation reactions. While the reaction of both $Pt_2(\mu_2\text{-}S)_2(PPh_3)_4$ and $Pt_2(\mu_2\text{-}S)_2(AsPh_3)_4$ with the alkylating agent MeI, promptly results in the monoalkylated cation $[Pt_2(\mu_2\text{-}S)(\mu_2\text{-}SMe)(EPh_3)_4]^+$ (E = As or P) as the reaction proceeds, the phosphine ligated complex reacts further to form the dicationic dialkylated complex which undergoes nucleophilic attack from the

iodide giving the product $[Pt_2(\mu_2\text{-}SMe)_2(PPh_3)_3I]^+$. The arsine complex does not follow this reaction pathway, it will rapidly form the monoalkylated complex but will not react further, with very little dialkylation occurring. The monomethylated complex from this reaction does not remain stable in solution for longer than 24 hours after the initial reaction; after this time it is no longer present within the mass spectrum.[54]

Attempts to dialkylate the arsine-ligated complex using alkylating agents that do not produce species that can undergo nucleophilic attack have also been investigated. This again demonstrates the lability of the arsine ligand and reaction rate of the complex. In reactions of $Pt_2(\mu_2\text{-}S)_2(EPh_3)_4$ (E = As or P) with $ClCH_2CH_2Cl$ over the same time frame. The phosphine-containing complex produces the dialkylated complex as its major product, whereas the arsine-containing complex produces the monoalkylated complex with insubstantial amounts of the dialkylated complex present.[54]

In the reactions with $ClCH_2CH_2Cl$ and other reactions where *n*-butylchloride is used as the alkylating agent, the increased lability of the ligand is made apparent by the minimal amount of the dialkylated complex that forms. Chloride, a weak nucleophile, is able to substitute for one of the arsine ligands resulting in $[Pt_2(\mu_2\text{-}SA)_2(AsPh_3)_3Cl]^+$ (A = Me or CH_2CH_2). The phosphine analogue of this complex does not undergo the same nucleophilic attack with chloride as the phosphine ligands are less labile.

With the coordination of arsine ligands to the $\{Pt_2(\mu_2\text{-}S)_2\}$ core there are geometrical changes to the bond lengths occurring with respect to the known phosphine analogues. The arsine ligated complex results in a longer Pt-As bond distance giving a weaker interaction between the two, this is observed between the crystal structures of the complex of the general form $Pt_2(\mu_2\text{-}S)_2(L)_2$ (L = $Ph_2As(CH_2)_2AsPh_3$, $Ph_2P(CH_2)_2PPh_3$).[55] The lesser *trans*-influence of the arsenic on the $\{Pt_2(\mu_2\text{-}S)_2\}$ core results in a decrease of the bond length between the platinum and sulfur atoms of the core. When the arsine ligated complex $Pt_2(\mu_2\text{-}S)_2(L)_2$ (L = $Ph_2As(CH_2)_2AsPh_3$) is co-ordinated to form the penta-nuclear $[\{Pt_2(\mu_3\text{-}S)_2\}_2(L)_2M]^{2+}$ complex, the effects of the arsine ligand are again

observed, as the S-M bonding interaction is lengthened when compared to phosphine analogues, as the electron density around the sulfurs is lessened with the arsine ligands present giving a weaker interaction.[55]

The arsine analogues of previously established phosphine ligands have been shown to be similar enough in most regards to produce structurally similar complexes.[54] The differences between the phosphines and arsines becomes apparent upon closer examination of the reaction chemistry of the $\{Pt_2(\mu_2\text{-}S)_2\}$ core, shown by the examples of the alkylation chemistry discussed.[54,55]

1.4 Water-Solubility with $\{Pt_2(\mu_2\text{-}S)_2\}$ Centred Complexes

All of the ligands and their accompanying platinum complexes that have been discussed previously are soluble in common organic solvents. This solubility is provided to the complex *via* the phenyl rings, that all the phosphine ligands mentioned share, and therefore complexes containing the $\{Pt_2(\mu_2\text{-}S)_2\}$ core completely lack any form of water-solubility while these phosphines are attached.

Attempts at synthesising water-soluble derivatives of the complex $Pt_2(\mu_2\text{-}S)_2(PPh_3)_4$ can be divided into two different methods. The first of which has been successfully achieved through the polyether functionalisation of the complex, this is the addition of a water-soluble chain to one of the μ_2-sulfur bridges without breaking the four-membered platinum sulfide ring, resulting in a bridging thiolate group.[56] The attachment of the polyether chain is performed by a monoalkylation reaction on the $\{Pt_2(\mu_2\text{-}S)_2\}$ core of the complex, reaction such as these have been well studied, and discussed here previously.[13–15]

1.4.1 Water-Solubility *via* Polyether Functionalisation

The successful water-soluble derivation of $Pt_2(\mu_2\text{-}S)_2(PPh_3)_4$ was produced with the attachment of a Jeffamine® chain acting as the polyether within the complex. Jeffamines® are polyetheramines consisting of a polyether backbone with terminal primary amino groups capping the ends of the chain.[56] For the chain to be bound to the μ_2-sulfur bridges, they first need to undergo a conversion into an alkylating agent. This step is achieved *via* a reaction to form the bromoethylurea derivative

of the chain. This method of derivation was implemented as alkyl bromides avoid the production of unwanted side reactions from nucleophilic halides. As they can undergo attack of the $\{Pt_2(\mu_2\text{-}S)_2\}$ core, this was discussed with regards to the use of alkyl iodides,[19] and have been discussed previously in Section 1.1.2 when mentioning MeI us as an alkylating agent.

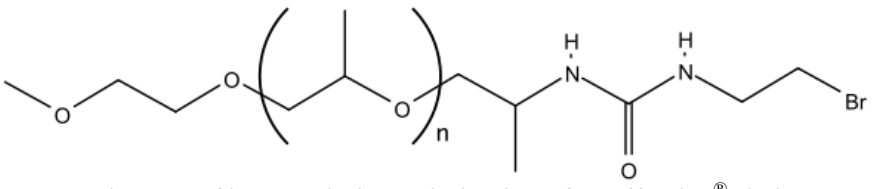

Figure 1.12: Diagram of bromoethylurea derivative of a Jeffamine® chain = R- Br, n = 3-17.

The alkylating agent is generated from the reaction between 2-bromoethylisocyanate ($Br(CH_2)_2NCO$) and the amine, (Jeffamine®) this reaction results in the bromoethylurea derivative of the chosen Jeffamine® chain, example in Figure 1.12. This reaction is carried out in hexane as both reactants are soluble, but the product is not. This allows for the easy separation and purification of the product from unreacted material present.[56]

The alkylation reaction between the bromoethylurea derivative and $Pt_2(\mu_2\text{-}S)_2(PPh_3)_4$ is carried out through a 1 hour long reflux of the reactants in methanol followed by 24 hours of stirring at ambient temperature. The reaction readily yields the desired product $[Pt_2(\mu_2\text{-}S)(\mu_2\text{-}SR)(PPh_3)_4]^+$ (R = Jeffamine® urea derivative as in Figure 1.12) which can be isolated with the appropriate counter anion (BPh_4^-).[56]

Attempts at generating the same derivative of the $Pt_2(\mu_2\text{-}S)_2(PPh_3)_4$ complex with shorter chain analogues has also been investigated using the chloro-functionalised polyethylene glycol (Cl-PEG), $Me(OCH_2CH_2)_nCl$. The reaction under the same methanol reflux preceded far slower then the alkylation reactions with the bromoethylurea derivative. Over this reaction time the Cl-PEG did result in detectable amounts of the desired product accompanied by the degradation of the $Pt_2(\mu_2\text{-}S)_2(PPh_3)_4$. In attempts to prevent this, the addition of NaBr was made to the reaction in order to convert the alkyl chlorides in to the more reactive

bromides. The desired reaction product was again isolated with the addition of a counter anion (BPh_4^-).[56]

The polyether functionalisation of $Pt_2(\mu_2\text{-}S)_2(PPh_3)_4$ successfully resulted in water-soluble complexes, it was determined that the longer chain derivations of $Pt_2(\mu_2\text{-}S)_2(PPh_3)_4$ yielded complexes of greater solubility. This was determined through the preparation of saturated solutions that were analysed for platinum content by ICP MS.[56]

The method of polyether functionalisation to achieve water-soluble $\{Pt_2(\mu_2\text{-}S)_2\}$ centred complexes is viable but introduces significant limitations on the chemistry of the complexes once produced. The $\{Pt_2(\mu_2\text{-}S)_2\}$ core as covered previously in Sections 1.1 and 1.2 has a flexible hinge angle through the μ_2- sulfur bridges that comprise the ring system. Through these bridging atoms the complexes that contain the $\{Pt_2(\mu_2\text{-}S)_2\}$ cores gain the ability to act as a metalloligand towards a large variety of heterometals.[3–5] The derivatisation of the $\{Pt_2(\mu_2\text{-}S)_2\}$ core through the alkylation of one or both of the μ_2-sulfur bridges provides complexes containing the $\{Pt_2(\mu_2\text{-}S)_2\}$ core a wide and interesting chemistry to explore. When polyether functionalisation is used to provide water-solubility to the complex, one of the coordination sites on the μ_2-sulfur bridges is occupied; this limits the complexes ability to coordinate, accompanied by a restriction of the flexibility of the hinge angle.

1.4.2 Water-Solubility *via* Phosphine Ligands

Water-solubility has been achieved with drawbacks that restrict the reactivity of the complexes prepared. The desire to have water-soluble $\{Pt_2(\mu_2\text{-}S)_2\}$ centred complexes with unaltered μ_2-sulfur bridges, can only be achieved *via* a second, unexplored method. This implements suitable water-soluble phosphine ligands, which allows the central $\{Pt_2(\mu_2\text{-}S)_2\}$ core to remain unaltered and retain the flexibility and reactivity of the organic-soluble analogues.

This method of achieving water-solubility for $\{Pt_2(\mu_2\text{-}S)_2\}$ complexes has not been documented in the literature as time of writing, so is the focus of the research undertaken here. The aim of this project was to synthesise and

characterise complexes of the general form $Pt_2(\mu_2\text{-}S)_2(L)_4$, where L = the ligands PTA, $[TPPMS]^-$, TCEP. The methods chosen to be investigated included a biphasic ligand exchange reaction between $Pt_2(\mu_2\text{-}S)_2(PPh_3)_4$ and the ligand. Another synthetic method investigated were the reactions of the platinum complexes in the general form *cis*-$PtCl_2L_2$, (L = PTA, $[TPPMS]^-$, TCEP) in a benzene suspension with $Na_2S{\cdot}9H_2O$. This is a slight alteration to the metathesis reaction between *cis*-$PtCl_2(PPh_3)_2$ and $Na_2S{\cdot}9H_2O$ to prepare $Pt_2(\mu_2\text{-}S)_2(PPh_3)_4$.[2] Upon the successful synthesis of water-soluble complexes, such as $Pt_2(\mu_2\text{-}S)_2(L)_4$ (L = PTA, $[TPPMS]^-$, TCEP) efforts will be taken for a complete characterisation through ESI-MS, NMR, and X-ray crystallography.

Chapter 2:
Synthesis of 1,3,5-Triaza-7-phosphaadamantane (PTA) Complexes

2.1 Synthesis and Characteristics of PTA

This chapter primarily focuses on the ligand 1,3,5-triaza-7-phosphaadamantane, or PTA (Figure 2). PTA is a small, water-soluble phosphine that has been shown to act as a ligand towards group 10 transition metals forming complexes with the general formula *cis*-$MCl_2(PTA)_2$ (M = Ni, Pd, Pt)[57,58]. PTA can also act as a ligand towards some of the other platinum group metals, such as rhodium[59]. The phosphine has also demonstrated the ability to provide water-soluble metal complexes, and it therefore has the potential to be used in complexes containing the $\{Pt_2(\mu_2\text{-}S)_2\}$ core to provide solubility. This hypothesis is lent credence as the common starting materials for $Pt_2(\mu_2\text{-}S)_2(L)_4$ complexes are of the general form *cis*-$PtCl_2L_2$ (L = phosphine ligand)[2] which has been reported for PTA.[60]

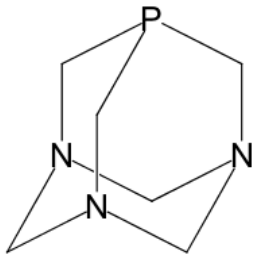

Figure 2: Structure of 1,3,5-triaza-7-phosphaadamantane, PTA.

The synthesis of PTA was undertaken using established literature methods,[61] with the reaction between tetrakis(hydroxymethyl)phosphonium chloride ($P(CH_2OH)_4Cl$) and sodium hydroxide (NaOH) to form the intermediate $P(CH_2OH)_3$. This was followed by reaction with hexamethylenetetramine and formaldehyde, giving PTA, followed by evaporation and recrystallisation.

During the routine collection of mass spectra and NMR spectra of the ligand after synthesis, small variations from stated literature observations were recorded, and are discussed briefly below.

The mass spectrum of the phosphine ligand was obtained, along with the $^{31}P\{^1H\}$ NMR to ensure the purity of the sample. Small amounts of the oxide were found to be present. The positive-ion ESI mass spectrum clearly showed the most

intense ion as the protonated PTA, ($[PTA+H]^+$ 158.13 *m/z*), but PTA=O was not observed. Less intense ions were also present, primarily attributed to lingering contaminants inside the instrument. The $^{31}P\{^1H\}$ NMR revealed two chemical shift values both in agreement with the literature while D_2O was used as the solvent; a strong sharp resonance for PTA at -98.5 ppm and a weak resonance for PTA=O at -2.9 ppm.[61] These $^{31}P\{^1H\}$ NMR data confirmed that there were only two phosphine compounds present; the desired PTA product and a small amount of its oxide.

The ^1H NMR of PTA that was synthesised here showed something in the spectrum not previously described in the literature. The literature[61] only reported three hydrogen resonances, a doublet at 3.9 ppm with a coupling constant of $^2J_{H\text{-}P}$ 9 Hz for the 6 (PCH_2N) hydrogen atoms and a singlet at 4.42 ppm for the 6 (NCH_2N) hydrogen atoms.[61]

This was not the case for the ^1H NMR spectrum that was collected here. The doublet at 3.9 ppm was consistent with their observations, but at 4.42 ppm there were discrepancies, visible in Figure 2.1. The spectrum shows two AB doublets at 4.49 ppm and 4.44 ppm both with $^2J_{H\text{-}H}$ 12 Hz geminal coupling. These will be due to the difference in environments for the axial and equatorial hydrogens along

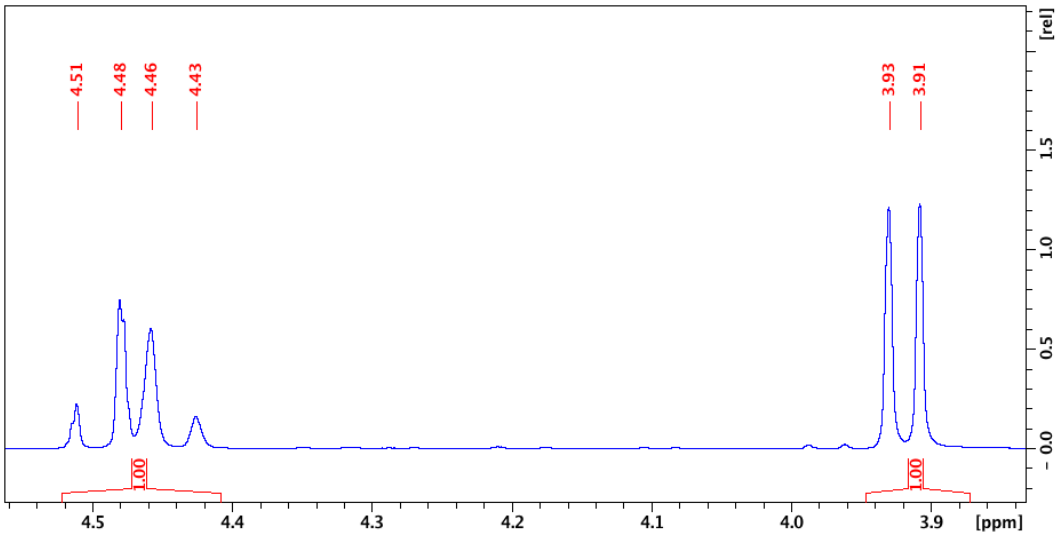

Figure 2.1: ^1H NMR of PTA, showing the 3 proton environments. One environment for the 6 hydrogen atoms of (PCH_2N) is represented by the doublet at 3.9 ppm. Two hydrogen environments represented by the two doublets at 4.49 and 4.44 ppm for the 6 hydrogen atoms of (NCH_2N). Recorded on a 400 MHz NMR spectrometer in D_2O.

the bottom of the ring at (NCH_2N) (Figure 2). The integration of the 2 AB doublets matches that of the doublet at 3.9 ppm. This was consistent with the conclusion that the pairs of doublets at 4.4 ppm are a result of the differing environments for the 3 axial and 3 equatorial hydrogen atoms.

2.2 Synthesis of *cis*-$PtCl_2(PTA)_2$

The platinum complex used as the starting material in further reactions with $Na_2S{\cdot}9H_2O$ was *cis*-$PtCl_2(PTA)_2$. Its synthesis and notable characteristics are discussed below. The complex *cis*-$PtCl_2(PTA)_2$ was synthesised with the use of established literature methods from $PtCl_2(cod)$.[60]

The complex *cis*-$PtCl_2(PTA)_2$ is water-soluble but not inert. It undergoes a reaction with water that leads to the decomposition of the platinum complex and the production of PTA oxide. A small amount of water-stability can be achieved with an excess of PTA in solution.[58] The decomposition of the platinum complex is proposed,[58] to occur through oxidative addition of water producing a hydridohydroxo M(IV) species. This allows for the oxidation of PTA and at some point in the reaction pathway the intermediate $[PtCl(PTA)_3]^+$ is produced.[58] This water instability has also been documented in other group 10 metal complexes of

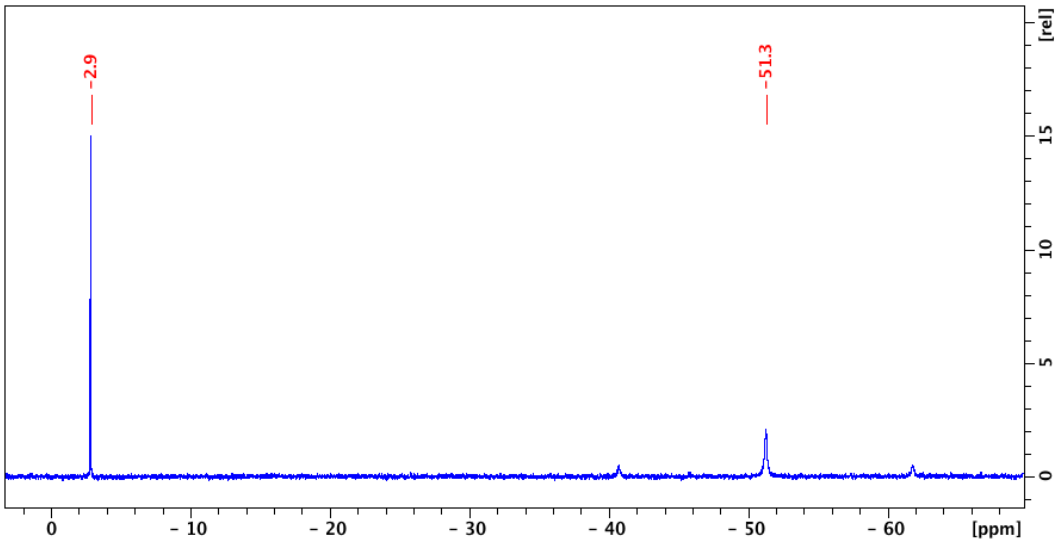

Figure 2.2: The $^{31}P\{^1H\}$ NMR spectrum of *cis*-$PtCl_2(PTA)_2$, immediately after dissolution in D_2O. PTA=O, s, -2.9 ppm and *cis*-$PtCl_2(PTA)_2$ s, -51.3 ppm, $^1J_{Pt\text{-}P}$ 3410 Hz. Recorded at 162 MHz on a 400 MHz NMR spectrometer.

the general form *cis*-$MCl_2(PTA)_2$ (M = Pt, Pd, Ni), and the order of reactivity of these metal complexes with water was that of Pt > Pd > Ni.[58]

Here these findings are corroborated with the use of $^{31}P\{^1H\}$ NMR of *cis*-$PtCl_2(PTA)_2$ in a D_2O solution. The solution began colourless and over 1 hour became increasingly yellow, and then turning brown after approximately a week. The $^{31}P\{^1H\}$ NMR spectrum recorded immediately after preparing this sample is shown in Figure 2.2. It shows two peaks of interest; a strong PTA oxide resonance at -2.9 ppm and a second resonance of *cis*-$PtCl_2(PTA)_2$ at -51.3 ppm with $^1J_{Pt\text{-}P}$ coupling of 3410 Hz. Both of these are consistent with the literature values.[60,61]

The $^{31}P\{^1H\}$ NMR spectrum of the same sample was recorded two weeks later (Figure 2.3). The sample showed an almost negligible signal for the platinum complex at -51.3 ppm, (Figure 2.2 compared with Figure 2.3). Additionally, the $^1J_{Pt\text{-}P}$ coupling satellites were not distinguishable from the base line, and an increase in the PTA oxide peak along with the appearance of two other phosphorus chemical shifts were observed.

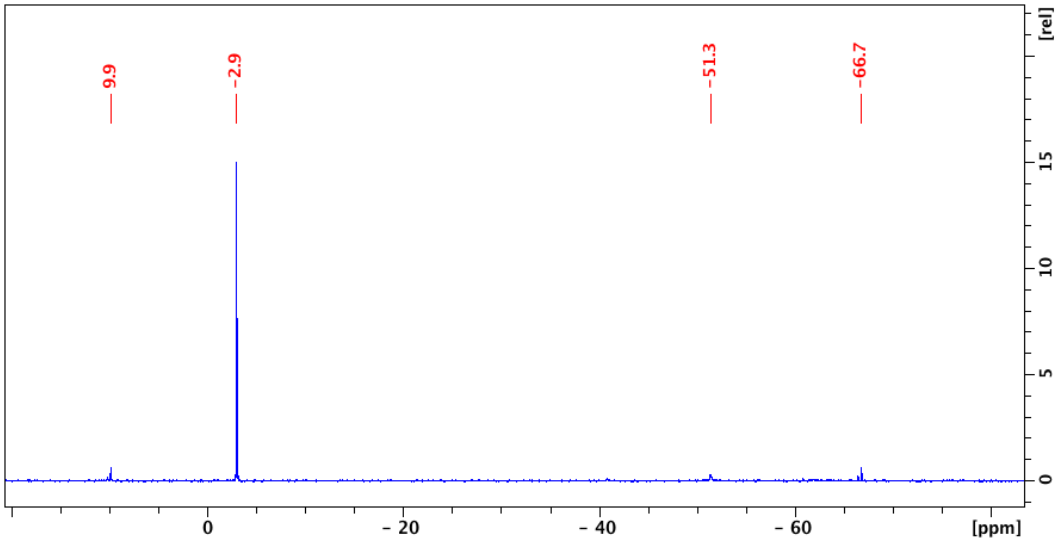

Figure 2.3: $^{31}P\{^1H\}$ NMR spectrum of *cis*-$PtCl_2(PTA)_2$ in D_2O, two weeks after dissolution. PTA=O s, -2.8 ppm. *cis*-$PtCl_2(PTA)_2$ s, 51.3 ppm. Recorded at 162 MHz on a 400 MHz NMR spectrometer.

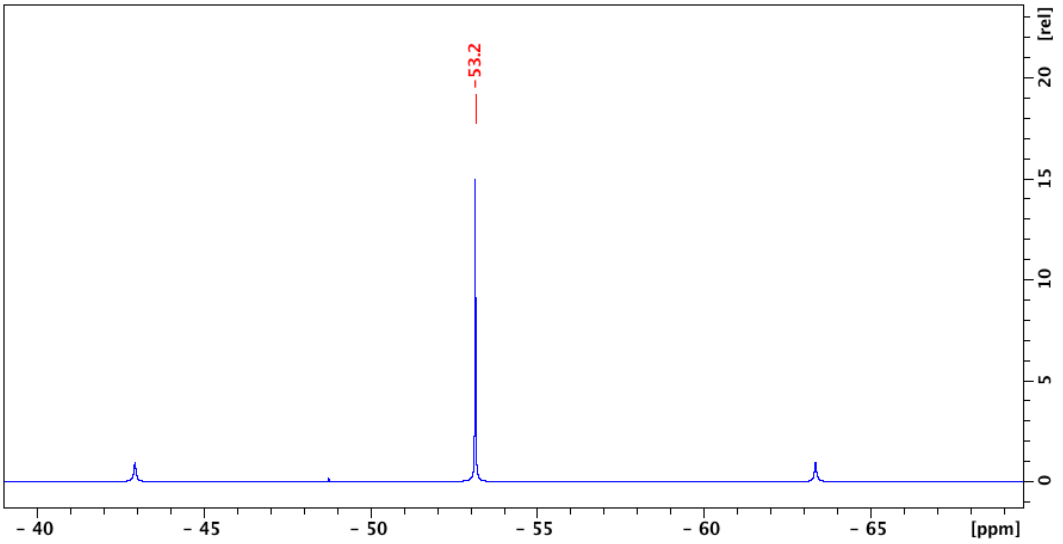

Figure 2.4: The $^{31}P\{^{1}H\}$ NMR of *cis*-$PtCl_2(PTA)_2$ s, -53.2 ppm $^{1}J_{Pt\text{-}P}$ 3308 Hz, immediately after dissolution in DMSO-d_6. Recorded at 162 MHz on a 400 MHz NMR spectrometer.

A clean $^{31}P\{^{1}H\}$ NMR spectrum of *cis*-$PtCl_2(PTA)_2$ with no decomposition was obtained in DMSO-d_6 (Figure 2.4), demonstrating the purity of the platinum complex synthesised. The spectrum showed that no PTA oxide was present at the start, only the sharp resonance of *cis*-$PtCl_2(PTA)_2$ and its satellites were observed and are in agreement with the literature for *cis*-$PtCl_2(PTA)_2$ in DMSO-d_6.[62]

2.2.1 An Investigation of *cis*-$PtCl_2(PTA)_2$ Using ESI Mass Spectrometry

The complex *cis*-$PtCl_2(PTA)_2$ was used as the starting material in later reactions, so was investigated using ESI mass spectrometry in order to place the characteristics and behaviour of any products synthesised from this complex in a greater context. This was also done for analogous complexes of *cis*-$PtCl_2(PTA)_2$ for comparison purposes.

This study demonstrated that in the presence of excess chloride, the species $[PtCl_3(PTA)_2]^-$ at 614.97 *m/z* was observed, in the negative-ion ESI mass spectrum at a CEV of -150 V with a MeOH solvent. Platinum prefers to form four-coordinate (square planar) complexes,[63] so the location of the third chloride is of interest. It is possible that the chloride was interacting with the platinum forming a five-coordinate complex, but an alternative possibility was that the

chloride interacts through a hydrogen atom of the PTA (Figure 2.5). The C-H bond was expected to be slightly more polar with the presents of the nitrogen adjacent to it, promoting a chloride interaction through a hydrogen atom. The ion $[PtCl_3(PTA)_2]^-$ observed may have contributions from both possibilities in Figure 2.5. A five-coordinated platinum PTA complex, $[PtI_2(PTA)_3]\cdot CH_3OH$, has previously been documented in the literature.[64] This complex differs from the suspected five-coordinate complex observed here as the halogen used was iodide and three phosphine ligands were present. Hydrogen interactions through the slightly polar C-H bonds have been documented in the X-ray crystal structures of PTA complexes with chloride counter ions. An example of this is $[Au(PTA)_4]Cl\cdot 2H_2O$,[65] (TIRDON, CSD), where the short contacts are shown in the crystal structure between the three hydrogen atoms on one face of the PTA and the chloride anion.

The negative-ion ESI spectrum of *cis*-$PtCl_2(PTA)_2$ shows the ions $[PtCl_3(PTA)_2]^-$ along with $[(PtCl_2(PTA)_2)_2+Cl]^-$ (Figure 2.6). As mentioned the ion $[PtCl_3(PTA)_2]^-$ could be the result of five-coordinate platinum as per 1 of Figure 2.5 or a hydrogen interaction as in 2 of Figure 2.5, it would also be possible for

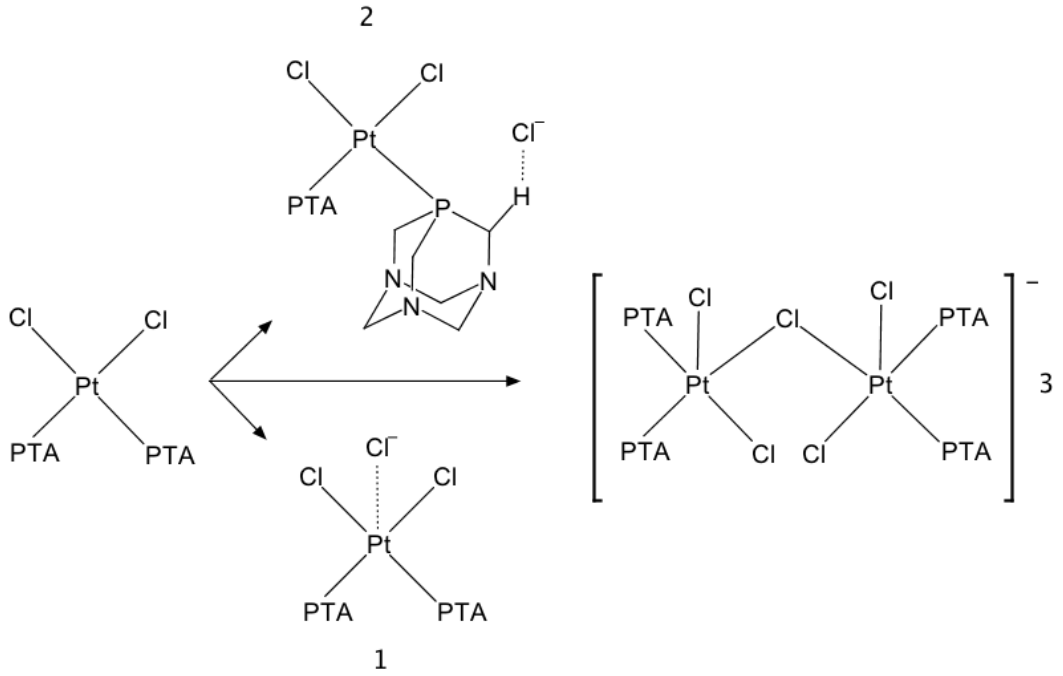

Figure 2.5: Two possible structures of the $[PtCl_3(PTA)_2]^-$.
1) The 5-coordinate platinum complex.
2) Interaction of chloride through a hydrogen atom of PTA.
3) Bridged chloride ion observed.

the hydrogen bonding interaction to occur through the N-CH_2-N hydrogen atom not just P-CH_2-N, as both C-H bonds would have a slight increase in polarity from the adjacent atoms. The ion observed $[(PtCl_2(PTA)_2)_2+Cl]^-$ at 1194.96 *m/z* (Figure 2.6) could be from a bridging chloride complex 3 of Figure 2.5, which could provide evidence for a five-coordinate platinum, or possibly a hydrogen bonding interaction (C-H···Cl···H-C) between two *cis*-$PtCl_2(PTA)_2$ complexes sharing the chloride. The positive-ion ESI spectra readily showed the adducts with sodium and potassium $[PtCl_2(PTA)_2+Na]^+$ and $[PtCl_2(PTA)_2+K]^+$. These adducts are likely to form through a nitrogen of the PTA as it allows for the coordination of the sodium and potassium cations.

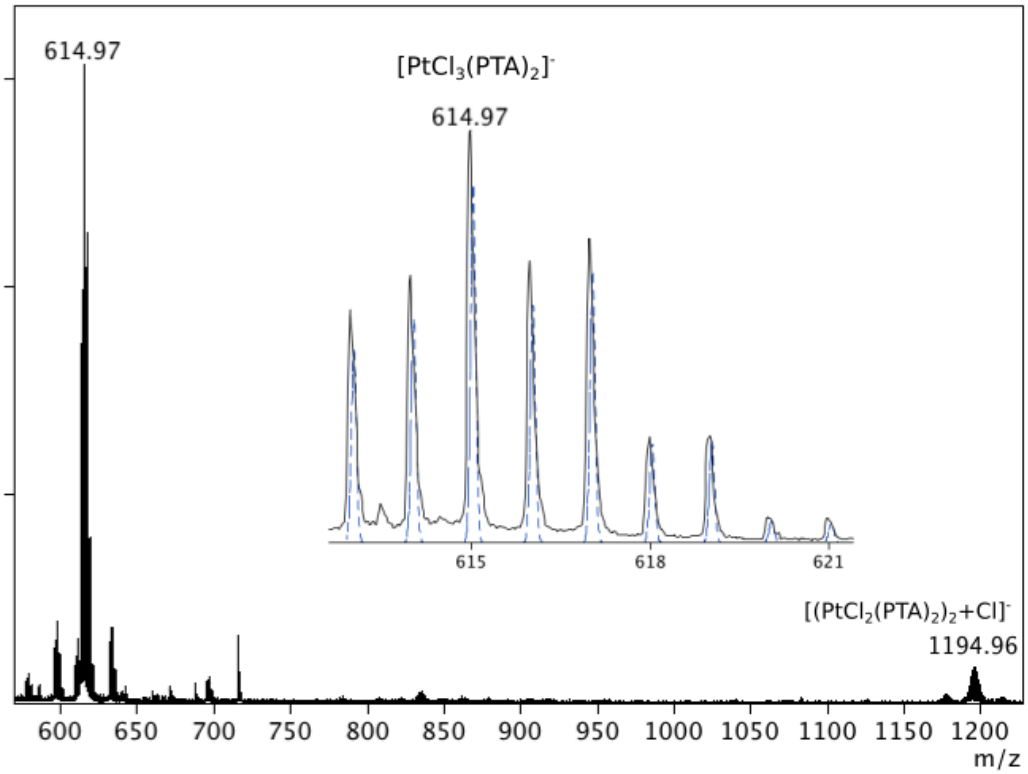

Figure 2.6: The negative-ion ESI mass spectrum of *cis*-$PtCl_2(PTA)_2$ (no additional chloride), showing the ions $[PtCl_3(PTA)_2]^-$ and $[(PtCl_2(PTA)_2)_2+Cl]^-$. The inset spectrum shows both the observed (solid line) and calculated (dashed line) isotope patterns of $[PtCl_3(PTA)_2]^-$. CEV -150 V, MeOH solution.

The potential coordination of chloride to other *cis*-$PtCl_2(L)_2$ (L = phosphine) complexes was examined to see if the size of the phosphine ligand affects its formation. Mass spectra were obtained for the complexes *cis*-$PtCl_2(PTA)_2$ and *cis*-$PtCl_2(PPh_3)_2$ with excess chloride added *via* NaCl. This allowed for the examination of how ligand bulk and steric hindrance can effect the formation of

the possible five-coordinate complex, or alternatively if the lack of a viable C-H for the chloride interaction would effect formation. It was suspected that the PPh_3 ligand would provide enough bulk to prevent the addition of chloride to the platinum along with lacking a polar C-H bond for the chloride interaction to occur, while the smaller phosphine ligand, PTA, had already been shown to be capable of this addition, but through which bonding mode was unknown.

The resulting negative-ion ESI mass spectrum for *cis*-$PtCl_2(PTA)_2$ with added chloride (NaCl) again showed the formation of $[PtCl_3(PTA)_2]^-$ along with $[(PtCl_2(PTA)_2)_2+Cl]^-$, and the adducts $[PtCl_2(PTA)_2+Na]^+$ and $[PtCl_2(PTA)_2+K]^+$ were again observed in the positive-ion ESI spectrum, the potassium ions in solution were adventitious coming from solvent or glassware. The spectra of the triphenylphosphine analogue also showed the sodium adduct *cis*-$[PtCl_2(PPh_3)_2+Na]^+$, however the negative-ion ESI spectrum of *cis*-$PtCl_2(PPh_3)_2$ with excess chloride did not show a peak for the species $[PtCl_3(PPh_3)_2]^-$. This suggests that the size of the phosphine ligand was what influences the coordination of the additional chloride ion, with bulkier groups such as triphenylphosphine preventing the coordination of the chloride from occurring. The counter point to this is that if the chloride interaction occurs between a hydrogen atom of a polar C-H bond in the PTA (2 of Figure 2.5), this interaction will not occur in the negative-ion ESI mass spectrum for *cis*-$PtCl_2(PPh_3)_2$ as it lacks the necessary polar C-H bonding interaction for $[PtCl_3(PPh_3)_2]^-$ to be observed.

The negative-ion ESI spectra of the complexes *cis*-$PdCl_2(PTA)_2$ and *cis*-$PtCl_2(PMe_3)_2$ with the addition of NaCl to provide the excess chloride were also recorded. The ion $[PdCl_3(PTA)_2]^-$ complex was seen within the spectrum, similar to that of the platinum analogue. Palladium possesses an increased lability so will lose a phosphine ligand more readily than platinum complexes. This can be seen with the comparison of intensities between the ion $[PdCl_3(PTA)_2]^-$ and its fragment $[PdCl_3(PTA)]^-$ (Figure 2.7). The monophosphine ion fragment $[PdCl_3(PTA)]^-$ was at a far greater intensity than the diphosphine ion $[PdCl_3(PTA)_2]^-$. The analogous monophosphine fragment of the platinum complex was not present at the same level of intensity in the spectrum when excess

chloride is used and the same skimmer and capillary exit voltages are applied to provide identical fragmentation conditions. This demonstrates the palladium atoms' increased lability over platinum, as it was readily fragmented, losing a

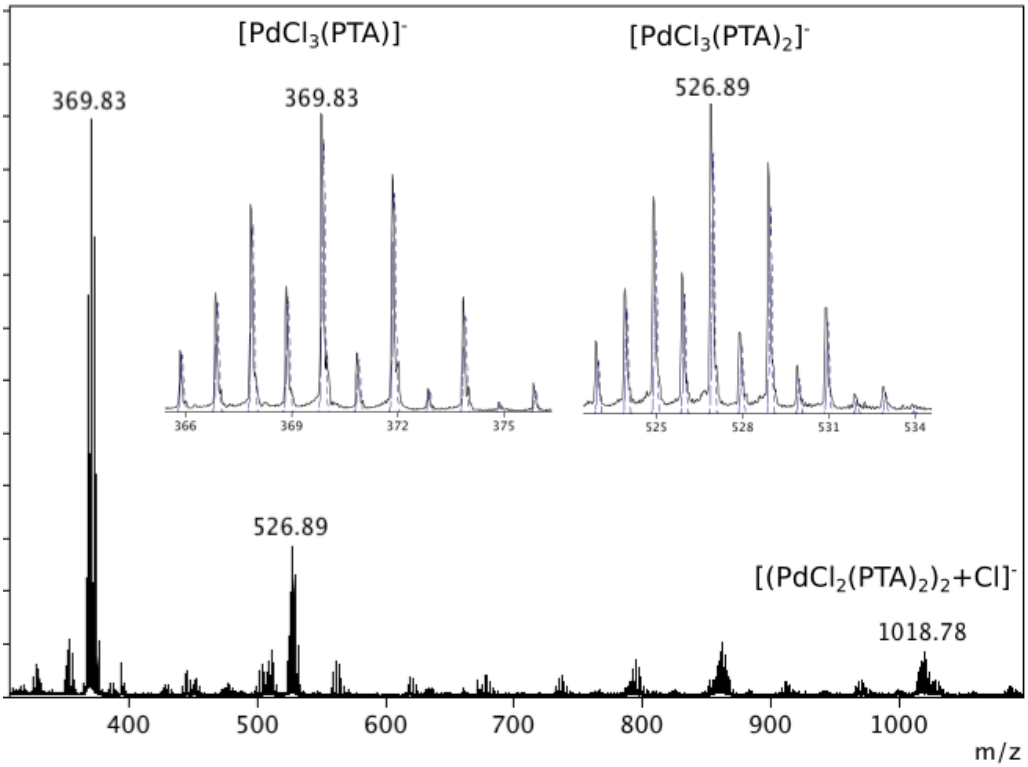

Figure 2.7: The negative-ion ESI mass spectrum of *cis*-$PdCl_2(PTA)_2$ with excess chloride as NaCl. The inset spectra displays both observed and calculated isotope patterns for $[PdCl_3(PTA)_2]^-$ and $[PdCl_3(PTA)]^-$. CEV -150 V, MeOH solution.

phosphine ligand in the ionisation process where the platinum complex does not. It was expected that the fragment $[PdCl_3(PTA)]^-$ would be at a lower intensity at decreased skimmer and capillary exit voltages, as more of the complete ion $[PdCl_3(PTA)_2]^-$ would be present in its place. It was also expected that an increase in voltage would be accompanied by an increase in fragmentation, leading to fewer $[PdCl_3(PTA)_2]^-$ ions. What was observed, however, was that the intensity of the monophosphine remained relatively consistent throughout the alteration in skimmer and capillary exit voltages, while an increase in $[PdCl_3(PTA)_2]^-$ was witnessed at lower voltages. These results, showing a consistent $[PdCl_3(PTA)]^-$ ion intensity and fluctuations in the intensity of $[PdCl_3(PTA)_2]^-$ as the voltage was changed, suggests that the *cis*-$PdCl_2(PTA)_2$ complex used had impurities of $[PdCl_3(PTA)]^-$ to begin with.

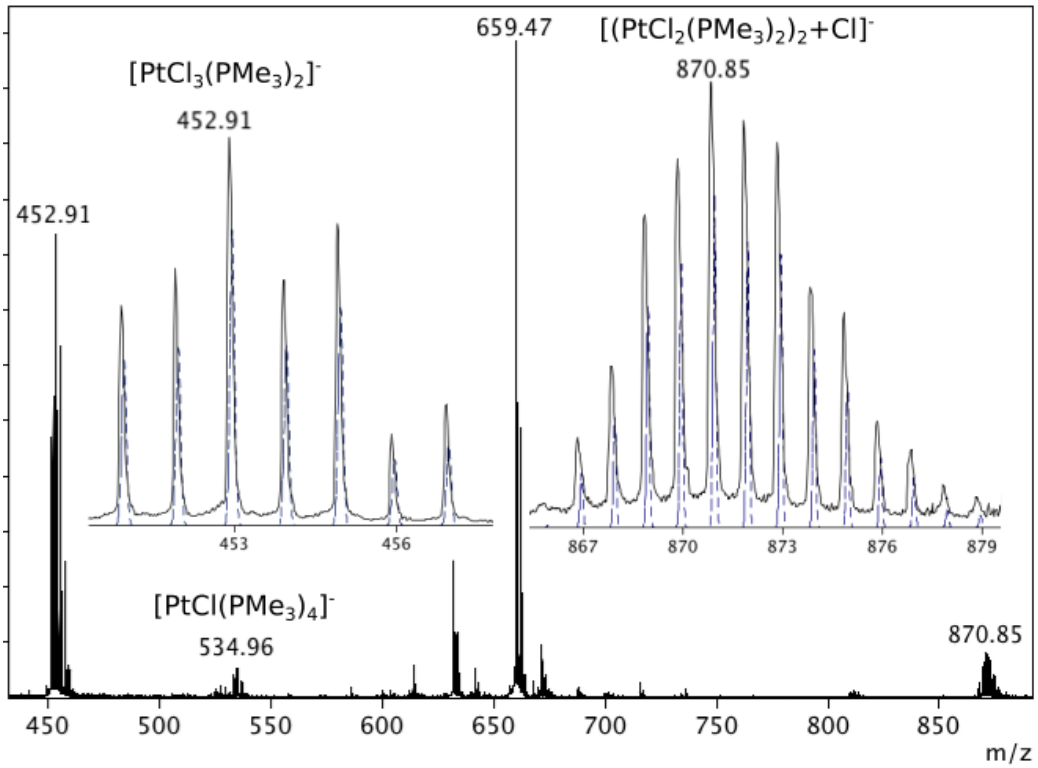

Figure 2.8: The negative-ion ESI mass spectrum of *cis*-$PtCl_2(PMe_3)_2$ with excess chloride in the form of NaCl, The inset spectra shows the calculated and observed isotope patterns for $[PtCl_3(PMe_4)_2]^-$, $[PtCl_2(PMe_3)_2]_2$+$Cl]^-$. The ion at 659.47 *m/z* is a non-platinum complex present in the ESI-MS. CEV -150 V, MeOH solution.

Another phosphine analogue investigated was *cis*-$PtCl_2(PMe_3)_2$. This also showed the formation of the chloride adduct $[PtCl_3(PMe_3)_2]^-$ (Figure 2.8), confirming that the two PMe_3 phosphine ligands result in minimal steric bulk, allowing for the addition of the third chloride to the complex. This addition of the chloride to form $[PtCl_3(PMe_3)_2]^-$ has to occur through a five-coordinate platinum, as the PMe_3 ligand lacks a polar C-H bond for the interaction to occur through a hydrogen atom. This was again in contrast with *cis*-$PtCl_2(PPh_3)_2$ where no $[MCl_3L_2]^-$ anion was visible in the negative-ion ESI spectrum, as both chloride additions are not possible. An ion was observed at 534.69 *m/z* which matched the mass and isotope pattern of $[PtCl(PMe_3)_4]^-$, this would be an unusual species to observe as it will require the platinum to be in the Pt(0) state when it started as Pt(II). The ion at 659.47 *m/z* was a non-platinum complex present in the ESI-MS spectrum, comprising of a carbon isotope pattern and remains unidentified.

The positive-ion ESI mass spectra of *cis*-$PdCl_2(PTA)_2$ and *cis*-$PtCl_2(PMe_3)_2$ were also obtained. Two pairs of methanol solutions were prepared in Eppendorf tubes,

a pair of *cis*-$PdCl_2(PTA)_2$ solutions and a pair of *cis*-$PtCl_2(PMe_3)_2$ solutions. NaCl was added to one of each pair in order to observe the sodium adduct of the general form $[MCl_2(L)_2+Na]^+$ (M = Pd, Pt. L = PTA, PMe_3). The spectra resulting from this addition of NaCl resulted in both of the sodium adducts, $[PdCl_2(PTA)_2+Na]^+$ and $[PtCl_2(PMe_3)_2+Na]^+$ being observed within their respective positive-ion ESI mass spectra. The aggregate platinum complex $[(PtCl_2(PMe_3)_2)_2+Na]^+$ was observed but not the palladium analogue.

A single drop of pyridine (Pyr) was added to the remaining tube of each pair in order to determine if pyridine is capable of exchanging for the chloride in both complexes, which would result in the generation of ions of the general form $[MCl(L)_2(Pyr)]^+$ (M = Pd, L = PTA or M = Pt, L = PMe_3). The pyridine exchange was successful and the complexes $[PdCl(PTA)_2(Pyr)]^+$ and $[PtCl(PMe_3)_2(Pyr)]^+$ were both visible at capillary exit voltages of 90 V, the fragment $[PdCl(PTA)(Pyr)]^+$ was observed at this CEV as well. Upon increasing the capillary exit voltage to 140 V the pyridine complex ions of the general form

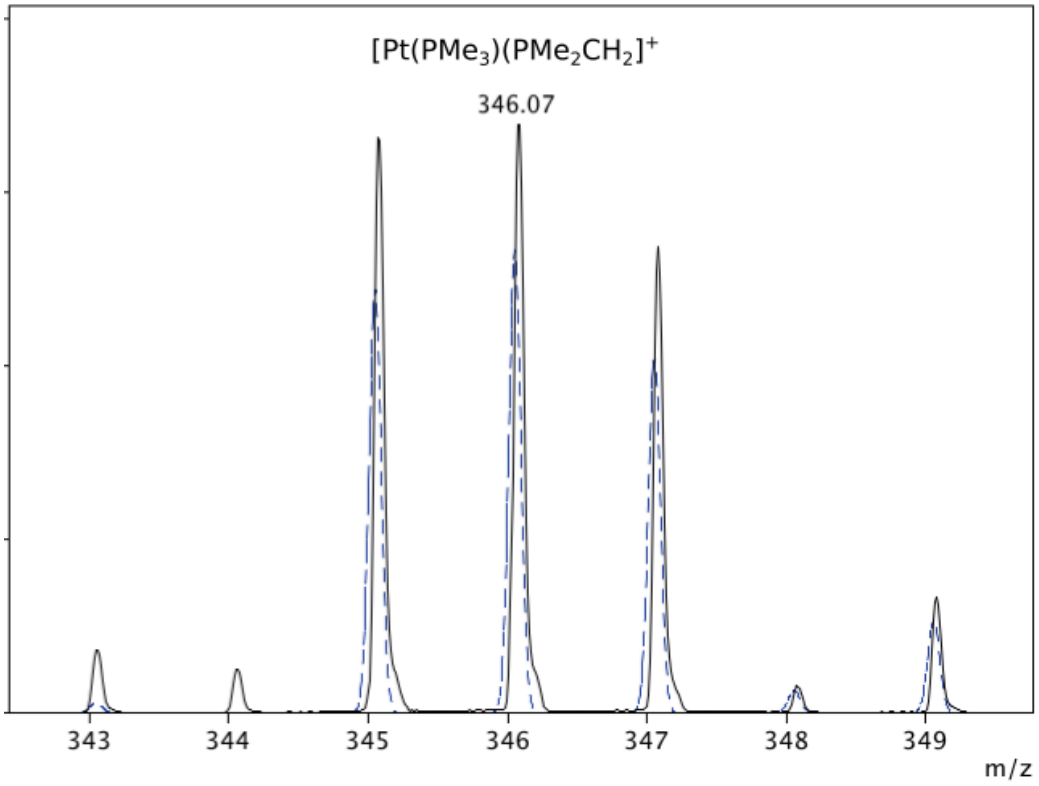

Figure 2.9: The positive-ion ESI spectrum of *cis*-$[PtCl_2(PMe_3)_2]$ showing the observed isotope pattern of the ion $[Pt(PMe_3)(PMe_2CH_2)]^+$ with its calculated isotope pattern overlaid (dotted blue lines). CEV 180 V, MeOH solution.

$[(MCl(L)_2(Pyr)]^+$ (M = Pd, L = PTA or M = Pt, L = PMe_3), fragmented resulting in the loss of pyridine and an increased intensity of the fragment ions $[PdCl(PTA)_2]^+$, and $[PtCl(PMe_3)_2]^+$.

The pyridine substitution was also attempted with the starting complex *cis*-$PtCl_2(PTA)_2$. The exchange between pyridine and the chloride was readily observed in the mass spectrum with the presence of the ion $[PtCl(PTA)_2(Pyr)]^+$ when a capillary exit voltage of 150 V was used. For the previous platinum and palladium complexes the capillary exit voltages required for the ion to be visible was much lower (90 V), indicating the Pt-Pyr bond formed after the addition of pyridine to *cis*-$PtCl_2(PTA)_2$ was stronger than the same bond in the analogous complexes. This was expected for the palladium complex (*cis*-$PdCl_2(PTA)_2$) as the metal centre was more labile and this is shown with the ion $[PdCl(PTA)_2(Pyr)]^+$ requiring lower CEV to be observed, but was not expected for the platinum analogue (*cis*-$PtCl_2(PMe_3)_2$) as it also required the lower CEV of 90 V for the ion $[PtCl(PMe_3)_2(Pyr)]^+$ to be observed in the spectrum, where the ion $[PtCl(PTA)_2(Pyr)]^+$ was visible at the CEV of 150 V.

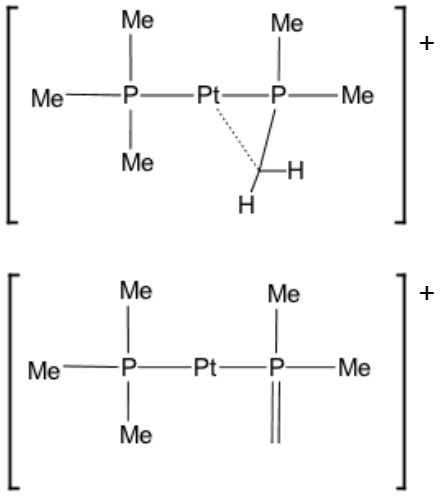

Figure 2.10: Proposed bonding modes of $[Pt(PMe_3)(PMe_2CH_2)]^+$. Top cyclometalation, bottom unbound.

During the investigation of positive-ion ESI mass spectra of *cis*-$PtCl_2(PMe_3)_2$, an interesting ion, $[Pt(PMe_3)(PMe_2CH_2)]^+$ 346.07 *m/z* was observed (Figure 2.9). This ion results from the initial complex *cis*-$PtCl_2(PMe_3)_2$ fragmenting and losing both chlorides and one of the methyl hydrogen atoms. Two possible bonding modes for this ion are either a cyclometalation or the CH_2 remaining unbound (Figure 2.10). This cation was

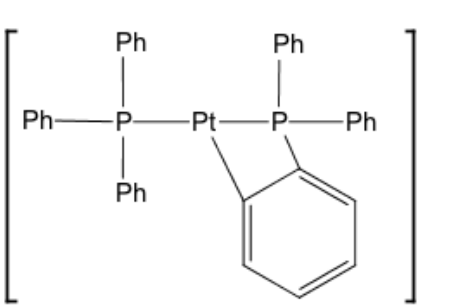

Figure 2.11: Cyclometalated fragment ion of *cis*-$[PtCl_2(PPh_3)_2]$.

first observed in the spectrum when a capillary exit voltage of 140 V was used. Increasing the voltage caused an increase in observed fragmentation, correlating to an increase in the intensity of the $[Pt(PMe_3)(PMe_2CH_2)]^+$ cation. This cation gave the strongest peak in the spectrum with a capillary exit voltage of 210 V. This was determined with the positive-ion ESI mass spectra of *cis*-$PtCl_2(PMe_3)_2$ being recorded over various capillary exit voltages between 60 V and 240 V.

This type of cyclometalated cation can form readily with triphenylphosphine ligands in the mass spectra of *cis*-$PtCl_2(PPh_3)_2$ (Figure 2.12) and other analogous complexes which have been documented in the literature.[66] The cation $[Pt(PPh_3)(PPh_2C_6H_4)]^+$ results in a four-membered ring system (Figure 2.11). For the newly observed cation $[Pt(PMe_3)(PMe_2CH_2)]^+$ to achieve the same cyclometalation, it would require the formation of a three-membered ring system (Figure 2.10). This would make the ring very strained, making it likely that no cyclometalation was occurring in the mass spectrometer and that the CH_2 group of the cation is uncoordinated (Figure 2.10).

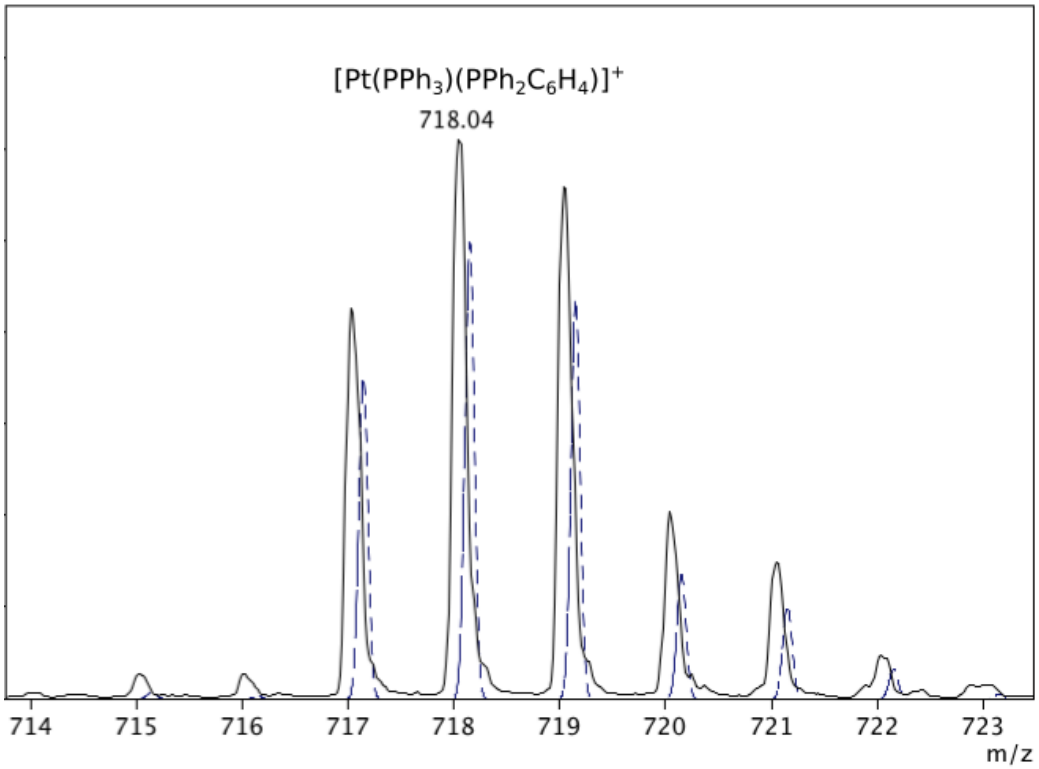

Figure 2.12: Positive-ion ESI mass spectrum of *cis*-$PtCl_2(PPh_3)_2$, showing the cyclometalated cation fragment $[Pt(PPh_3)(PPh_2C_6H_4)]^+$ with the observed (solid line) and calculated (dashed line) isotope patterns. CEV 150 V, MeOH solution.

2.3 Synthesis and Characterisation of $Pt_2(\mu_2\text{-}S)_2(PTA)_4$

The complex *cis*-$PtCl_2(PTA)_2$ was reacted with $Na_2S{\cdot}9H_2O$ in a benzene suspension in an attempt to form $Pt_2(\mu_2\text{-}S)_2(PTA)_4$. This was the same literature method implemented with *cis*-$PtCl_2(PPh_3)_2$ to form $Pt_2(\mu_2\text{-}S)_2(PPh_3)_4$ and hence this was the first synthetic route initially trialled for its effectiveness.[2] The starting material *cis*-$PtCl_2(PTA)_2$ has been thoroughly documented and characterised, through the use of $^{31}P\{^1H\}$ NMR investigation of the decomposition in a D_2O solution over time, that has been discussed previously (Section 2.2). Along with being mentioned in the literature to lack water-stability.[58] The addition of water to the reaction suspension could only be minimised to an extent, as the sodium sulfide used was the nonahydrate form. This would have caused some decomposition of *cis*-$PtCl_2(PTA)_2$ and resulted in the formation of some PTA=O which was unavoidable.

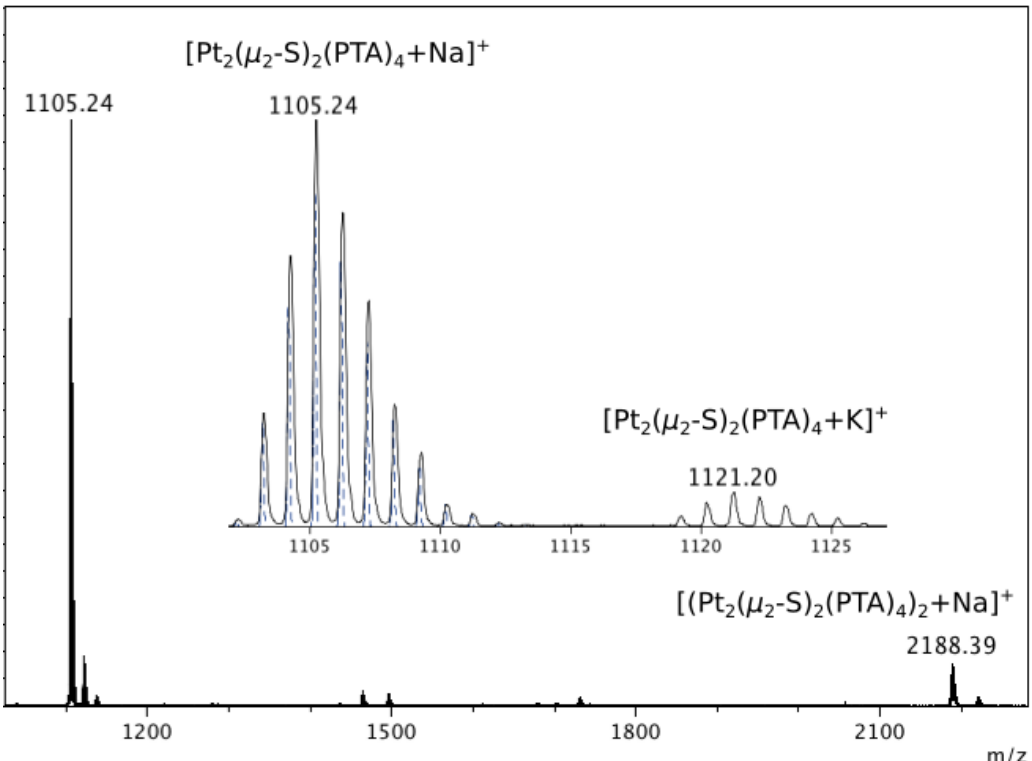

Figure 2.13: Initial positive-ion ESI mass spectrum of the isolated solid, $Pt_2(\mu_2\text{-}S)_2(PTA)_4$. Significant ions are listed in Table 2. The inset spectrum shows the observed isotope patterns for $[Pt_2(\mu_2\text{-}S)_2(PTA)_4+Na]^+$ and $[Pt_2(\mu_2\text{-}S)_2(PTA)_4+K]^+$ along with the calculated pattern (dashed line) for $[Pt_2(\mu_2\text{-}S)_2(PTA)_4+Na]^+$. CEV 150 V, water/MeOH (2:5) solution.

The solid was recovered from the benzene suspension after the 24 hours mixing period *via* filtration with a Büchner funnel, followed by drying under a vacuum. The isolated solid possessed a slight yellow-green colouration. The reaction did proceed successfully, as is indicated by the initial positive-ion ESI mass spectrum (Figure 2.13). This spectrum showed various ions that could only result from a successful reaction. The ions observed are listed in Table 2.

The sodium adduct $[Pt_2(\mu_2\text{-}S)_2(PTA)_4+Na]^+$ was the signal with the highest intensity in the mass spectrum, which was expected because sodium ions were present in the mixture from the excess of $Na_2S{\cdot}9H_2O$ that was used. In the synthesis of the complex $Pt_2(\mu_2\text{-}S)_2(PPh_3)_4$ the filtered product would normally be washed with water to remove the sodium salts. Due to the water-solubility of the $Pt_2(\mu_2\text{-}S)_2(PTA)_4$ synthesised here however, another method was needed. The water-solubility of this new complex became apparent in the preparation of the mass spectrum samples, as it required the addition of water to the MeOH solution for dissolution to occur.

Table 2: Observed ions in the positive-ion ESI mass spectrum of isolated $Pt_2(\mu_2\text{-}S)_2(PTA)_4$ in a water/MeOH (2:5) solution.

Ion (*m/z*)	Calculated (*m/z*)	Formula
1105.24	1105.17	$[Pt_2(\mu_2\text{-}S)_2(PTA)_4Na]^+$
1121.20	1121.14	$[Pt_2(\mu_2\text{-}S)_2(PTA)_4K]^+$
1137.20	1137.16	$[Pt_2(\mu_2\text{-}S)_2(PTA)_4O_2Na]^+$
2188.39	2188.35	$[(Pt_2(\mu_2\text{-}S)_2(PTA)_4)_2Na]^+$

The initial method trialled to remove the sodium salts was to preferentially dissolve the $Pt_2(\mu_2\text{-}S)_2(PTA)_4$ in methanol to allow for the filtration of NaCl or unreacted Na_2S that remained. The solution started as a green colour as was the initial solid. After 24 hours of evaporation in a desiccator under constant vacuum, a colour change occurred. The solution turned orange with a hint of green, and a fine orange precipitate was present. Rotary evaporation was avoided during this stage as it was unknown if the complex was temperature sensitive. The positive-ion ESI mass spectrum of the orange solution showed a lower intensity for the ion $[Pt_2(\mu_2\text{-}S)_2(PTA)_4+Na]^+$ and showed far more organic, non-platinum complex

peaks present with greater intensity than when the spectra was first obtained (inset spectrum Figure 2.14).

The orange decomposition solution demonstrated a larger variety of $Pt_2(\mu_2\text{-}S)_2(PTA)_4$ ions, with more oxides present and 2+ ions accompanying the expected sodium adduct $[Pt_2(\mu_2\text{-}S)_2(PTA)_4+Na]^+$ seen in (Figure 2.14). The ion assignment is within the accompanying Table 2.1. After 48 hours the solvent had completely evaporated, leaving behind a precipitate that was primarily coloured orange with flecks of white. It is proposed these flecks are the result of solid NaCl that was not removed. The mass spectrum of the solid isolated from evaporation showed the $[Pt_2(\mu_2\text{-}S)_2(PTA)_4+Na]^+$ ion at a lower intensity than the spectrum obtained from solution before evaporation was complete, and had fewer ions overall (Figure 2.15).

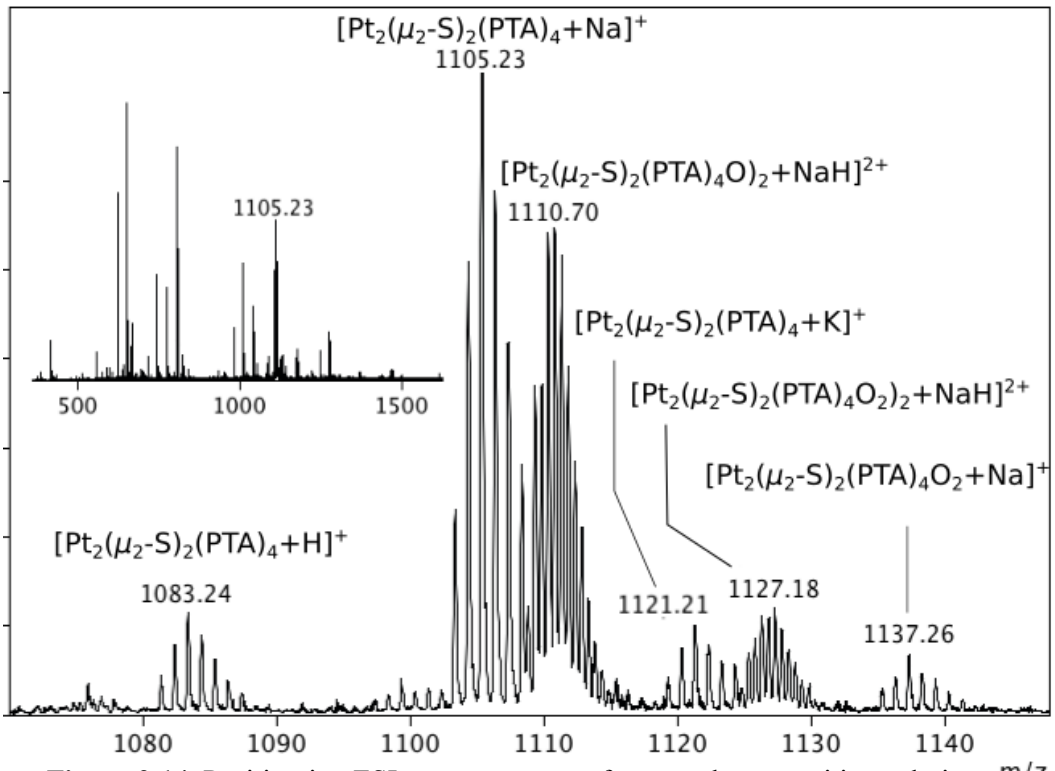

Figure 2.14: Positive-ion ESI mass spectrum of orange decomposition solution. Table 2.1 lists the ions present. The inset spectrum shows the entire recorded spectrum. CEV 150 V, water/MeOH (2:5) solution.

Table 2.1: Identified ions of various $Pt_2(\mu_2\text{-}S)_2(PTA)_4$ species seen in Figure 2.14.

Ions (*m/z*)	Calculated (*m/z*)	Formula
1083.24	1083.19	$[Pt_2(\mu_2\text{-}S)_2(PTA)_4+H]^+$
1105.23	1105.17	$[Pt_2(\mu_2\text{-}S)_2(PTA)_4+Na]^+$
1110.70	1110.17	$[(Pt_2(\mu_2\text{-}S)_2(PTA)_4O)_2+NaH]^{2+}$
1121.21	1121.14	$[Pt_2(\mu_2\text{-}S)_2(PTA)_4O+K]^+$
1127.18	1127.17	$[(Pt_2(\mu_2\text{-}S)_2(PTA)_4O_2)_2+NaH]^{2+}$
1137.26	1137.16	$[Pt_2(\mu_2\text{-}S)_2(PTA)_4O_2+Na]^+$

Several oxidised species of $Pt_2(\mu_2\text{-}S)_2(PTA)_4$ were observed in the positive-ion ESI mass spectra, tabulated in Table 2.1. The oxidation of the analogous PPh_3 complex, through the bridging sulfides has been documented in the literature.[67] The X-ray crystal structure of the oxidised and protonated complex $Pt_2(\mu_2\text{-}S_2O_2H)(PPh_3)_4$ has been obtained; this reaction did require a strong oxidant or a catalyst of Sc^{3+}/Ln^{3+} to be used, to obtain a significant yield.[67]

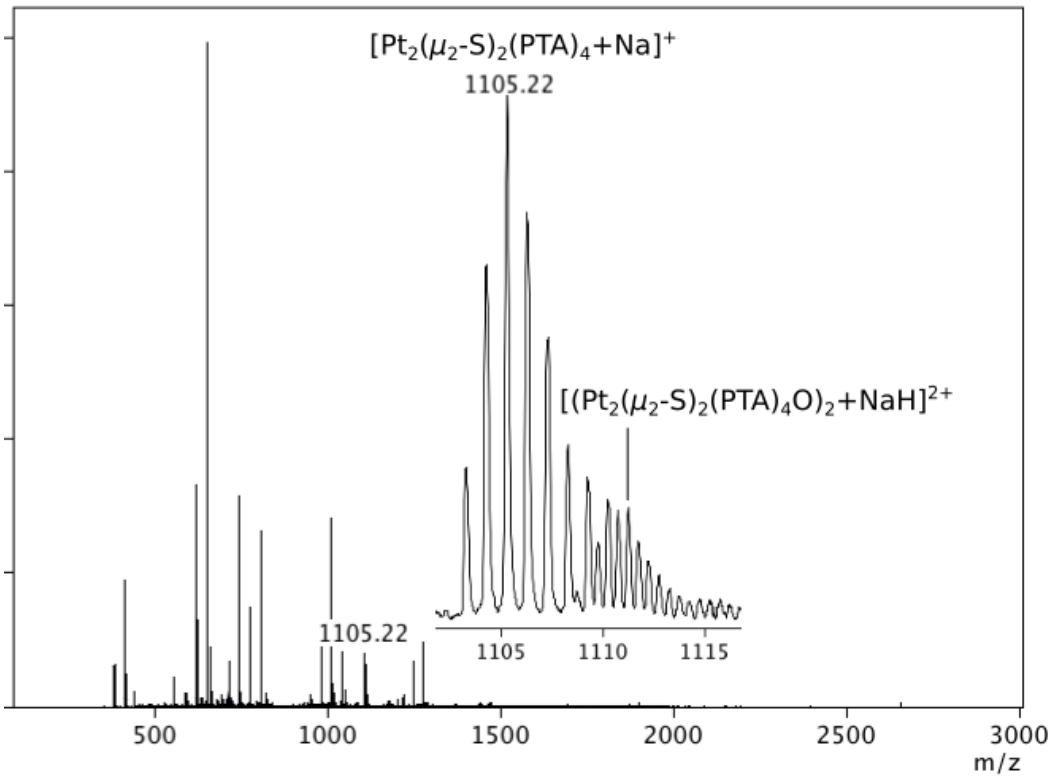

Figure 2.15: Positive-ion ESI mass spectrum of the final decomposition product of $Pt_2(\mu_2\text{-}S)_2(PTA)_4$. Inset spectrum of platinum complexes present. CEV 150 V, water/MeOH (2:5) solution.

The decreasing intensity of the $Pt_2(\mu_2\text{-}S)_2(PTA)_4$ ions over time (Figure 2.13- Figure 2.15) and the appearance of a significant number of non-platinum ions, combined with the colour change, suggests that partial decomposition had occurred during the attempted purification procedure. Interestingly, it can be determined that the larger variety of ions seen in Figure 2.14 from the orange solution are possibly only present in solution or generated as a direct result of the mass spectrometry ionisation technique. As they are not visible in the spectrum of the final solid isolated after evaporation was complete Figure 2.15, where only the sodium adduct $[Pt_2(\mu_2\text{-}S)_2(PTA)_4+Na]^+$ was prominent, alongside the overlapping oxidised complex $[(Pt_2(\mu_2\text{-}S)_2(PTA)_4O)_2+NaH]^{2+}$.

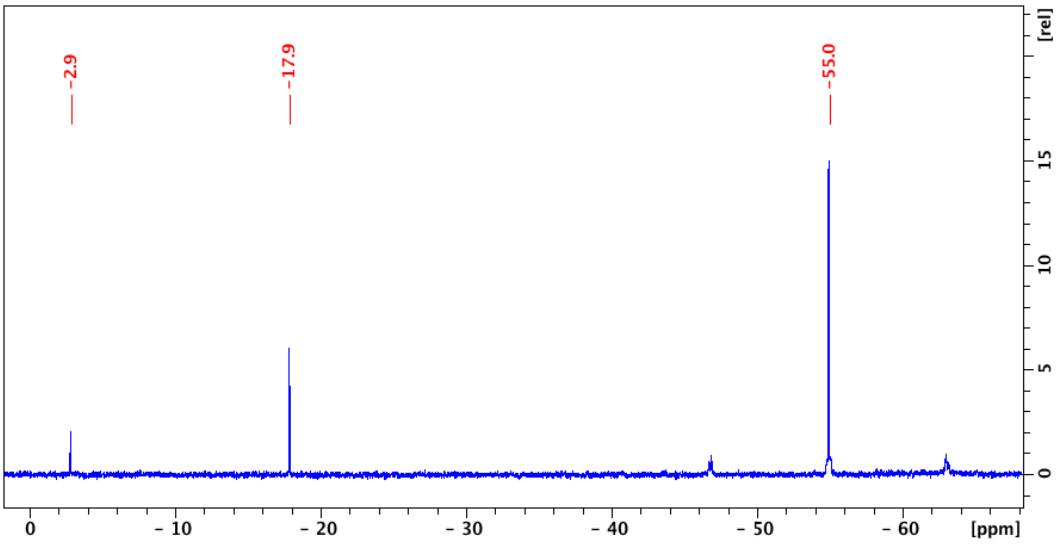

Figure 2.16: The $^{31}P\{^1H\}$ NMR of the orange solid product of $Pt_2(\mu_2\text{-}S)_2(PTA)_4$. PTA=O s, -2.9 and PTA=S s, -17.9 ppm. $Pt_2(\mu_2\text{-}S)_2(PTA)_4$ s, -55.0 ppm, $^1J_{Pt\text{-}P}$ 2617 Hz. Recorded at 162 MHz on a 400 MHz NMR spectrometer in D_2O.

The $^{31}P\{^1H\}$ NMR of the now orange solid supports the claim that the various species recorded do not reside outside of the ESI mass spectrometer as they were not shown to be present in the NMR spectra, it also provides evidence that less decomposition has occurred in the orange solid, than the mass spectra (Figure 2.13- Figure 2.15) and colour change has suggested. The $^{31}P\{^1H\}$ NMR spectrum showed one phosphorus resonance at -54.9 ppm with $^1J_{Pt\text{-}P}$ coupling of 2640 Hz suspected to be $Pt_2(\mu_2\text{-}S)_2(PTA)_4$, along with two more phosphorus resonances at -2.9 and -17.9 ppm, which were attributed to PTA=O and PTA=S (Figure 2.16). Both the oxide and sulfide chemical shifts are in good agreement with reported values,[61,68] along with the authentic samples of PTA=O and PTA=S that were

synthesised and NMR spectra recorded here. Small amounts of PTA oxide were present in the starting material, PTA sulfide however was produced in the reaction with $Na_2S{\cdot}9H_2O$ or was a result of the partial decomposition Figure 2.16.

The complex $Pt_2(\mu_2\text{-}S)_2(PTA)_4$ has a $^1J_{Pt\text{-}P}$ coupling constant of approximately 2600 Hz, in comparison to the starting material for this complex, *cis*-$PtCl_2(PTA)_2$ having an approximate $^1J_{Pt\text{-}P}$ coupling of 3300 Hz. Upon the formation of the $\{Pt_2(\mu_2\text{-}S)_2\}$ core, the coupling between the platinum and phosphorus atoms has decreased. This indicates that the sulfide bridging groups have a greater *trans*-influence in $Pt_2(\mu_2\text{-}S)_2(PTA)_4$ when compared to the chloride groups of *cis*-$PtCl_2(PTA)_2$.

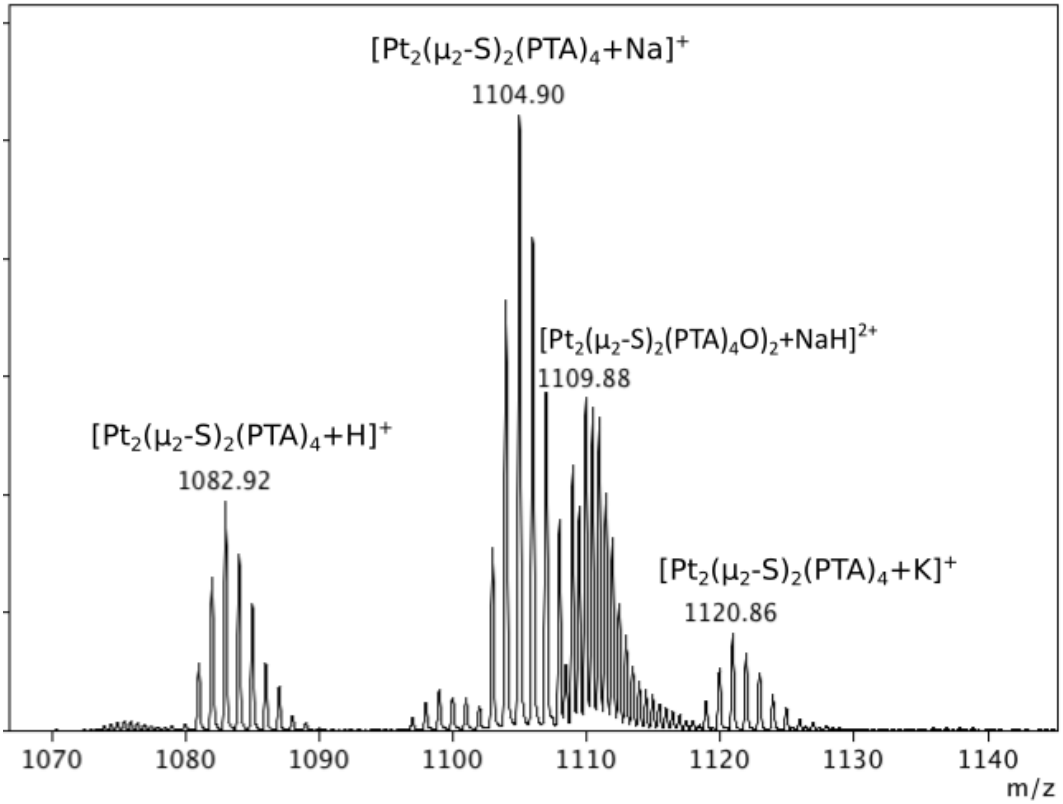

Figure 2.17. Positive-ion ESI mass spectrum of $Pt_2(\mu_2\text{-}S)_2(PTA)_4$ after two weeks at ambient temperature. Sodium and potassium adducts, accompanied by the protonated ion, are recorded. CEV 150 V, water/MeOH (2:5) solution.

The partial decomposition of the complex means it was not stable under certain conditions. A second sample of $Pt_2(\mu_2\text{-}S)_2(PTA)_4$ was prepared to undergo a low temperature thermal decomposition assessment over two weeks. This sample was filtered out of the benzene suspension and washed with benzene, no further attempts were made to purify the sample and remove the sodium salts. The solid

sample was placed in a sealed airtight vessel and stored at 4°C for the duration of the assessment. Samples were removed periodically, dissolved in a water/MeOH solution and the positive-ion ESI mass spectra were recorded. No decomposition was visibly observed and there was little alteration in the mass spectra obtained. This indicates that the sample is stable when stored at low temperature.

An ambient temperature thermal decomposition assessment was undertaken next, whereupon the same sealed sample was kept at ambient temperature for two weeks. During this time a slight colour change was observed and by the end of the two weeks the sample had become increasingly yellow (compared to the initial slight green colouration). The sample was left for further observations at ambient temperature and after 18 days the sample of $Pt_2(\mu_2\text{-}S)_2(PTA)_4$ was completely yellow. Over the same time period the odour of H_2S gradually decreased, that resulted from the impurities that remained in the sample.

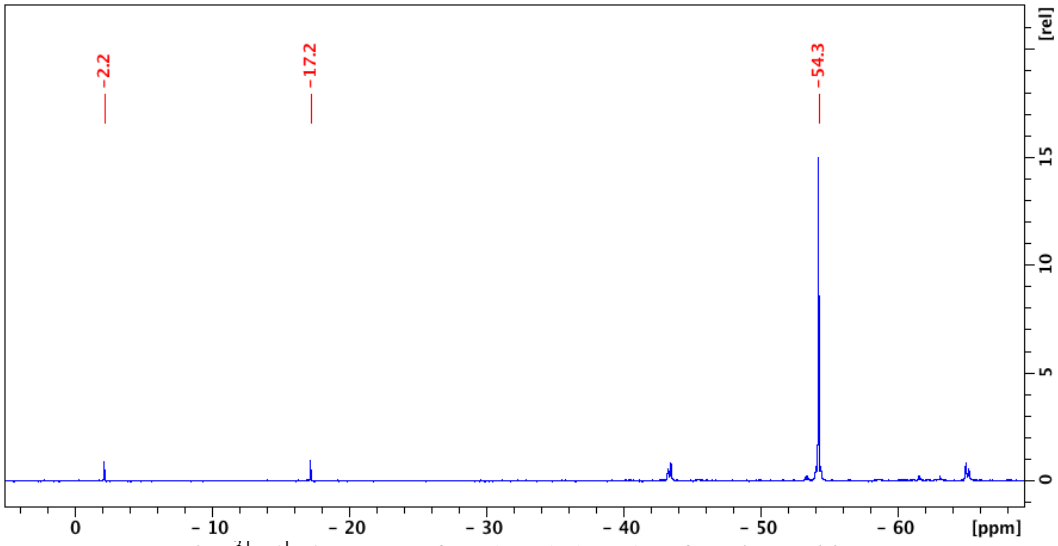

Figure 2.18: The $^{31}P\{^1H\}$ NMR of $Pt_2(\mu_2\text{-}S)_2(PTA)_4$ after the ambient temperature thermal decomposition assessment. The chemical shifts present are $Pt_2(\mu_2\text{-}S)_2(PTA)_4$ at -54.3 ppm $^1J_{Pt\text{-}P}$ 2616 Hz, $^3J_{Pt\text{-}P}$ 45.5 Hz PTA=O at -2.2 ppm and PTA=S at 17.2 ppm. Recorded at 121.5 MHz on a 300 MHz NMR spectrometer in D_2O.

In the beginning of the ambient temperature thermal decomposition assessment the only ion of $Pt_2(\mu_2\text{-}S)_2(PTA)_4$ visible was that of the sodium adduct $[Pt_2(\mu_2\text{-}S)_2(PTA)_4+Na]^+$ and the positive-ion ESI spectra remained this way until nine days had passed. The spectrum that was collected after fourteen days of ambient temperature storage had noticeable changes (Figure 2.17), with the presence of several more adduct and oxide ions now recorded. All of these 'new' ions were

previously visible in Figure 2.15, the positive-ion ESI spectrum of the orange partial decomposition solution, that resulted from the failed purification attempt during the first synthesis of $Pt_2(\mu_2\text{-}S)_2(PTA)_4$. The notable difference between the two spectra was that for the now yellowed sample only the adduct ions are present and one oxide; no other non-platinum ions were present. By comparison, as for the partial decomposition solution there were significant numbers of non-platinum and platinum complexes resulting from oxidation that were recorded. The ions observed in Figure 2.17 are the protonated form of the $Pt_2(\mu_2\text{-}S)_2(PTA)_4$ complex, along with the sodium and potassium adducts, accompanied by the oxidised species $[(Pt_2(\mu_2\text{-}S)_2(PTA)_4O)_2+NaH]^{2+}$ which is overlapping with $[Pt_2(\mu_2\text{-}S)_2(PTA)_4+Na]^{+}$.

The $^{31}P\{^1H\}$ NMR of the now yellow $Pt_2(\mu_2\text{-}S)_2(PTA)_4$ after the ambient temperature thermal decomposition assessment confirmed that there was only one platinum complex present with Pt-P bonding, with a resonance at -54.2 ppm and a $^1J_{Pt\text{-}P}$ coupling of 2616 Hz, $^3J_{Pt\text{-}P}$ 45.5 Hz (Figure 2.18). This spectrum was the first observation of $^3J_{Pt\text{-}P}$ coupling, this arises from the phosphorus atoms coupling with the platinum atom three bonds away on the other side of the $\{Pt_2(\mu_2\text{-}S)_2\}$ core. This is in a similar order of magnitude as other observed $^3J_{Pt\text{-}P}$ coupling constants for $[Pt_2(\mu_2\text{-}I)_2(dppm)_2](BF_4)_2$ $^3J_{Pt\text{-}P}$ 30 Hz, $[Pt_2(\mu_2\text{-}OH)_2(PMe_3)_4](NO_3)_2$ $^3J_{Pt\text{-}P}$ 10 Hz.[36,69] The other phosphorus resonances observed were attributed to small amounts of PTA=O at -2.1 ppm and PTA=S at -17.2 ppm. From all the spectra recorded it can be confidently stated that the slow progression of $Pt_2(\mu_2\text{-}S)_2(PTA)_4$ to a yellow solid was not a result of the decomposition of the platinum complex. Along with this the oxidised species ion recorded in the positive-ion ESI mass spectrum (Figure 2.17) was a result of the ESI mass spectrum, as the $^{31}P\{^1H\}$ NMR confirms only one platinum complex was present. The alternative to this is the oxidised species were formed in the sample and has a high ionisation efficiency, which leads it to be over-represented in the ESI-MS spectrum. The $^{31}P\{^1H\}$ NMR is a more accurate representation of what species are present and the only platinum phosphine complex observed is $Pt_2(\mu_2\text{-}S)_2(PTA)_4$. Later larger scale synthesis of $Pt_2(\mu_2\text{-}S)_2(PTA)_4$ yielded the same yellow solid after a short time.

During further experimentation an alternative route of synthesis was found, through a ligand exchange reaction between $Pt_2(\mu_2\text{-}S)_2(cod)_2$ and PTA. The cod platinum complex discovery and synthesis is discussed in a later chapter where it is more relevant (Chapter 4.3 - 4.3.1).

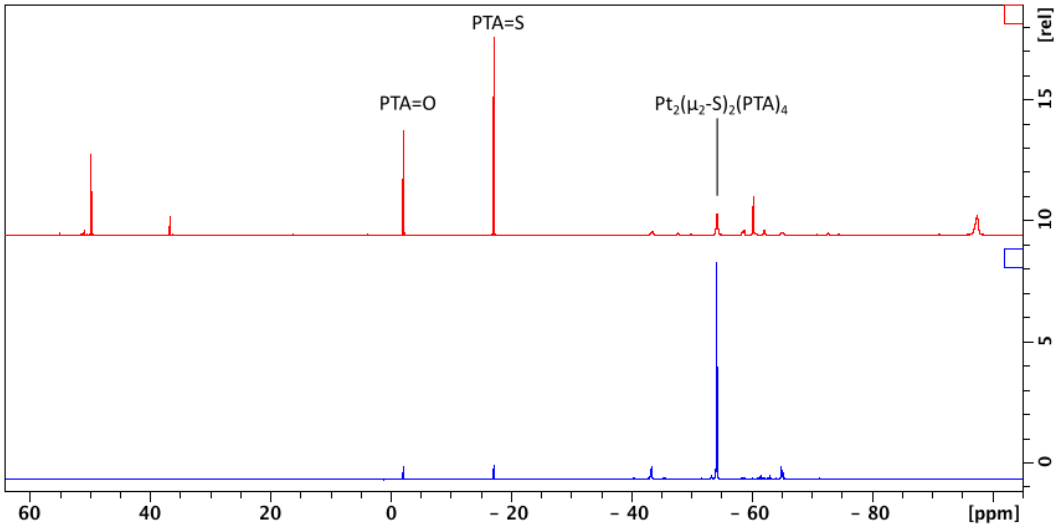

Figure 2.19: The $^{31}P\{^1H\}$ NMR spectra of $Pt_2(\mu_2\text{-}S)_2(PTA)_4$ from the ligand exchange reaction with $Pt_2(\mu_2\text{-}S)_2(cod)_2$ (top) compared with the spectrum from *cis*-$PtCl_2(PTA)_2$ reactions with $Na_2S{\cdot}9H_2O$ (bottom). Recorded at 121.5 MHz on a 300 MHz NMR spectrometer in D_2O.

The $^{31}P\{^1H\}$ NMR of the product from this alternative synthetic method revealed that, although $[Pt_2(\mu_2\text{-}S)_2(PTA)_4+H]^+$ and $[Pt_2(\mu_2\text{-}S)_2(PTA)_4+Na]^+$ were the only ions observed in the positive-ion ESI mass spectrum, the $Pt_2(\mu_2\text{-}S)_2(PTA)_4$ complex was not produced as a pure solid. There were many phosphorus resonances present in the $^{31}P\{^1H\}$ NMR spectrum, but only one of them (-54.3 ppm) was assigned to $Pt_2(\mu_2\text{-}S)_2(PTA)_4$, and the $^1J_{Pt\text{-}P}$ coupling was not distinguishable from the baseline. It was only determined that this resonance was the complex $Pt_2(\mu_2\text{-}S)_2(PTA)_4$ through comparison with a previous spectrum recorded Figure 2.19. The spectrum on top comes from the $Pt_2(\mu_2\text{-}S)_2(cod)_2$ ligand exchange, with its highest intensity resonances resulting from PTA=O and PTA=S (-2.3 and -17.2 ppm, respectively). The bottom spectrum is Figure 2.18, used here for comparison. This demonstrates the high ionisation efficiency of $Pt_2(\mu_2\text{-}S)_2(PTA)_4$ complex as if the positive-ion ESI mass spectrum was the only evidence collected this would have suggested that the reaction proceeded to form

$Pt_2(\mu_2\text{-}S)_2(PTA)_4$ with very little by-products, the $^{31}P\{^1H\}$ NMR reveals this was not what occurred.

Attempts at growing crystals for the purpose of gaining the X-ray crystal structure of $Pt_2(\mu_2\text{-}S)_2(PTA)_4$ were attempted, but no crystals suitable for X-ray crystallography could be obtained.

The sample of $Pt_2(\mu_2\text{-}S)_2(PTA)_4$ synthesised from the reaction with $Na_2S{\cdot}9H_2O$, that was prepared for $^{31}P\{^1H\}$ NMR in D_2O, providing the spectra in Figure 2.18 was allowed to stand at ambient temperature to determine if the complex was stable while in solution. The $^{31}P\{^1H\}$ NMR 17 days after dissolution occurred revealed resonances for $Pt_2(\mu_2\text{-}S)_2(PTA)_4$ at -54.3 ppm accompanied by two other resonances at -58.6, -62.2 ppm, which have not been observed previously. The resonances of greatest intensity are PTA=O at -2.2 ppm and PTA=S at -17.2 ppm, as shown in Figure 2.20 (top spectrum). The resonance at -54.3 ppm was only attributed to $Pt_2(\mu_2\text{-}S)_2(PTA)_4$ through the comparison with the previously obtained spectra, as the $^1J_{Pt\text{-}P}$ satellites are not present.

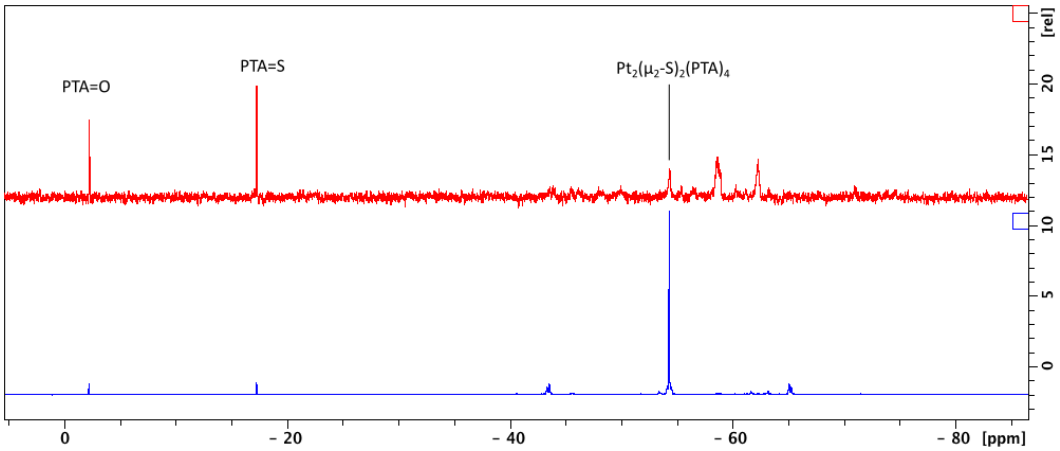

Figure 2.20: $^{31}P\{^1H\}$ NMR comparison spectra of $Pt_2(\mu_2\text{-}S)_2(PTA)_4$ upon dissolution (bottom) and 17 days after (top). Identified resonances PTA=O s, -2.2 ppm. PTA=S s, -17.2 ppm. $Pt_2(\mu_2\text{-}S)_2(PTA)_4$ s, -54.3 ppm, $^1J_{Pt\text{-}P}$ 2616 Hz, $^2J_{Pt\text{-}P}$ 45 Hz. Recorded at 121.5 MHz on a 300 MHz NMR spectrometer in D_2O.

The $^{31}P\{^1H\}$ NMR spectrum comparison in Figure 2.20, is not completely adequate: the bottom spectrum was recorded over a span of 17 hours (overnight), whereas the top spectrum was recorded over 1 hour. At this stage of research the 400 MHz NMR was unable to record $^{31}P\{^1H\}$ NMR spectra, and the 300 MHz NMR was periodically malfunctioning; spectra could only be recorded over a

short time frame. The top spectrum of Figure 2.20 does suggest that $Pt_2(\mu_2\text{-}S)_2(PTA)_4$ was unstable while in a D_2O solution, with strong PTA=O and PTA=S resonances accompany by the unidentified resonances at -58.6 and -62.2 ppm, but a longer acquisition time spectrum would have needed to be acquired to determine if the resonances at -58.6 and -62.2 ppm were platinum complexes through possible $^1J_{Pt\text{-}P}$ couplings. The $^{31}P\{^1H\}$ NMR spectra collected (Figure 2.20) along side the findings of the attempted purification step does suggest that $Pt_2(\mu_2\text{-}S)_2(PTA)_4$ lacks solvent stability.

2.4 Synthesis of $[Pt_2(\mu_3\text{-}S)_2(PTA)_4Rh(cod)]Cl$

As the complex $Pt_2(\mu_2\text{-}S)_2(PTA)_4$ is an analogue of $Pt_2(\mu_2\text{-}S)_2(PPh_3)_4$, a brief ESI mass spectrometric investigation was performed to determine if the $\{Pt_2(\mu_2\text{-}S)_2\}$ core of the PTA complex shares the same reactivity, acting as a metalloligand towards heterometal centres through the electron-rich sulfur bridges. Examples of various metalloligand behaviour are the complexes; $[Pt_2(\mu_3\text{-}S)_2(PPh_3)_4Rh(cod)]X$ ($X = Cl^-$, PF_6^-, BPh_4^-), and $[Pt_2(\mu_3\text{-}S)_2(PPh_3)4(M)]$ ($M = Tl^+$, $Pb(NO_3)^+$, $GaCl_2^+$, $InCl_3$, $HgCl_2$) have all been documented,[9,10,34,70] with the X-ray crystal structure of $[Pt_2(\mu_3\text{-}S)_2(PPh_3)_4Rh(cod)]PF_6$ being reported.[70]

A small scale reaction of $Pt_2(\mu_2\text{-}S)_2(PTA)_4$ with $[RhCl(cod)]_2$ was investigated to observe if the cation $[Pt_2(\mu_3\text{-}S)_2(PTA)_4Rh(cod)]^+$ would readily form and thus be visible in the positive-ion ESI mass spectrum. This was carried out in a eppendorf tube with small quantities of $Pt_2(\mu_2\text{-}S)_2(PTA)_4$ with $[RhCl(cod)]_2$ in a MeOH solution that was mixed continuously for five minutes. The cation $[Pt_2(\mu_3\text{-}S)_2(PTA)_4Rh(cod)]^+$ was observed, the intensity of which was orders of magnitude larger than all other ions present in the spectrum. All other ions were negligible in comparison, indicating the cation $[Pt_2(\mu_3\text{-}S)_2(PTA)_4Rh(cod)]^+$ is observed readily in the mass spectrometer. Before the reaction solution was analysed, samples of both $Pt_2(\mu_2\text{-}S)_2(PPh_3)_4$ and then $[RhCl(cod)]_2$ were analysed to check for any impurities present, so that they could be accounted for if they were also recorded in the mass spectrum of the reaction solution.

Using the synthetic method of $[Pt_2(\mu_3\text{-}S)_2(PPh_3)_4Rh(cod)]Cl$,[70] with minor alterations, a larger scale synthesis of $[Pt_2(\mu_3\text{-}S)_2(PTA)_4Rh(cod)]Cl$ was undertaken. The reaction did not proceed as described in the literature,[70] as a precipitate formed in solution. The desired product was isolated by first filtration

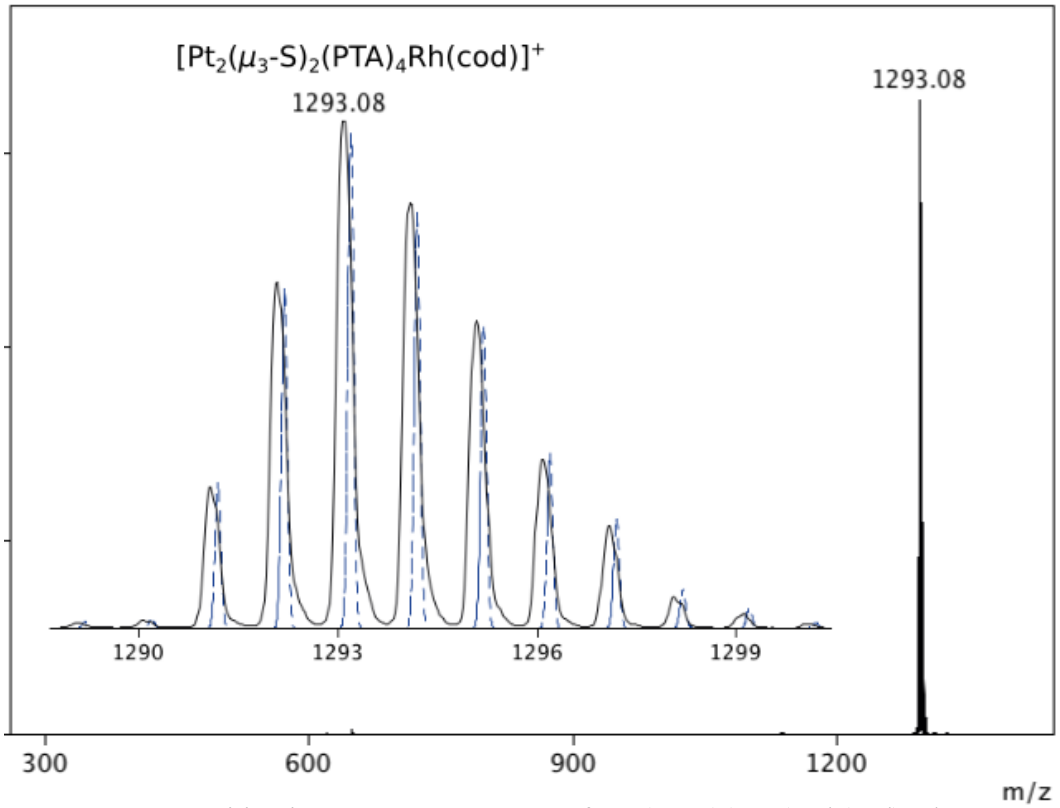

Figure 2.21: Positive-ion ESI mass spectrum of $[Pt_2(\mu_3\text{-}S_2)(PTA)_4Rh(cod)]Cl$. Inset spectrum shows observed (solid line) and calculated (dashed line) isotope patterns. CEV 150V, MeOH solution.

of the precipitate, which was placed in a desiccator to dry, then evaporation of the reaction solution, which gave a dark maroon coloured solid. The positive-ion ESI mass spectrum of this solid is shown in Figure 2.21. The precipitate that was filtered out of the solution after drying was dark grey, almost black. The positive-ion ESI mass spectrum of this solid in methanol showed the presence of $[Pt_2(\mu_3\text{-}S)_2(PTA)_4Rh(cod)]^+$ but of a far lesser intensity then the solid obtained by evaporation of the solvent. The black solid did not appear to be very soluble in methanol but readily dissolved in water. The positive-ion ESI mass spectrum obtained in a water/methanol (2:5) solution revealed a number of cations that all lack platinum isotope patterns, which were not observed when methanol on its own was used as a solvent. The ion $[Pt_2(\mu_3\text{-}S)_2(PTA)_4Rh(cod)]^+$ was again observed just as in the methanol sample at a significantly low intensity. This

provides evidence that trace amounts are trapped within the solid precipitate but it was not the desired product of this reaction, no starting material was present in this spectrum either, possibly some form of decomposition product.

The $^{31}P\{^{1}H\}$ NMR of the maroon solid isolated from evaporation (Figure 2.22) demonstrates clearly that it is the complex $[Pt_2(\mu_3\text{-}S)_2(PTA)_4Rh(cod)]Cl$, as there are only three phosphorus resonances in the spectrum. PTA oxide and sulfide are observed (PTA=O s,-2.2 ppm. PTA=S s, -17.2 ppm) in small quantities, that originated from the sample of $Pt_2(\mu_2\text{-}S)_2(PTA)_4$. The $[Pt_2(\mu_3\text{-}S)_2(PTA)_4Rh(cod)]Cl$ is the final phosphorus resonance at -56.8 ppm with satellites of $^{1}J_{Pt\text{-}P}$ 2965 Hz. Both the phosphorus resonance and the coupling constant of $Pt_2(\mu_3\text{-}S)_2(PTA)_4Rh(cod)]Cl$ differ slightly in comparison to the starting complex of $Pt_2(\mu_2\text{-}S)_2(PTA)_4$ at s, -54.3 ppm, $^{1}J_{Pt\text{-}P}$ 2616 Hz, the $^{3}J_{Pt\text{-}P}$ coupling was not observed. The large $^{1}J_{Pt\text{-}P}$ coupling of 2616 Hz is consistent with the *trans*-influence of sulfide. The PPh_3 analogue $[Pt_2(\mu_3\text{-}S)_2(PPh_3)_4Rh(cod)]Cl$ has a slightly larger coupling constant at $^{1}J_{Pt\text{-}P}$ 3151 Hz, with $^{3}J_{Pt\text{-}P}$ 19.5 Hz.[70] The $^{3}J_{Pt\text{-}P}$ coupling was not observed for $[Pt_2(\mu_3\text{-}S)_2(PTA)_4Rh(cod)]Cl$.

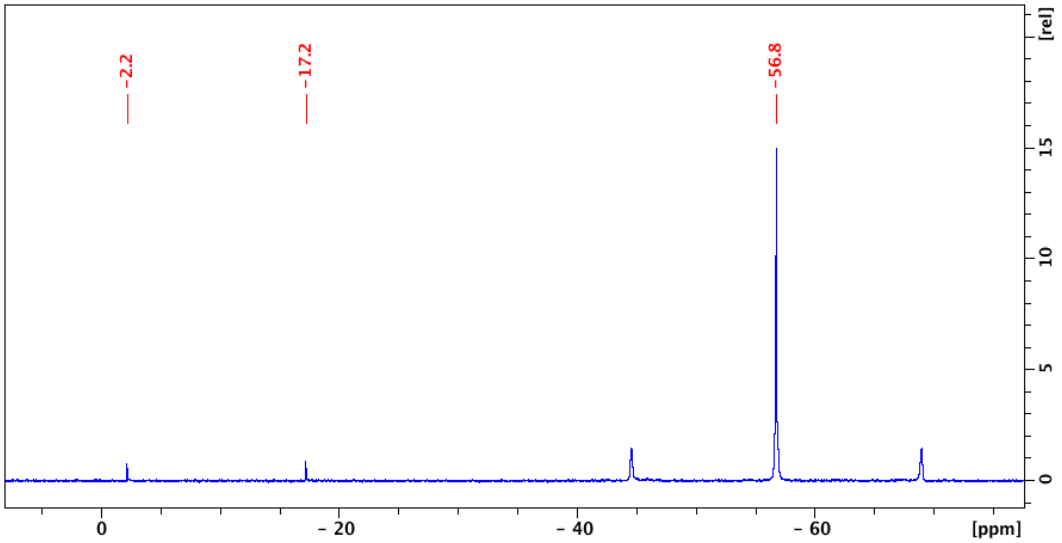

Figure 2.22: $^{31}P\{^{1}H\}$ NMR of $[Pt_2(\mu_3\text{-}S)_2(PTA)_4Rh(cod)]Cl$ in D_2O. PTA=O s, -2.2 ppm. PTA=S s -17.2 ppm. $[Pt_2(\mu_3\text{-}S)_2(PTA)_4Rh(cod)]Cl$ s, -56.8 ppm, $^{1}J_{Pt\text{-}P}$ 2965 Hz. Recorded at 121.5 MHz on a 300 MHz NMR spectrometer.

The synthesis for $[Pt_2(\mu_3\text{-}S)_2(PTA)_4Rh(cod)]Cl$ confirms the ability of $Pt_2(\mu_2\text{-}S)_2(PTA)_4$ to act as a metalloligand towards suitable metal ligand pairs e.g. Rh(cod). Attempts at growing crystals of $[Pt_2(\mu_3\text{-}S)_2(PTA)_4Rh(cod)]X$ (X = Cl^-,

BF_4^-, BPh_4^-) for the purpose of gaining the X-ray crystal structure were made, but no crystals suitable for X-ray crystallography were obtained. Solutions of $Pt_2(\mu_3\text{-}S)_2(PTA)_4Rh(cod)]Cl$ in methanol were prepared and excess of $NaBF_4$, $NaBPh_4$ were added to each followed by the addition of water. This was planned to force precipitation of the $[Pt_2(\mu_3\text{-}S)_2(PTA)_4Rh(cod)]X$ (X = BF_4^-, BPh_4^-) salts. No precipitation occurred, samples of the solution were left to undergo slow evaporation in attempts to grow crystals, none suitable for X-ray crystallography were obtained.

2.5 Investigation of Alternative Sulfide Sources in the Synthesis of $Pt_2(\mu_2\text{-}S)_2(PTA)_4$

The method that has been used with the monoplatinum starting materials to synthesise the $\{Pt_2(\mu_2\text{-}S)_2\}$ core has involved the use of sodium sulfide nonahydrate to provide the sulfide ion in the reaction. This is an effective reactant and is suited for the task of producing non water-soluble complexes such as $Pt_2(\mu_2\text{-}S)_2(PPh_3)_4$ as during the filtration step, the product can be washed with water to remove the sodium salt by-products and the excess sodium sulfide that may be dispersed or clumped in amongst the $Pt_2(\mu_2\text{-}S)_2(PPh_3)_4$.

Upon the successful synthesis of $Pt_2(\mu_2\text{-}S)_2(PTA)_4$ the inadequacies of sodium sulfide for this reaction became apparent. The product of the reaction and the whole aim of this project was to make water-soluble complexes that contain the $\{Pt_2(\mu_2\text{-}S)_2\}$ core. The removal of sodium salt by-products and excess sodium sulfide became significantly more difficult, as washing with water was no longer possible as the by-products and product have similar solubilities.

2.6 Attempted Synthesis of $Pt_2(\mu_2\text{-}S)_2(PTA)_4$ with a Sulfide Ion Exchange Column

The synthesis of $Pt_2(\mu_2\text{-}S)_2(PTA)_4$ was attempted using a source of sulfide ions that was free from Na^+ ions to simplify the isolation of the product in the pure state. A sulfide ion exchange column was constructed from Dowex 1X8 beads and $Na_2S{\cdot}9H_2O$. Sulfide exchange columns of this sort have been established

previously.[71] This column allowed for the reaction between *cis*-$PtCl_2(PTA)_2$ and the sulfide without the presence of near-inseparable sodium salts being produced.

After the construction of the column a solution of *cis*-$PtCl_2(PTA)_2$ in methanol was flushed through. The resulting eluent was evaporated until dry using a rotary evaporator, giving a solid, which appeared white when finally divided, but which appeared yellow when collected together.

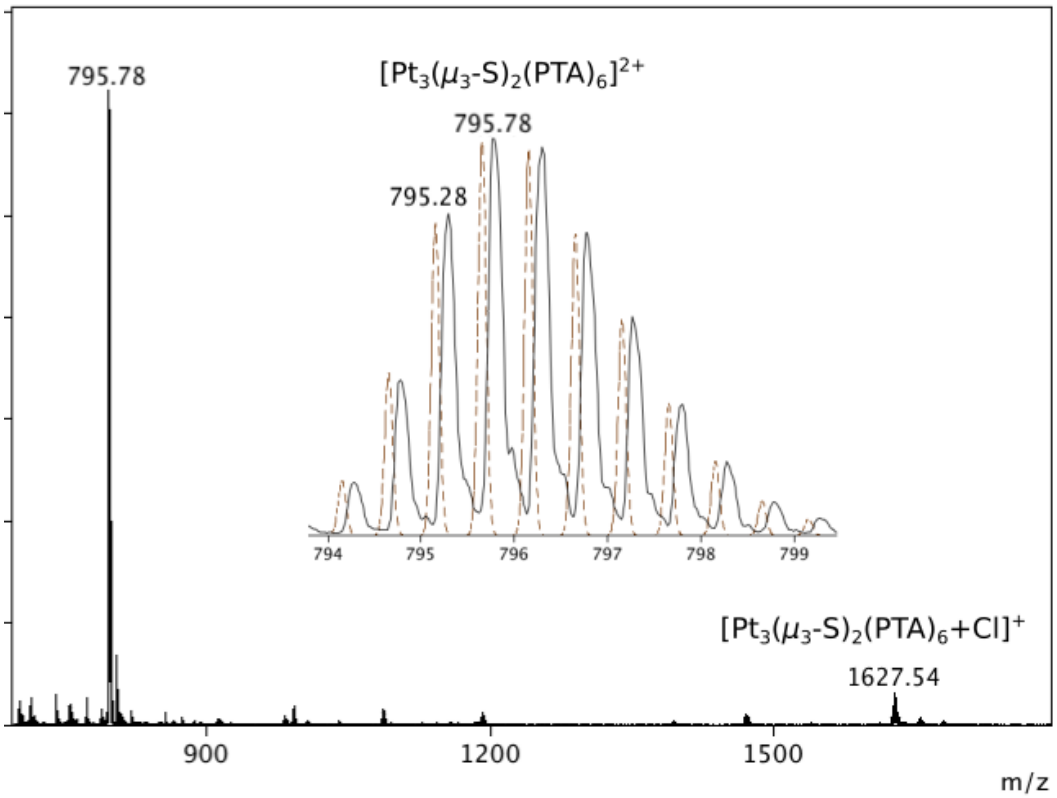

Figure 2.23: Positive-ion ESI mass spectrum showing the triplatinum complexes $[Pt_3(\mu_3\text{-}S)_2(PTA)_6]^{2+}$ and $[Pt_3(\mu_3\text{-}S)_2(PTA)_6\text{+}Cl]^+$. The inset spectrum shows both the observed (solid line) and calculated (dashed line) isotope pattern for $[Pt_3(\mu_3\text{-}S)_2(PTA)_6]^{2+}$. The peak separation of 0.5 *m/z* confirms the ion has a 2+ charge. CEV 150 V, water/MeOH (2:5) solution.

The positive-ion ESI mass spectrum of the product revealed a singular multi-platinum complex ion of a strong intensity, corresponding to the ion $[Pt_3(\mu_3\text{-}S)_2(PTA)_6]^{2+}$. The ion $[Pt_3(\mu_3\text{-}S)_2(PTA)_5\text{+}Cl]^+$ was also visible (Figure 2.23). When the capillary exit voltage was increased to 210 V, a considerable number of fragment ions appeared or increased in intensity, two of which were identified as $[Pt_3(\mu_3\text{-}S)_2(PTA)_5\text{+}Cl]^+$ (1470.44 *m/z*) and $[Pt_3(\mu_3\text{-}S)_2(PTA)_6\text{+}Cl]^+$ (1627.54 *m/z*). The product $Pt_2(\mu_2\text{-}S)_2(PTA)_4$ was not present in the spectrum at these voltages. The counter anion for these species was unknown, however the possibilities were

Cl^- or S^{2-}. Chloride is the most likely of the two as S^{2-} is likely to react to form $Pt_2(\mu_2\text{-}S)_2(PTA)_4$.

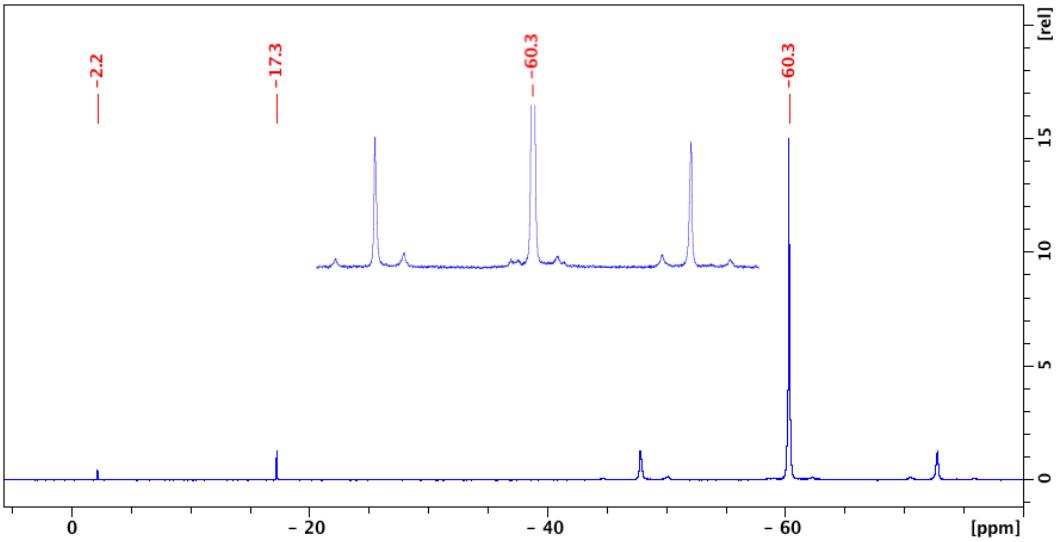

Figure 2.24: $^{31}P\{^1H\}$ NMR of $[Pt_3(\mu_3\text{-}S)_2(PTA)_6]^{2+}$ in D_2O. PTA=O s -2.2 ppm. PTA=S s, -17.3 ppm, $[Pt_3(\mu_3\text{-}S)_2(PTA)_6]^{2+}$ s, -60.3 ppm $^1J_{Pt\text{-}P}$ 3041 Hz. The inset spectrum is the magnified -60.3 ppm resonance showing the smaller satellites. Spectrum recorded at 121.5 MHz on a 300 MHz NMR spectrometer.

The $\{Pt_2(\mu_2\text{-}S)_2\}$ core is a known metalloligand and has been documented coordinating to a third metal centre through the μ_2-sulfur bridges.[24] The triplatinum $\{Pt_3(\mu_3\text{-}S)_2\}^{2+}$ core is established, and can be readily formed with dppm, and PMe_2Ph ligands.[37,46,72] The analogous triplatinum PTA complex observed here has not been documented in the literature previously.

The $^{31}P\{^1H\}$ NMR of the $[Pt_3(\mu_3\text{-}S)_2(PTA)_6]^{2+}$ species as seen in Figure 2.24 shows a strong single phosphorus resonance at -60.3 ppm with platinum satellites clearly visible, small amounts of PTA oxide and sulfide are present in the spectrum as their resonances were also observed. From this spectrum it can be safely stated that the synthesis of $[Pt_3(\mu_3\text{-}S)_2(PTA)_6]^{2+}$ yielded the complex in a relatively pure state, as no other platinum phosphine complexes are visible in the spectrum.

Due to the symmetry of the $\{Pt_3(\mu_3\text{-}S)_2\}^{2+}$ core and the abundance of both ^{31}P and ^{195} Pt nuclei, this results in four differing isotopomers of the $\{Pt_3(\mu_3\text{-}S)_2\}^{2+}$ core each giving slightly different NMR resonances, as the $\{Pt_3(\mu_3\text{-}S)_2\}^{2+}$ core will occur with one, two, or all three of the platinum atoms being NMR active. This

complexity gives rise to several smaller satellites from the differing $^{1}J_{Pt\text{-}P}$ and $^{3}J_{Pt\text{-}P}$ couplings occurring, these can be seen as the small resonances either side of the larger $^{1}J_{Pt\text{-}P}$ satellites in Figure 2.24. The smaller resonances present in the spectrum do agree with prior NMR investigations into the $\{Pt_3(\mu_3\text{-}S)_2\}^{2+}$ core completed for the analogous complex $[Pt_3(\mu_3\text{-}S)_2(PMe_2Ph)_6]^{2+}$.[72] The $\{Pt_3(\mu_3\text{-}S)_2\}^{2+}$ core has very similar $^{1}J_{Pt\text{-}P}$ values in both complexes (PTA) $^{1}J_{Pt\text{-}P}$ 3041 Hz, and (PMe_2Ph) $^{1}J_{Pt\text{-}P}$ 3202 Hz.[72]

Attempts at growing crystals through vapour diffusion of $[Pt_3(\mu_3\text{-}S)_2(PTA)_6]^{2+}$ for the purpose of gaining the X-ray crystal structure were made, but no crystals suitable for X-ray crystallography were obtained.

2.7 Attempted Synthesis of $Pt_2(\mu_2\text{-}S)_2(PTA)_4$ Direct from $Pt_2(\mu_2\text{-}S)_2(PPh_3)_4$

These series of experiments detail the attempted synthesis of the platinum complex $Pt_2(\mu_2\text{-}S)_2(PTA)_4$ from the triphenylphosphine analogue $Pt_2(\mu_2\text{-}S)_2(PPh_3)_4$ by a simple ligand exchange reaction between the triphenylphosphine of the platinum complex and unbound PTA. This would allow the removal of sodium salts from the synthesis of $Pt_2(\mu_2\text{-}S)_2(PTA)_4$. Phosphine exchange on involving $Pt_2(\mu_2\text{-}S)_2(L)_4$ (L = phosphine) has been demonstrated previously, albeit with close analogues of PPh_3,[73] and not yet PTA.

This was attempted using two different variants of the same reaction. The first was a biphasic ligand exchange reaction; the reaction mixture was comprised of two immiscible solvents that the reactants have differing solubilities in. Water and toluene were chosen for this. The unbound PTA readily dissolved in the water and remained there, while the liberated PPh_3 dissolved in toluene and again remained there. The desired outcome of this reaction was that the $Pt_2(\mu_2\text{-}S)_2(PPh_3)_4$ underwent stepwise exchange by PTA, the complex becoming increasingly more water-soluble and moving into the water layer of the reaction mixture as the liberated PPh_3 dissolved in the toluene. It was expected that during the reaction some form of $Pt_2(\mu_2\text{-}S)_2(PPh_3)_m(PTA)_n$ (n = 1-4, m = 4-n) would be found in the

water layer. These reactions were performed with four different ratios of $Pt_2(\mu_2\text{-}S)_2(PPh_3)_4$:PTA (1:1, 1:2, 1:3, 1:4).

The solutions for the biphasic ligand exchange reaction were stored at ambient temperature, stirred rapidly for seven days and analysed with ESI mass spectrometry. The notable results that were gained from these reaction attempts were that ligand exchange does occur between bound PPh_3 and the unbound PTA in solution, however the $\{Pt_2(\mu_2\text{-}S)_2\}$ cores during the ligand exchange do not stay intact. The mass spectrum of the water phase (after the phases left to settle) showed platinum complex ions with isotope patterns for complexes that have triplatinum sulfur $\{Pt_3(\mu_3\text{-}S)_2\}^{2+}$ cores in various stages of substitution between PPh_3 and PTA (Table 2.2). Small amounts of the starting material $Pt_2(\mu_2\text{-}S)_2(PPh_3)_4$ were also still present, the intensity of completely substituted $\{Pt_3(\mu_3\text{-}S)_2\}^{2+}$ complexes increased with the ratio of PTA, the reaction with the 1:4 ratio was the most successfully substituted and is what is shown in Figure 2.25. The platinum complex ion possessing the greatest intensity in the positive-ion ESI mass spectrum was that of the completely substituted $[Pt_3(\mu_3\text{-}S)_2(PTA)_6]^{2+}$ complex, which is the same complex that was synthesised with the use of a sulfide ion exchange column (Section 2.6). The exchange column results in a significantly purer product as it is the only ion present in the mass spectra at relevant intensity (Figure 2.23) and the only platinum phosphine complex present in the $^{31}P\{^1H\}$ NMR (Figure 2.24) (Section 2.6), as opposed to the various trinuclear ions present in the water phase that were observed for this reaction.

Table 2.2: The various $[Pt_3(\mu_3\text{-}S)_2(L)_6]^{2+}$ species present in differing stages of ligand substitution between PTA and PPh_3.

Ion (*m/z*)	Calculated (*m/z*)	Formula
796.21	795.65	$[Pt_3(\mu_3\text{-}S)_2(PTA)_6]^{2+}$
813.70	814.56	$[Pt_3(\mu_3\text{-}S)_2(PTA)_6\text{+}ClH]^{2+}$
848.71	848.16	$[Pt_3(\mu_3\text{-}S)_2(PTA)_5(PPh_3)_1]^{2+}$
901.23	900.66	$[Pt_3(\mu_3\text{-}S)_2(PTA)_4(PPh_3)_2]^{2+}$
953.74	953.17	$[Pt_3(\mu_3\text{-}S)(PTA)_3(PPh_3)_3]^{2+}$
1470.29	1470.19	$[Pt_3(\mu_3\text{-}S)_2(PTA)_5\text{+}Cl]^{+}$
1627.38	1627.27	$[Pt_3(\mu_3\text{-}S)_2(PTA)_6\text{+}Cl]^{+}$
1732.40	1732.28	$[Pt_3(\mu_3\text{-}S)_2(PTA)_5(PPh_3)\text{+}Cl]^{+}$

The positive-ion ESI mass spectrum of the water phase is shown in Figure 2.25 for the 1:4 reaction. The ion assignments are within the accompanying Table 2.2. The successfully identified substituted complexes and their adducts observed in the mass spectrum all possess a trinuclear $\{Pt_3(\mu_3\text{-}S)_2\}^{2+}$ core. No ligand-substituted complex ions were present with a dinuclear $\{Pt_2(\mu_2\text{-}S)_2\}$ core in either the positive- or negative-ion ESI mass spectra.

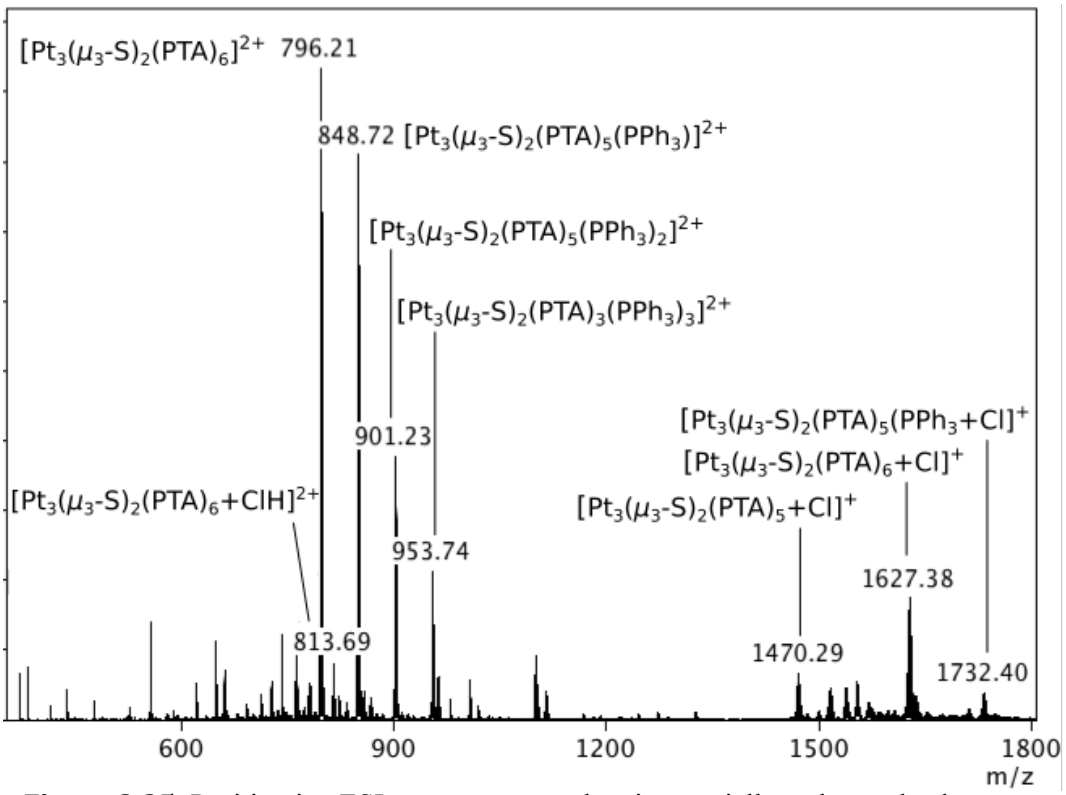

Figure 2.25: Positive-ion ESI mass spectrum showing partially and completely substituted trinuclear complexes of the general form $[Pt_3(\mu_3\text{-}S)_2(PTA)_n(PPh_3)_m]^{2+}$ (n = 1-6, m = 6-n). CEV 150 V, water/MeOH (2:5) solution.

The second variant of this reaction was performed using a monophasic reaction mixture, with methanol and toluene implemented as co-solvents. This again resulted in the complete and partially substituted triplatinum complexes identified in Table 2.2.

The experiment was repeated with only the starting complex $Pt_2(\mu_2\text{-}S)_2(PPh_3)_4$ and the co-solvents water and toluene, to investigate if the ligand PTA or the solvents and conditions were responsible for the fragmentation of the $\{Pt_2(\mu_2\text{-}S)_2\}$ core and formation of the $\{Pt_3(\mu_3\text{-}S)_2\}^{2+}$ core, and not the ligand exchange reaction. This experiment resulted in no $[Pt_3(\mu_3\text{-}S)_2(PPh_3)_6]^{2+}$ being present in the

mass spectrum or any other triplatinum complex, providing evidence that the formation of the triplatinum core $\{Pt_3(\mu_3\text{-}S)_2\}^{2+}$ was in fact the result of the interaction with the phosphine ligand PTA and not from the reaction conditions.

The complex $[Pt_3(\mu_3\text{-}S)_2(PTA)_6]^{2+}$ is a water-soluble platinum sulfide, the synthesis of which was the goal of this research, but as the third platinum is occupying the bonding site on the sulfur bridges, it severely limits the reactivity of the complex.

Multiple samples of the water phase from this experiment were removed and allowed to evaporate, with the intention of obtaining crystals of one of the triplatinum complexes. Only an orange micro-crystalline solid was obtained, which was not suitable for X-ray crystallography. The positive-ion ESI mass spectrum of this solid showed the complexes shown in Table 2.2 accompanied by the slight increase in intensity of the chloride adducts. Other ions were present with discernible platinum influences on their isotope patterns but remained unassignable.

2.8 Conclusion

Experimentation on the water-soluble phosphine PTA successfully resulted in the synthesis of three new and novel platinum complexes. The first complex synthesised and the one with the most potential for further research was $Pt_2(\mu_2\text{-}S)_2(PTA)_4$. With the synthesis of this platinum sulfide complex the primary objective of the research project was achieved, as the PTA ligand provides the $\{Pt_2(\mu_2\text{-}S)_2\}$ core with complete water-solubility. However, the complex was shown to lack long-term stability while in solution and a synthetic method to yield a pure product could not be derived. During the attempts to discover a synthetic method that excluded sodium salt by-products using a sulfide exchange column, a method was found to synthesise $[Pt_3(\mu_3\text{-}S)_2(PTA)_6]^{2+}$ as a pure product. $Pt_2(\mu_2\text{-}S)_2(PTA)_4$ was shown through its reaction with $[RhCl(cod)]_2$ to still possess the ability to act as a metalloligand toward heterometals, with the synthesis of $[Pt_2(\mu_3\text{-}S)_2(PTA)_4\,Rh(cod)]Cl$.

Further work into the synthesis of $Pt_2(\mu_2\text{-}S)_2(PTA)_4$ to yield a purifiable product was done and is expanded on in Chapter 3.

2.9 Experimental

The general experimental work and chemical suppliers, accompanied by the equipment parameters are detailed in Appendix 1.

2.9.1) Synthesis of cis-$PtCl_2(PTA)_2$

The literature method was used,[60] with $PtCl_2$(cod) (0.967 g, 2.5 mmol) and PTA (0.813 g, 5.1 mmol). The reaction was performed under a N_2 atmosphere. Yield 1.38 g (92%).

$^{31}P\{^1H\}$ NMR: s, -53.2 ppm, $^1J_{Pt\text{-}P}$ 3307 Hz. (DMSO-d_6) recorded at 162 MHz on a 400 MHz NMR spectrometer.

2.9.2) First Synthesis of $Pt_2(\mu_2\text{-}S)_2(PTA)_4$

First synthesis: The literature method for the synthesis of $Pt_2(\mu_2\text{-}S)_2(PPh_3)_4$,[2] with the alteration that *cis*-$PtCl_2(PTA)_2$ (0.0522 g, 0.09 mmol) in place of *cis*-$PtCl_2(PPh_3)_2$ and $Na_2S{\cdot}9H_2O$ (0.12 g, 0.49 mmol) in a benzene suspension (10 mL) this had an off-white (light yellow-brown) colouration. The suspension was continually stirred for 48 h after which the solids suspended in solution collected in the bottom of the flask, sticking there as a light brown paste. The suspension was filtered using a number 4-glass frit and a Büchner funnel, and washed with benzene (5 mL), the solid collected was a light green-brown pastel, the filtrate collected was tinted yellow.

The solid collected from filtration underwent a purifications step to preferentially dissolve the present sodium salts in MeOH, this lead to the partial decomposition of $Pt_2(\mu_2\text{-}S)_2(PTA)_4$ while in solution.

2.9.3) Second Synthesis of $Pt_2(\mu_2\text{-}S)_2(PTA)_4$

Second synthesis: was repeated as per Section 2.9.2, with the only purification step being the filtration from the benzene suspension. Product was used for thermal decomposition assessments.

$Pt_2(\mu_2\text{-}S)_2(PTA)_4$: $^{31}P\{^1H\}$ NMR s, -54.3 ppm, $^1J_{Pt\text{-}P}$ 2616 Hz (D_2O) recorded at 121.5 MHz on a 300 MHz NMR spectrometer.

2.9.4) Third Synthesis of $Pt_2(\mu_2\text{-}S)_2(PTA)_4$

Third Synthesis: was repeated as per Section 2.9.2. The literature method for the synthesis of $Pt_2(\mu_2\text{-}S)_2(PPh_3)_4$,[2] with the alteration that of *cis*-$PtCl_2(PTA)_2$ (0.418 g, 0.72 mmol) in place of *cis*-$PtCl_2(PPh_3)_2$ and $Na_2S{\cdot}9H_2O$ (0.86 g, 3.5 mmol) in a benzene suspension (10 mL) continually stirred for 48 h. After collection of the solid and washing with benzene (5 mL), no further purification attempts were made. The solid was dried under vacuum.

2.9.5) Synthesis of $[Pt_3(\mu_3\text{-}S)_2(PTA)_6]^{2+}$, Sulfide Exchange Column

The column was prepared from a glass pasteur pipette plugged with glass wool (4 mm) pushed to the bottom, to hold the beads in place.

The glass pasteur pipette was then filled with Dowex 1X8 beads (4 cm deep). The column was then washed with distilled water (15 mL) followed by methanol (15 mL). The eluent was discarded.

A solution of sodium sulfide in methanol was prepared, (200 mg, 10 mL) and the solution passed down the column, (producing a colour change from orange to brown.) The column was further washed with methanol till a fresh sample of the eluent tested clear, when a drop of $Pb^{2+}_{(aq)}$ was added to it. ($Pb^{2+}_{(aq)}$ was prepared by the dissolution of a sample (small spatula full) of lead nitrate in distilled water (5 mL)). If the eluent formed a black precipitate of PbS further washing was needed. (10 mL of methanol was needed, before running clean).

When the column was running clean, with no excess of sulfide ions, a solution of *cis*-$PtCl_2(PTA)_2$ (0.01 g, 0.02 mmol,) in methanol (15 mL) was passed down the column, followed by methanol (15 mL). The eluent was collected in a 100 mL round bottom flask and then evaporated to dryness using a rotary evaporator, producing a white solid that was shown by ESI-MS to contain $[Pt_3(\mu_3\text{-}S)_2(PTA)_6]^{2+}$. The column was rendered safe for disposal after 2M HCl (10 mL) was flushed down it in a fume hood followed by methanol (15 mL) (producing a colour change from brown to orange).

$[Pt_3(\mu_3\text{-}S)_2(PTA)_6]^{2+}$: $^{31}P\{^1H\}$ NMR s, -60.3 ppm, $^1J_{(Pt\text{-}P)}$ 3041 Hz (D_2O) recorded at 121.5 MHz on a 300 MHz NMR spectrometer.

2.9.6) Synthesis of $[Pt_2(\mu_3\text{-}S)_2(PTA)_4Rh(cod)]Cl$

The literature method for the synthesis of $[Pt_2(\mu_3\text{-}S)_2(PPh_3)_4Rh(cod)]Cl$,[70] with the alteration that $Pt_2(\mu_2\text{-}S)_2(PTA)_4$ (0.054 g, 0.05 mmol) prepared from 2.9.4 was used in place of $Pt_2(\mu_2\text{-}S)_2(PPh_3)_4$ and $[RhCl(cod)]_2$ (0.0123 g, 0.02 mmol). The solvent used was methanol (60 mL) in place of THF. After stirring for 1 hour the resulting precipitate which gave the solution a brown colouration was filtered off, the maroon filtrate was collected in a 100 mL round bottom flask and then evaporated to dryness with the use of a rotary evaporator.

The deposition of $[Pt_2(\mu_3\text{-}S)_2(PTA)_4Rh(cod)]Cl$ occurred as a maroon solid in the 100 mL round bottom flask during rotary evaporation. The solid obtained from filtration after drying was dark grey/black with a mass of 0.0557 g.

$[Pt_2(\mu_3\text{-}S)_2(PTA)_4Rh(cod)]Cl$: $^{31}P\{^1H\}$ NMR s, -56.8 ppm, $^1J_{Pt\text{-}P}$ 2965 Hz (D_2O) recorded at 121.5 MHz on a 300 MHz NMR spectrometer.

2.9.7) Attempted Synthesis of $Pt_2(\mu_2\text{-}S)_2(PTA)_4$ via a Biphasic Ligand Exchange

This reaction was prepared using a suitable sealable sample vial containing the biphasic reaction solvents of distilled water (20 mL) and toluene (20 mL). Added to the vial was $Pt_2(\mu_2\text{-}S)_2(PPh_3)_4$ (0.04 g, 0.026 mmol) and PTA (0.016, 0.106 mmol) in a 1:4 molar ratio. The sealable vial was stirred continuously for 7 days. During the stirring the $Pt_2(\mu_2\text{-}S)_2(PPh_3)_4$ as an orange mass floated in the aqueous phase and around the phase boundary. This was simultaneously repeated with ratios of 1:1, 1:2, 1:3, $Pt_2(\mu_2\text{-}S)_2(PPh_3)_4$ to PTA.

2.9.8) Attempted Synthesis of $Pt_2(\mu_2\text{-}S)_2(PTA)_4$ via a Monophasic Ligand Exchange

An exact replica of 2.9.7 *with* MeOH (20 mL) and toluene (20 mL) as co-solvents was used. The solvents were allowed to settle before samples of the aqueous phase were taken for positive-ion ESI mass analysis, results are discussed in Section 2.7.

2.9.9) Synthesis of PTA Sulfide

A solution of PTA (small spatula full) in distilled water and powdered elemental sulfur (small spatula full) were stirred continually in distilled water at 60 °C over 3 h. The phosphine sulfide was obtained by evaporation of the solvent after undissolved and unreacted solids were filtered off.

PTA=S**:** $^{31}P\{^1H\}$ NMR: s, -17.2 ppm (D_2O) recorded at 121.5 MHz on a 300 MHz NMR spectrometer.

2.9.10) Synthesis of PTA Oxide

PTA oxide was prepared through the reaction of a small sample of *cis*-$PtCl_2(PTA)_2$ in an excess of water.[58]

PTA=O: $^{31}P\{^1H\}$ NMR: s, -2.9 ppm (D_2O) recorded at 121.5 MHz on a 300 MHz NMR spectrometer.

Chapter 3: Thioacetamide as a Sulfide Ion Source for the Synthesis of the $\{Pt_2(\mu_2\text{-}S)_2\}$ Core

3.1.0 Initial Investigation of Thioacetamide as a Sulfide Ion Source

During the investigations into alternative sulfide ion sources, thioacetamide ($CH_3C(S)NH_2$) was explored as it could be used as a possible alternative source of sulfide for the formation of $Pt_2(\mu_2\text{-}S)_2(PTA)_4$. This would occur *via* a well studied hydrolysis reaction which is pH dependent.[74] In the presence of a basic solution the hydrolysis of thioacetamide yields thioacetic acid and an ammonium ion, thioacetic acid undergoes further hydrolysis with OH^- to yield hydrogen sulfide and acetate. In the presence of an acidic solution the hydrolysis of thioacetamide yields hydrogen sulfide and acetamide as the major products; acetamide then undergoes hydrolysis to an ammonium ion and acetate.[74] Both of these routes end up providing the hydrogen sulfide that would form the $\{Pt_2(\mu_2\text{-}S)_2\}$ core. It was thought the by-products produced from thioacetamide's hydrolysis, would be easier to remove than the sodium salt by-products described in Section 2.5. As the acetic acid from the acetate and acetamide are soluble in benzene so could be removed *via* filtration. Thioacetamide has been shown to be a viable source of sulfide ions, as it has been used as such in the synthesis of many other metal sulfides e.g. Cd, Zn, Pb, Cu.[75–77]

Due to the nature of the results gathered the thioacetamide work has been separated from the prior work into alternative sulfide ion sources for the synthesis of $Pt_2(\mu_2\text{-}S)_2(PTA)_4$ (Section 2.5).

To first determine if this alteration to an established reaction method,[2] was viable, it was attempted with *cis*-$PtCl_2(PPh_3)_2$ in a benzene suspension under the same conditions as prior reactions, as $Pt_2(\mu_2\text{-}S)_2(PPh_3)_4$ is known to be stable and formed from S^{2-} in benzene.[2] The only alteration was the addition of 1.5 mL of water, to promote the hydrolysis of thioacetamide (eq1) and therefore to provide H_2S in solution, as a source of sulfide for the formation of the $\{Pt_2(\mu_2\text{-}S)_2\}$ core.

$$CH_3C(S)NH_2 + H_2O \rightarrow CH_3C(O)NH_2 + H_2S \qquad (eq1)$$

The reaction between *cis*-$PtCl_2(PPh_3)_2$ and $CH_2C(S)NH_2$ did not proceed as anticipated and the desired product was not found to be present in the benzene suspension. The mass spectra of the suspension and the off-white/cream solid obtained *via* filtration of the reaction mixture showed the cation $[Pt(CH_3C(S)NH)(PPh_3)_2]^+$ as the most intense peak in the spectrum (Figure 3). This species has not been previously reported in the literature. The other ions present that were identified are within the accompanying Table 3. When the CEV was lowered to 60 V from 150 V ions of another product *trans*-$Pt(SC(O)CH_3)_2(PPh_3)_2$ became visible in the mass spectrum.

Table 3: Identified ions that accompanied $[Pt(CH_3C(S)NH)(PPh_3)_2]^+$.

CEV(V)	Ion (*m/z*)	Calculated (*m/z*)	Formula
150	792.94	793.15	$[Pt(CH_3C(S)NH)(PPh_3)_2]^+$
	717.94	718.14	$[Pt(PPh_3)(PPh_2C_6H_4)]^+$
	530.94	531.06	$[Pt(CH_3C(S)NH)(PPh_3)]^+$
60	868.90	870.14	$[Pt(SC(O)CH_3)_2(PPh_3)_2+H]^+$
	891.86	892.12	$[Pt(SC(O)CH_3)_2(PPh_3)_2+Na]^+$

The reaction was repeated twice more: one an exact replica of the first reaction, while the second was altered by performing the reaction under reflux. The replica reactions were done in the interest of understanding why the filtrate of the benzene water suspension in the first synthetic attempt was distinctly yellow. The replica reaction with no alterations had no filtration step at the end. The reaction mixture was allowed to evaporate, providing a yellow solid, as opposed to the original off-white/cream colouration. A comparison between the two was undertaken, in order to hopefully determine what resulted in the yellow colouration.

The positive-ion ESI mass spectrum of the yellow solid showed clearly the cation $[Pt(CH_3C(S)NH)(PPh_3)_2]^+$. An increased intensity of the ions $[Pt(SC(O)CH_3)_2(PPh_3)_2+H]^+$ and its adduct ion $[Pt(SC(O)CH_3)_2(PPh_3)_2+Na]^+$ was also observed, and both of these ions were also now visible when a capillary exit

voltage of 150 V was used. These ions were the result of thioacetamide being hydrolysed, resulting in the formation of *trans*-$Pt(SC(O)CH_3)_2(PPh_3)_2$ during the reaction.

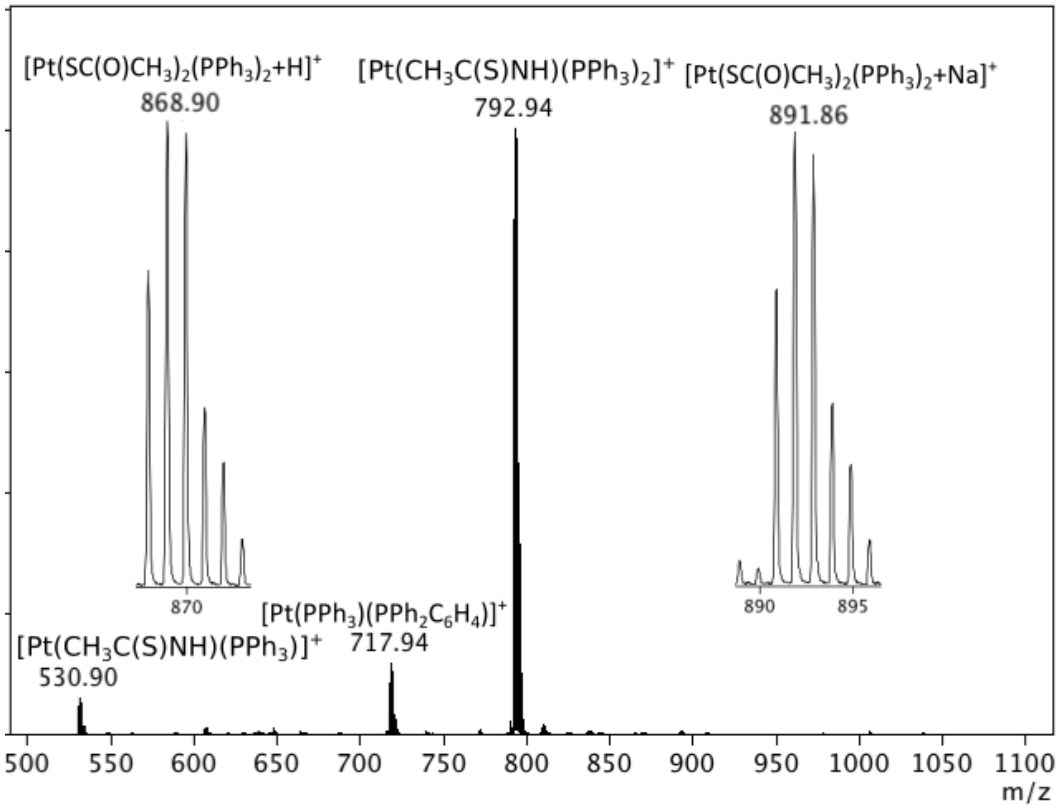

Figure 3: Positive-ion ESI mass spectrum showing major ions of the reaction products of *cis*-$PtCl_2(PPh_3)_2$ and $CH_3C(S)NH_2$ in a methanol solution with a CEV of 150 V.
The inset spectra show the isotope patterns of ion side products that were present at a CEV of 60 V and that increased in intensity during the second repeated synthesis.

The $^{31}P\{^1H\}$ NMR of both the yellow and off-white solids did show phosphine ligated platinum complexes which were identifiable as they had $^1J_{Pt\text{-}P}$ coupling. The $^{31}P\{^1H\}$ NMR spectrum of the yellow solid revealed that there are 3 visible phosphorus environments present with $^1J_{Pt\text{-}P}$ coupling, data given in Table 3.1 with proposed assignments. The $^{31}P\{^1H\}$ NMR spectrum of the first synthesis, off-white solid reveals the same 3 phosphorus environments but only one resonance was of a high enough intensity to have visible phosphorus-platinum coupling (21.3 ppm, $^1J_{Pt\text{-}P}$ 2557 Hz) (Table 3.1). This peak was the strongest in both spectra but may not result from the *cis*-$[Pt(CH_3C(S)NH)(PPh_3)_2]^+$ species, as this complex should result in two different phosphorus environments of similar intensities each with $^2J_{P\text{-}P}$ coupling giving doublets. Therefore it is possible is responsible for the other 2 phosphorus environments in both spectra. In the

spectrum of the yellow solid isolated from evaporation the $^{1}J_{Pt\text{-}P}$ coupling is visible for all three resonances, while in the spectrum of the off-white synthesis two resonances are of an intensity so low that no phosphorus-platinum coupling is visible Figure 3.1. The largest resonance in both spectra could result from another complex with only one phosphorus environment, possibly the *trans*-$Pt(SC(O)CH_3)_2(PPh_3)_2$ species as it was observed in the mass spectrum for both solids (Figure 3).

Table 3.1: $^{31}P\{^{1}H\}$ NMR of both syntheses of $[Pt(CH_3C(S)NH)(PPh_3)_2]^+$.

Second Synthesis, Yellow		First Synthesis, Off-white		Suspected Assignments
δ(ppm)	$^{1}J_{Pt\text{-}P}$ (Hz)	δ(ppm)	$^{1}J_{Pt\text{-}P}$ (Hz)	
17.2	2981	17.2		$[Pt(CH_3C(S)NH)(PPh_3)_2]^+$
21.3	2543	21.3	2543	*tans*-$Pt(SC(O)CH)_2(PPh_3)_2$
23.4	2781	23.4		$[Pt(CH_3C(S)NH)(PPh_3)_2]^+$

Accompanying these chemical shifts in both spectra are peaks attributed to triphenylphosphine oxide (43.3 ppm), triphenylphosphine sulfide (26.4 ppm), and triphenylphosphine (-4.7 ppm).[78] Triphenylphosphine sulfide has a significantly more intense peak in the spectrum obtained from the yellow solid which was isolated from evaporation Figure 3.1 bottom spectrum, indicating the oxide was originally lost in the eluent during filtration. This is also applicable to the two

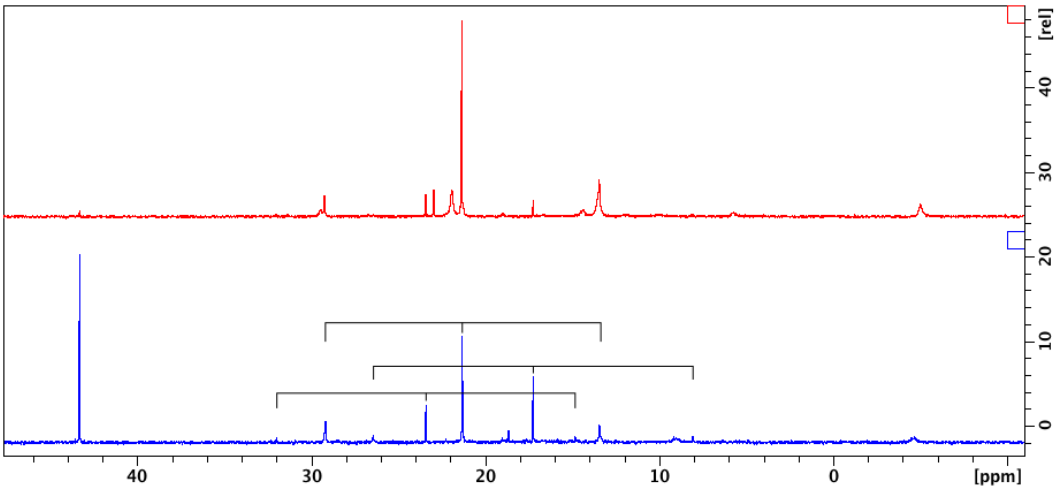

Figure 3.1: The $^{31}P\{^{1}H\}$ NMR of both filtered (top) and evaporated (bottom) synthesis of $[Pt(CH_3C(S)NH)(PPh_3)_2]^+$ produced. Significant platinum complex chemical shifts are listed in Table 3. **(**Black lines indicate couplings) Spectra were recorded at 162 MHz on a 400 MHz NMR spectrometer in $CDCl_3$.

other platinum complexes with smaller resonances, as they are also diminished in the sample that was filtered.

Other noticeable differences in the two spectra are a small number of phosphorus shifts that lack platinum coupling and only appear in one of the two spectra. The most notable are the broad resonance at 21.9 ppm and the sharp resonance at 22.9 ppm, both of which are seen only in the spectrum of the filtered sample (Figure 3.1, top spectrum).

It was later determined that complexes containing $[Pt(CH_3C(S)NH)(PPh_3)_2]X$ (X = suitable anion) were not solvent stable for long periods in $CDCl_3$. The comparison between $^{31}P\{^1H\}$ NMR spectra in Figure 3.1 were collected with $CDCl_3$ as the solvent. In order to provide increased accuracy in this preliminary investigation, the spectra will have needed to be re-recorded with the use of DMSO-d_6 as the solvent, as the complex was observed to have greater solvent stability while dissolved in DMSO-d_6. This was determined to be unnecessary as the platinum complexes present $[Pt(CH_3C(S)NH)(PPh_3)_2]X$ and *trans*-$Pt(SC(O)CH_3)_2(PPh_3)_2$ were characterised in later research (Sections 3.1.1 and 3.2).

The third reaction carried out was altered from the previous two only in that it was done under reflux, as an attempt to get the reaction to proceed to the desired product $Pt_2(\mu_2\text{-}S)_2(PPh_3)_4$ from a reaction of *cis*-$PtCl_2(PPh_3)_2$ with $CH_3C(S)NH_2$ in a benzene suspension with 1.5 mL of water. The reaction only ran for 1.5 hours and started with the solution having a yellow colouration just as the previous two reactions did. The solution quickly became orange within 5 minutes, red within 15-20 minutes, and then became brown after 40 minutes. No further colour changes were observed.

The mass spectra of both the brown reaction mixture and the solid obtained after it was evaporated to dryness showed a large array of various ions. Most of these ions were not platinum complexes, based on the isotope patterns observed. The ions that did display a platinum isotope pattern were not ones seen previously, and most could not be identified. The ion $[Pt(CH_3C(S)NH)(PPh_3)_2]^+$ was observed at low intensities. Accompanying all of the non-platinum and unidentified platinum

ions was a very low intensity $[Pt_2(\mu_2\text{-}S)_2(PPh_3)_4]^+$ ion, meaning a part of the reaction did proceed as desired, though to a negligible extent.

3.1.1 X-ray Crystal Structure of *trans*-$Pt(SC(O)CH_3)_2(PPh_3)_2$

For the first two attempted syntheses of $[Pt(CH_3C(S)NH)(PPh_3)_2]^+$ (yellow solid obtained by evaporation, off-white solid obtained by filtration), attempts at growing crystals through vapour diffusion of dichloromethane and diethyl ether were performed on the isolated product. A significant portion of what formed was micro-crystalline and unsuitable for X-ray crystallography. From the second synthesis, the yellow solid, crystals of *trans*-$Pt(SC(O)CH_3)_2(PPh_3)_2$ were successfully grown, they were yellow and clear, a darker shade then the powdered solid first collected.

Crystal structure data are given in Figure 3.2 and tables of bond lengths (Table 3.2) and angles (Table 3.3) are summarised. Accompanying data are listed within Appendix II.

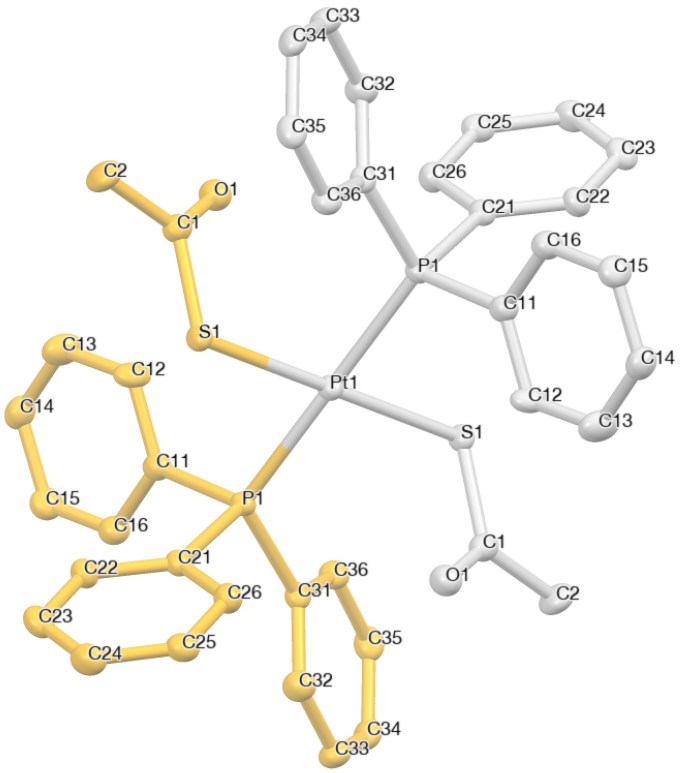

Figure 3.2: Structure of *trans*-$Pt(SC(O)CH_3)_2(PPh_3)_2$.

Table 3.2: Bond lengths of *trans*-$Pt(SC(O)CH_3)_2(PPh_3)_2$.

Atom	Atom	Length/Å	Atom	Atom	Length/Å
Pt1	P1	2.3131(11)	P1	C31	1.840(5)
Pt1	$P1^1$	2.3131(11)	S1	C1	1.762(5)
Pt1	$S1^1$	2.3319(10)	O1	C1	1.218(6)
Pt1	S1	2.3319(10)	C1	C2	1.516(7)
P1	C11	1.825(5)			

Table 3.3: Bond angles of *trans*-$Pt(SC(O)CH_3)_2(PPh_3)_2$.

Atom	Atom	Atom	Angle/°	Atom	Atom	Atom	Angle/°
$P1^1$	Pt1	P1	180	C31	P1	C11	100.0(2)
S1	Pt1	$P1^1$	92.39(4)	C1	S1	$Pt1^1$	105.14(17)
$S1^1$	Pt1	P1	92.39(4)	C22	C21	P1	122.9(4)
S1	Pt1	P1	87.61(4)	C26	C21	P1	117.5(3)
$S1^1$	Pt1	$P1^1$	87.61(4)	C12	C11	P1	120.8(4)
$S1^1$	Pt1	S1	180	C16	C11	P1	120.5(4)
C21	P1	Pt1	110.83(16)	C32	C31	P1	122.2(4)
C11	P1	Pt1	114.83(16)	C36	C31	P1	118.3(4)
C11	P1	C21	104.9(2)	O1	C1	S1	125.2(4)
C31	P1	Pt1	119.97(15)	C2	C1	S1	113.6(4)
C31	P1	C21	104.6(2)	C2	C1	O1	121.2(4)

The crystal structure of this complex bears a strong similarity to the known palladium analogue, sharing the same triclinic crystal system and $P\bar{1}$ space group.[79] The key differences between the two structures, apart from the metals, is how the complex is orientated in the unit cell. The platinum complex has the metal centre located on an inversion point, while the metal centre of the palladium complex is situated in the centre of the unit cell. This is the only major difference that occurs between the platinum and palladium analogues, the metal-phosphorus and metal-sulfur bond lengths are within the margin of error to be considered the same, along with that of the bond angles.

3.2 Synthesis and Isolation of $[Pt(CH_3C(S)NH)(PPh_3)_2]^+$

Efforts were taken to synthesise and isolate the cation $[Pt(CH_3C(S)NH)(PPh_3)_2]^+$ by use of a counter anion. Two counter anions, BF_4^- and BPh_4^-, were used to force precipitation of the platinum complex out of the methanol reaction solution of *cis*-$PtCl_2(PPh_3)_2$ and thioacetamide. The mass spectra of both products showed the

$[Pt(CH_3C(S)NH)(PPh_3)_2]^+$ ion. The BPh_4^- salt was light pink whereas the BF_4^- was a light peach colour.

The starting colouration was notable in that during the attempts at growing crystals through vapour diffusion, the dichloromethane solution in which both the BPh_4^- and BF_4^- salts were dissolved turned forest green over a few hours, the colour change also occurred for $CDCl_3$ samples while in NMR tubes. This solution slowly became more red over time for one BF_4^- sample as it was allowed to evaporate to dryness. When the BPh_4^- salt was dissolved in a dilute DMSO solution, the colouration was light pink, and it remained this colour over 2 days. The green transition occurred just like the dichloromethane solution after 5 days. Over several hours a microcrystalline solid of $[Pt(CH_3C(S)NH)(PPh_3)_2](BPh_4)$ was grown from a concentrated DMSO solution, however the crystals were not suitable for X-ray crystallography.

The $^{31}P\{^1H\}$ NMR spectrum of $[Pt(CH_3C(S)NH)(PPh_3)_2](BPh_4)$ in both $CDCl_3$ and DMSO-d_6 showed the expected resonances for this complex. Two phosphorus environments were observed, both with slightly different $^1J_{Pt\text{-}P}$ coupling constants (Table 3.4). Two resonances were observed due to the PPh_3 groups not being magnetically (or chemically) equivalent, this also leads to $^2J_{P\text{-}P}$ coupling resulting in these resonances being seen as a pair of doublets. The two phosphorus atoms are *trans* to donor atoms (S and N) having different *trans*-influences, resulting in different $^1J_{Pt\text{-}P}$ couplings for each. A PPh_3=S resonance was present, which is in close agreement with the literature value,[78] 44.0/ 43.0 ppm ($CDCl_3$ /DMSO-d_6) Table 3.4. The chemical shifts and $^1J_{Pt\text{-}P}$ couplings of $[Pt(CH_3C(S)NH)(PPh_3)_2](BPh_4)$ between the solvents $CDCl_3$ and DMSO-d_6 changes more then would be expected for a change in solvent. This suggests a possible interaction with DMSO while in solution, as DMSO is known to be a strongly coordinating solvent,[80] the difference may also suggest a reaction is occurring in one of the solvents.

Table 3.4: $^{31}P\{^{1}H\}$ NMR data of $[Pt(CH_3C(S)NH)(PPh_3)_2](BPh_4)$ in $CDCl_3$ / DMSO-d_6.

Resonance (ppm)	$^{2}J_{P\text{-}P}$ (Hz)	$^{1}J_{Pt\text{-}P}$ (Hz)
	Sample in $CDCl_3$	
8.7	18.8	3436
14.5	18.3	3151
44.1	-	-
	Sample in DMSO-d_6	
10.4	19.6	2969
13.0	18.9	3169
19.3	20.2	-
43.0	-	-

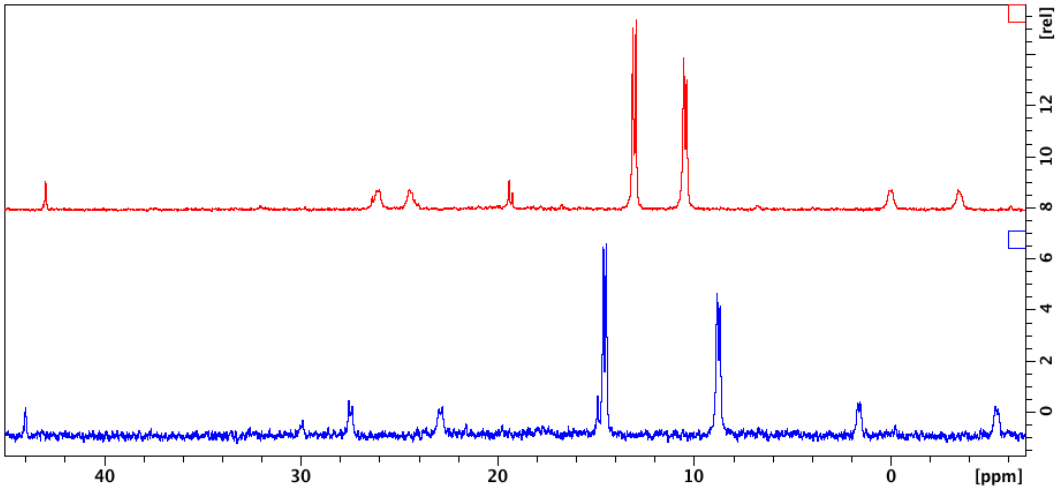

Figure 3.3: The $^{31}P\{^{1}H\}$ NMR spectrum of $[Pt(CH_3C(S)NH)(PPh_3)_2](BPh_4)$ in DMSO-d_6 (top) $CDCl_3$ (bottom), recorded at 121.5 MHz on a 300 MHz NMR spectrometer. The assignments of these spectrum are found within Table 3.4.

The $^{31}P\{^{1}H\}$ NMR of $[Pt(CH_3C(S)NH)(PPh_3)_2](BPh_4)$ in DMSO-d_6 had a fourth phosphorus resonance at 19.3 ppm, $^{2}J_{P\text{-}P}$ 20.2 Hz Figure 3.3 (top), this results from an unknown complex. If platinum coupling is present it is indistinguishable from the baseline. Interestingly this resonance was not observed in the $CDCl_3$ sample, so could be attributed to the possible coordination with DMSO-d_6. The $CDCl_3$ sample Figure 3.3 (bottom) spectrum shows a single resonance that overlaps with the resonance at 14.5 ppm that does not occur in the DMSO-d_6 sample and remains unidentified.

For both BF_4^- and BPh_4^- salts, the solutions prepared for NMR analysis (in $CDCl_3$ and DMSO-d_6) and the solutions prepared during the attempts at growing crystals from dichloromethane, all started as a pale yellow or pink solution. However,

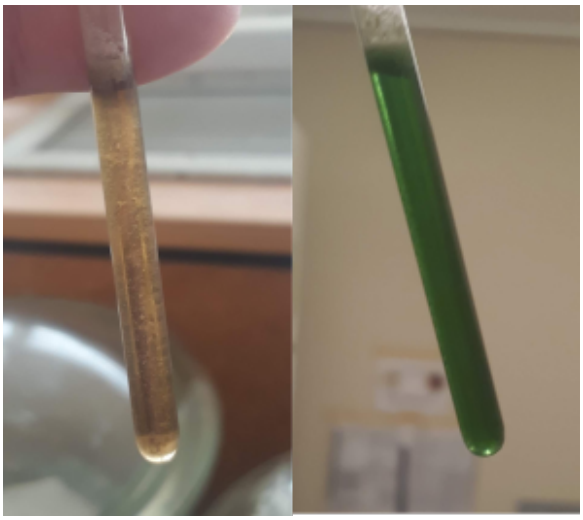

Figure 3.4.: The colour change of $Pt(CH_3C(S)NH)(PPh_3)_2](BPh_4)$ $CDCl_3$ solution. Left sunlight. Right fluorescent lighting.

after approximately three hours for a $CDCl_3$ sample, while under the fluorescent lighting of the laboratory environment, the sample became green Figure 3.4 (right). When exposed to sunlight the colour of the solution would change to a more yellow colouration Figure 3.4 (left). This observed colour change was reversible if the sample was then removed from the sunlight. During the 3-4 hour it took for the green transition to occur a very fine precipitate formed that collected at the top of the solution. This precipitate could not be filtered off using a number four-sintered glass frit.

A sample of $[Pt(CH_3C(S)NH)(PPh_3)_2](BPh_4)$ in dichloromethane was prepared and allowed to stand for several hours until completely green. The UV/Visible spectrum of this solution was recorded, showing stronger absorbance values at the wavelengths 380, 465, 603 nm (Figure 3.5) This shows the solution does not have a strong absorbance of red light (630-750 nm) to provide its complementary colour green, indicating something else is responsible for the green colouration. The complexes $[Pt(CH_3C(S)NH)(PPh_3)_2]X$ ($X = BF_4^-$, BPh_3^-) turn green while dissolved in chloroform and dichloromethane over several hours, but when a sample of $[Pt(CH_3C(S)NH)(PPh_3)_2](BPh_4)$ is dissolved in DMSO the solution retains the colouration of the solid, a light pink for several days before slowly turning green. The UV/Visible spectrum of the DMSO solution immediately after dissolution was recorded and is shown in Figure 3.5 as the dashed line, the only notable absorbance occurs at 485 nm, which is an appropriate absorbance for a solution to be light pink in colour.

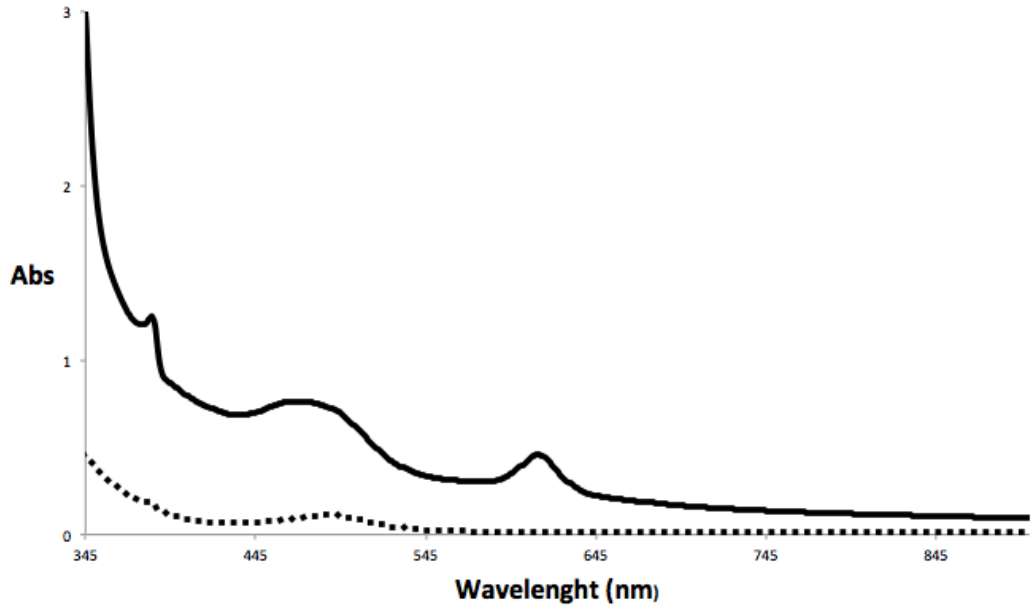

Figure 3.5: The UV/Visible absorbances of $[Pt(CH_3C(S)NH)(PPh_3)_2](BPh_4)$ in dichloromethane (solid line), and DMSO (dashed line) over wavelengths of 320-1100 nm. The three notable absorbances for the dichloromethane solution occurred at 380, 465, and 603 nm. The notable absorbance for the DMSO solution is at 485 nm.

The positive-ion ESI mass spectrum of $[Pt(CH_3C(S)NH)(PPh_3)_2](BPh_4)$ immediately after dissolution in a chloroform solution shows the ion $[Pt(CH_3C(S)NH)(PPh_3)_2]^+$ (793 *m/z*) as the only visible cation. After several hours the solution (completely green) had the positive-ion ESI mass spectrum re-recorded shown in Figure 3.6. This spectrum shows considerable decomposition, with various cations that contain recognisable platinum isotope patterns now visible. The ion of $[Pt(CH_3C(S)NH)(PPh_3)_2]^+$ (793.03 *m/z*) is significantly diminished in intensity, with the highest intensity ion at 809.99 *m/z* and has an isotope pattern that matches the ion $[Pt(CH_3C(S)NH)(PPh_3)_2O+H]^+$. The problem arises here as $[Pt(CH_3C(S)NH)(PPh_3)_2O+H]^+$ matches the isotope pattern in the spectrum recorded but this complex formally will have a neutral charge, with the Pt^{2+}, H^+ being neutralised by O^{2-}, $(CH_3C(S)NH)^-$. This decomposition product at 809.99 *m/z* is a monoplatinum complex, as contributions to the isotope pattern from a platinum atom can be observed, but the ligands and other coordinated groups remain unknown at this stage.

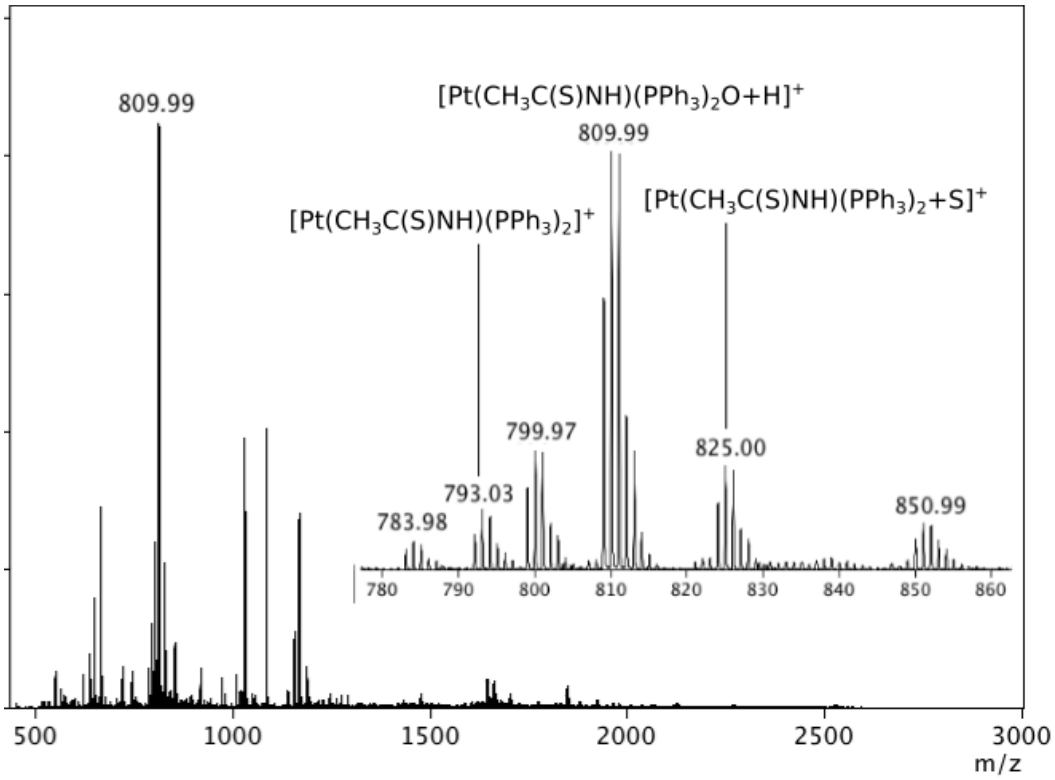

Figure 3.6: The positive-ion ESI mass spectrum of $[Pt(CH_3C(S)NH)(PPh_3)_2](BPh_4)$ in dichloromethane after 4 hours (completely green). CEV 150 V, MeOH solution.

The sample of $[Pt(CH_3C(S)NH)(PPh_3)_2](BPh_4)$ in DMSO slowly changed to green over a six day period. The $^{31}P\{^1H\}$ NMR was obtained to observe how the decomposition had affected the spectrum (Figure 3.7). The doublet of doublet resonances from $[Pt(CH_3C(S)NH)(PPh_3)_2](BPh_4)$ (Table 3.4) are observed in the decomposition spectrum with a significant increase of the PPh_3=S resonance at 43.0 ppm, accompanied by several new and unidentified single phosphorus resonances at 26.4, 25.2, 19.4 and 16.7 ppm.

The $^{31}P\{^1H\}$ NMR spectra in DMSO-d_6 over time (Figure 3.7), paired with the positive-ion ESI mass spectra in chloroform while green (Figure 3.6) provided evidence that $[Pt(CH_3C(S)NH)(PPh_3)$ (X = BF_4^-, BPh_4^-) lack solvent stability.

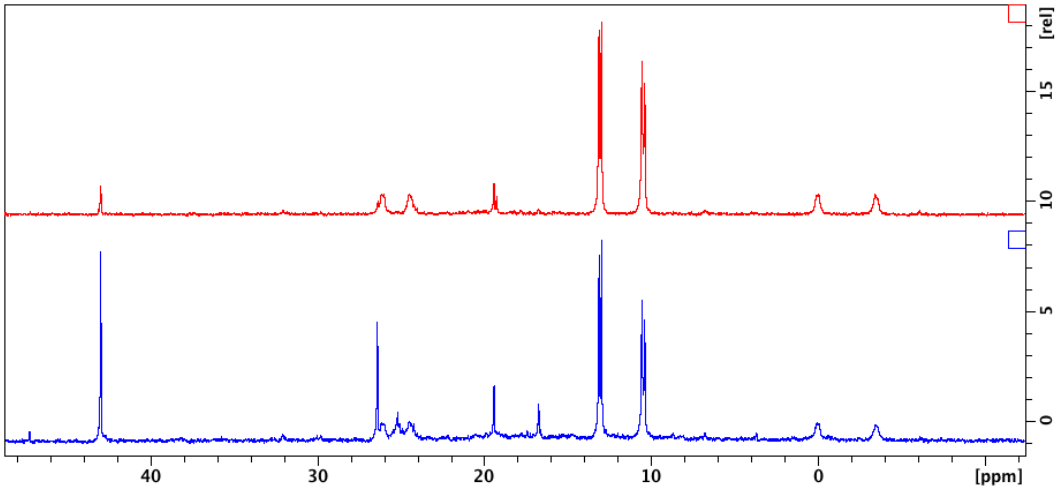

Figure 3.7 : $^{31}P\{^{1}H\}$ NMR of $[Pt(CH_3C(S)NH)(PPh_3)_2](BPh_4)$ in DMSO-d_6.Top spectrum, immediately after dissolution (light pink-yellow). Bottom spectrum, 6 days after dissolution (green). Recorded at 121.5 MHz on a 300 MHz NMR spectrometer.

3.3 Conclusion

The research undertaken during this study found that thioacetamide was not a viable alternative source of sulfide in the synthesis of the $\{Pt_2(\mu_2\text{-}S)_2\}$ core. This research also led to the synthesis of two new complexes.

The first complex, in the general form $[Pt(CH_3C(S)NH)(PPh_3)_2]X$ (X = suitable anion), was the primary product produced from the unsuccessful $\{Pt_2(\mu_2\text{-}S)_2\}$ core synthesis and was later isolated with the counter anions BPh_4^- and BF_4^-. The complex was characterised with $^{31}P\{^{1}H\}$ NMR and positive-ion ESI mass spectra, and was found to be lacking long-term solvent stability, with the solution turning green over time.

The second complex discovered during the unsuccessful attempt to use thioacetamide to form the $\{Pt_2(\mu_2\text{-}S)_2\}$ core was *trans*-$Pt(SC(O)CH_3)_2(PPh_3)_2$. This complex was a by-product of the reaction and was visible in mass spectra at low capillary exit voltages. It resulted from thioacetamide being hydrolysed before undergoing the reaction with the platinum starting material. Although this complex was a by-product, it was the only complex from which crystals suitable for X-ray crystallography were grown. The crystal structure was successfully collected and is comparable to that of the palladium analogue.

3.4 Experimental

The general experimental work and chemical suppliers, accompanied by the equipment parameters are detailed in Appendix 1.

3.4.1) Initial Reaction Between cis-$PtCl_2(PPh_3)_2$ and Thioacetamide

A modification of the literature method for synthesis of $Pt_2(\mu_2\text{-}S)_2(PPh_3)_4$ was used,[2] with *cis*-$PtCl_2(PPh_3)_2$ (0.05 g, 0.06 mmol), replacing $Na_2S{\cdot}9H_2O$ by thioacetamide (0.025 g, 0.33 mmol), in a benzene suspension (10 mL), with the addition of distilled water (1.5 mL) to promote the hydrolysis of the thioacetamide, the suspension was stirred for 48 hours.

The reaction suspension was yellow in the beginning of the 48 hour mixing period, over time becoming increasingly darker with a hint of orange almost at the end of the mixing. Upon filtration it was determined that the darker colouration was the result of the off-white solid in the suspension and the yellow benzene filtrate.

The positive-ion ESI mass spectrum of the solid collected revealed the reaction product to be 792.94 *m/z* $[Pt(PPh_3)_2(CH_2C(S)NH)]^+$ a counter anion of Cl^- was most probable as it was present in solution.

3.4.2) Second Reaction Between cis-$PtCl_2(PPh_3)_2$ and Thioacetamide

The reaction 3.4.1 was repeated the same, till the filtration step. The benzene suspension was allowed to evaporate to dryness, producing a yellow solid.

The positive-ion ESI mass spectrum of the yellow solid collected revealed a spectrum that closely resembled that of 3.4.1 with the greatest intensity cation being $[Pt(PPh_3)_2(CH_2C(S)NH)]^+$ and the lesser ion of $[Pt(PPh_3)_2(SC(O)CH_3)_2]^+$ visible.

3.4.3) Third Reaction Between cis-$PtCl_2(PPh_3)_2$ and Thioacetamide

The reaction 3.4.1 was repeated a third time with further alterations to the method. The reaction suspension was refluxed over 2.5 h followed by evaporating to dryness. During the reflux the reaction suspension changed from yellow to red-orange to brown, this being the colour of the final solid.

The positive-ion ESI mass spectrum of the brown solid collected showed a spectrum containing $[Pt(PPh_3)_2(CH_2C(S)NH)]^+$ and a small intensity of $[Pt_2(\mu_2\text{-}S)_2(PPh_3)_4+H]^+$ along with a large number of non-platinum and platinum complexes that remain unidentifiable.

The $^{31}P\{^1H\}$ NMR of the products collected from the 3.4.1-3.4.3 series of reactions are discussed in Section 3.1.

3.4.4) Synthesis of $[Pt(PPh_3)_2(CH_3C(S)NH)](BF_4)$

A methanol solution (10 mL) of *cis*-$PtCl_2(PPh_3)_2$ (0.02 g, 0.025 mmol) and thioacetamide (0.0091 g, 0.12 mmol) was stirred till complete dissolution occurred, (after 5 minutes of being stirred the reaction solution was clear and colourless), then after addition of triethylamine (2 drops), stirring was continued for 10 minutes the solution remained clear gaining a slight yellow tint.

An excess of $NaBF_4$ (approximately 0.8 g, 7.03 mmol) was added to the solution, and stirring continued until complete dissolution occurred. No precipitate was observed at this stage therefore distilled water (50 mL) was added, resulting in precipitation of a light peach solid. The mixture was filtered using a number 4-glass frit and a Büchner funnel. The frit was left in a desiccator under vacuum to dry. Final yield 0.0068 g (30%).

3.4.5) Synthesis of [Pt(PPh$_3$)$_2$(CH$_3$C(S)NH)](BPh$_4$)

This synthesis was an exact replica of the previous reaction 3.4.4; using *cis*-$PtCl_2(PPh_3)_2$ (0.1 g, 0.13 mmol) and thioacetamide (0.048 g, 0.064 mmol). $NaBPh_4$ was added in place of $NaBF_4$, giving a light pastel pink solid. Yield 0.19 g (81%).

$[Pt(PPh_3)_2(CH_3C(S)NH)](BPh_4)$ $^{31}P\{^1H\}$ NMR:

d, 14.5, $^1J_{Pt\text{-}P}$ 3151 Hz, $^2J_{P\text{-}P}$ (Hz) 18.3 Hz. d, 8.9 $^1J_{Pt\text{-}P}$ 3435 Hz, $^2J_{P\text{-}P}$ (Hz) 18.8 Hz ($CDCl_3$) 121.5 MHz on a 300 MHz NMR spectrometer.

d, 13.0, $^1J_{Pt\text{-}P}$ 3169 Hz, $^2J_{P\text{-}P}$ (Hz) 18.9 Hz d, 10.4, $^1J_{Pt\text{-}P}$ 2969 Hz, $^2J_{P\text{-}P}$ (Hz) 19.6 Hz (DMSO-d_6) 121.5 MHz on a 300 MHz NMR spectrometer.

Chapter 4: Synthesis of Monosulfonated Triphenylphosphine $[TPPMS]^-$ Complexes and Related Investigations

4.1 Synthesis and Characteristics of $[TPPMS]^-$

Monosulfonated triphenylphosphine $[TPPMS]^-$ $[PPh_2(C_6H_4SO_3)]^-$ (Figure 4) is a water-soluble derivative of triphenylphosphine, PPh_3. It is well established that triphenylphosphine can bond readily with the $\{Pt_2(\mu_2\text{-}S)_2\}$ core.[4] The water-solubility of $[TPPMS]^-$ is provided by the SO_3^- group that is meta-substituted on a single phenyl ring. It was considered that $[TPPMS]^-$ should be a suitable phosphine ligand to provide water-solubility to the $\{Pt_2(\mu_2\text{-}S)_2\}$ core, as the common precursor complex *cis*-$[PtCl_2(TPPMS)_2]K_2$ has already been documented,[81] and essentially $[TPPMS]^-$ is still a triphenylphosphine derivative with the added benefit of functioning as a charged-tagged phosphine ligand,[82] where all complexes prepared will be easily identified in the negative-ion ESI mass spectra.

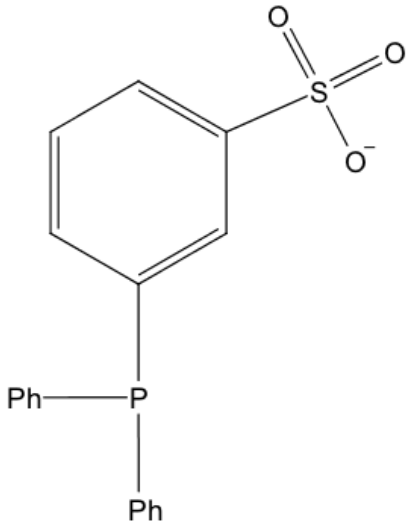

Figure 4: Diagram of $[TPPMS]^-$.

$[TPPMS]^-$ can be synthesised as the potassium salt $[TPPMS]K{\cdot}H_2O$, by reaction of PPh_3 and fuming sulfuric acid (30% SO_3:H_2SO_4) under a nitrogen atmosphere, a minor alteration was made here as tris(2-ethylhexyl)amine was added in place of tri-n-octylamine, due to availability. This was followed by several extraction and purification steps, ending with the precipitation from the addition of KOH to the solution.[83]

The ligand $[TPPMS]K$ and its trisulfonated counterpart $[TPPTS]K_3$ are water-soluble phosphine ligands that have been bound to various metal complexes in the general form $[MCl_2(TPPMS)_2]X_2$, $[MCl_2(TPPTS)_2]X_6$ (M = Pt, Pd, Ir, Ru) (X = Na, K).[81,83–85] $[TPPTS]K_3$ and $[TPPMS]K$ have found use as ligands providing

water-solubility in catalysis reactions. $[RuCl_2(TPPMS)_2]$ is used in the selective hydrogenation of cinnamaldehyde, through a hydrogen transfer with formate. $[Pd(TPPMS)_3]Na$ has been used for the alkylation of heteroaromatic halides through terminal alkynes,[85] while [TPPMS]X (X = Na, K) has been used as a ligand in the biphasic catalysis of hydroformylation reactions.[85]

4.2 Synthesis of *cis*-$[PtCl_2(TPPMS)_2]K_2$

The production of *cis*-$[PtCl_2(TPPMS)_2]K_2$ from the starting materials *cis*-$PtCl_2(L)$, (L = cod or DMSO) through a ligand substitution reaction in DMF solution with a 1:2 molar ratio of $[TPPMS]K \cdot H_2O$, resulted in an off-white precipitate. During the filtration step the solid liquefied slightly in air, becoming a yellow oily solid. Under vacuum the oily solid completely re-solidified, becoming a darker yellow solid with an orange tinge. The phase change from a fine off-white powder in solution to the sticky yellow solid upon exposure to air was interesting and not documented in the literature method used.[81] It was unknown if this was due to the rapid decomposition of the *cis*-$[PtCl_2(TPPMS)_2]K_2$ when exposed to air as a Schlenk line was not used for this synthesis, just the evacuation of the vessel with nitrogen. Thus the stability and sensitivity of the product were investigated. Three different samples relating to this reaction were analysed by mass spectra for comparison purposes: the final reaction solution (before precipitation), the white precipitate, and the final yellow product. This was undertaken in order to determine if decomposition of the product was occurring when the product was removed from solution. The negative-ion ESI spectra of the three different samples were virtually indistinguishable from each other, with no unique ion peaks or large differences in intensity.

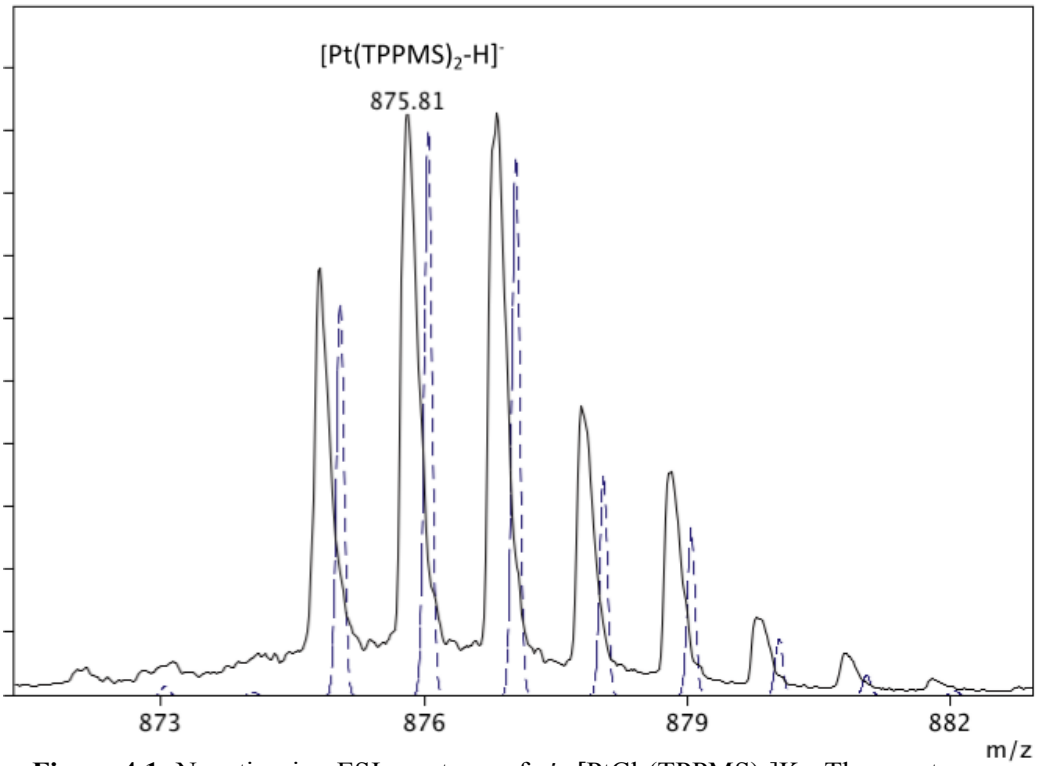

Figure 4.1: Negative-ion ESI spectrum of *cis*-$[PtCl_2(TPPMS)_2]K_2$. The spectrum shows the observed (solid line) and calculated (dashed line) isotope patterns for the anion $[Pt(TPPMS)_2\text{-}H]^-$. CEV= -150 V, MeOH solution.

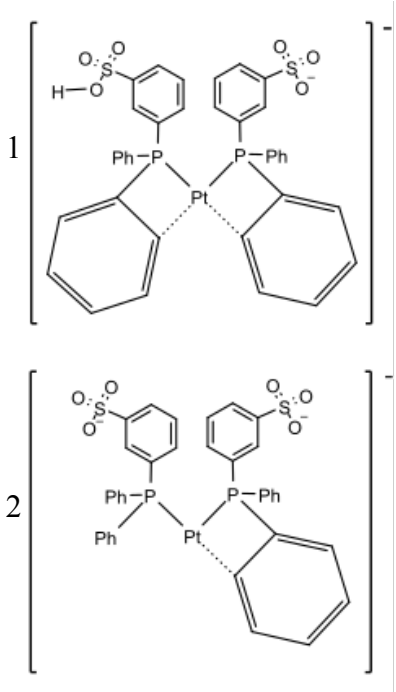

Figure 4.2: The proposed bonding modes of the anion $[Pt(TPPMS)_2\text{-}H]^-$.

The negative-ion ESI mass spectra for all three samples had their most intense peaks at 876 *m/z*. This peak corresponds to the ion $[Pt(TPPMS)_2\text{-}H]^-$ (Figure 4.1). The anion is comprised of a platinum centre bound to two $[TPPMS]^-$ ligands, with an undetermined amount of cyclometalation occurring. The proposed bonding modes for this anion are shown in Figure 4.2 bonding mode 1, where a phenyl ring of each ligand has undergone cyclometalation to the Pt centre, with the addition of one hydrogen atom forming a SO_3H, resulting in an ion with the 1- charge.

A second bonding mode is 2 in Figure 4.2, where only one of the Ph groups has cyclometalated, resulting in an ion with a 1- charge. Both of the two bonding modes in Figure 4.2 have the same mass, isotope pattern, and charge making it impossible to determine which ion was being observed in the negative-ion ESI mass spectra. Mono-cyclometalation of PPh_3 groups has been seen to occur in the mass spectra of *cis*-$PtCl_2(PPh_3)_2$ (Figures 2.11 & 2.12) along with other analogous complexes.[66] The di-cyclometalation of PPh_3 groups has not been documented for *cis*-$PtCl_2(PPh_3)_2$, as it would provide a neutral complex so would be unobservable in mass spectra. The positive-ion ESI mass spectrum of the analogous complex *cis*-$PtCl_2(PPh(C_6H_4OMe)_2)_2$ was obtained to provide additional supporting information. This complex has the potential to undergo both a mono- and di-cyclometalations while remaining a cation through the OMe groups bonded to the phenyl rings providing a site for protonation of any neutral, doubly cyclometalated complex. The resulting positive-ion ESI mass spectrum revealed the ion $[Pt(PPh(C_6H_4OMe)_2)_2\text{-}H]^+$ at 838.16 *m/z*, this ion was from the mono-cyclometalation of the complex.

If a di-cyclometalation was to occur the ion would have retained a 1+ charge, through one of the oxygen atoms protonating giving the same mass at 838.16 *m/z*, the addition of a drop of sodium and/or lithium brine to each ESI-MS sample of *cis*-$PtCl_2(PPh(C_6H_4OMe)_2)_2$ was made to promote the formation of a di-cyclometalated adduct ion with sodium or lithium, this would allow the ion to be distinguished from its mono-cyclometalated counterpart. The resulting positive-ion ESI mass spectra shows none of these adduct ions present, this provides additional evidence that PPh_3 ligands and analogues thereof prefer a mono-cyclometalation, meaning the ion of 876 *m/z* in Figure 4.1 would most likely be a result of bonding mode 2 in Figure 4.2.

Figure 4.3 shows the mass spectrum of the white precipitate and is representative of the spectra recorded for the three samples. The highest intensity peak is $[Pt(TPPMS)_2\text{-}H]^-$, 876.86 *m/z*, however there are various other platinum complex ions that were recorded in the spectrum also. The other platinum complexes present are potassium adducts or fragments of the complex *cis*-$[PtCl_2(TPPMS)_2]K_2$. The fragment ion $[PtCl(TPPM)\text{-}H]^-$ and the potassium adduct

$[PtCl(TPPMS)_2\text{-}H+K]^-$ are also suspected to have undergone cyclometalation. All of the ions that were successfully identified are listed within Table 4. Two other peaks with discernible platinum isotope patterns remain unidentified, with *m/z* values of 533.89 and 1070.77.

Table 4: Identified ions observed in the negative-ion ESI mass spectrum of *cis*-$[PtCl_2(TPPMS)_2]K_2$.

Ions (*m/z*)	Calculated (*m/z*)	Formula
340.98	341.04	$[TPPMS]^-$
356.56	357.04	$[TPPMS{=}O]^-$
570.86	570.97	$[PtCl(TPPMS)\text{-}H]^-$
876.86	876.04	$[Pt(TPPMS)_2\text{-}H]^-$
912.83	913.01	$[PtCl(TPPMS)_2]^-$
950.85	950.95	$[PtCl(TPPMS)_2\text{-}H+K]^-$
986.74	986.95	$[PtCl_2(TPPMS)_2+K]^-$

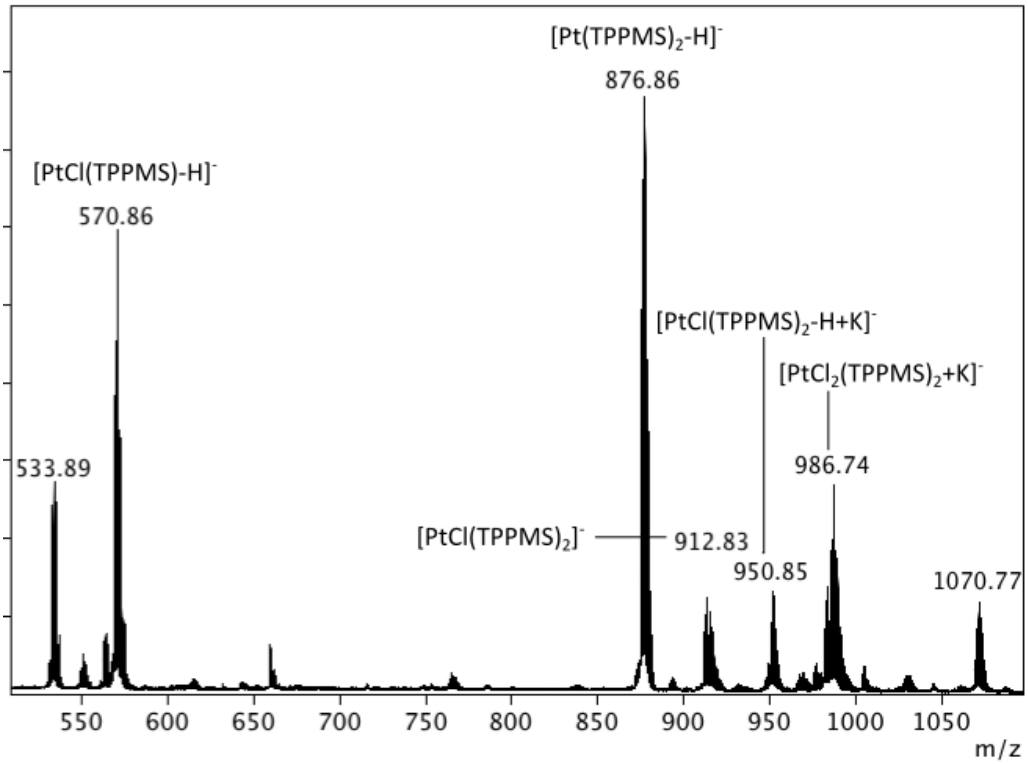

Figure 4.3: Negative-ion ESI mass spectrum of *cis*-$[PtCl_2(TPPMS)_2]K_2$ as a white precipitate. All peak assignments are listed in Table 4. CEV = -180 V MeOH solution.

The negative-ion ESI mass spectra of the three samples of *cis*-$[PtCl_2(TPPMS)_2]K_2$: the reaction solution, white precipitate, and the final yellow product after removal from solution, were recorded under the same ionisation

conditions. The three negative-ion ESI mass spectra for the three different samples are all the same, though a slight variation in ion intensity does occur. They all resembled Figure 4.3. These negative-ion ESI mass spectra on their own do not confirm that no decomposition or oxidation occurred during the transition between the fine white precipitate and sticky yellow solid. The spectra confirm the presence of the ions observed, that the complexes that form them are present in all three samples and have the same ionisation efficiency.

Another method used to investigate whether decomposition was occurring when the white precipitate changed to a sticky yellow solid, was to continuously repeat the final steps of the *cis*-$[PtCl_2(TPPMS)_2]K_2$ synthesis. This was done by redissolving the yellow product in DMF and adding diethyl ether again, thus forcing precipitation of the product as a fine white solid. The solid was then removed from solution, causing it to return to an oily yellow residue, before it dried into a yellow solid again in a desiccator. This process was repeated several times, with mass spectra obtained at each step. These spectra were all consistent with the previous spectrum obtained for the initial product (Figure 4.3 and Table 4). Therefore, it was concluded that the complex does not decompose during these transitions. If decomposition had occurred, the starting white precipitate would not be able to be repeatedly re-generated from the final product.

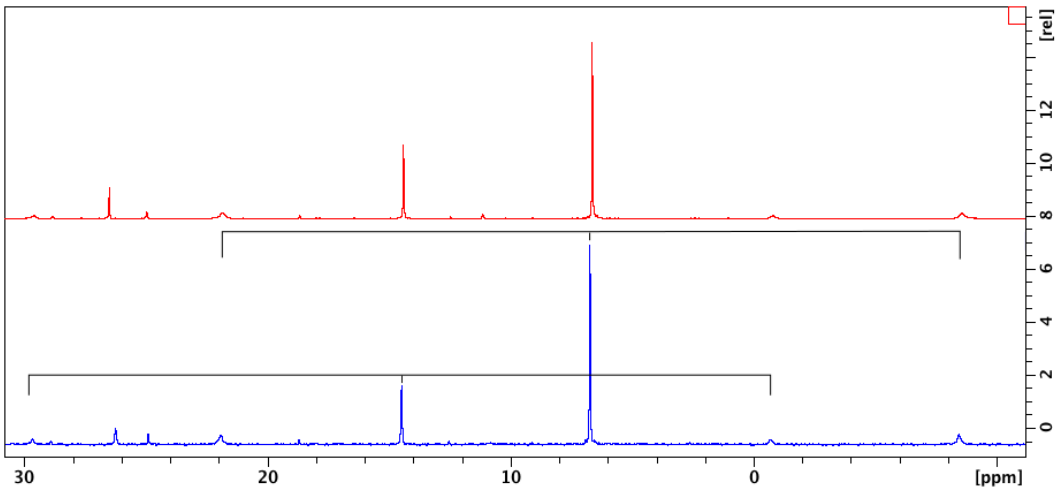

Figure 4.4: $^{31}P\{^{1}H\}$ NMR spectrum of *cis*-$[PtCl_2(TPPMS)_2]K_2$. The spectrum of the product as a white precipitate is on the bottom, while the spectrum of the product as a yellow solid is on the top. Both spectra are identical, the $^{1}J_{Pt\text{-}P}$ coupling are illustrated by solid black lines. Solvent DMSO-d_6, recorded at 121.5 MHz on a 300 MHz NMR spectrometer.

Further corroboration that no decomposition was occurring comes from the $^{31}P\{^{1}H\}$ NMR of both the white and yellow product. The two spectra (seen in Figure 4.4) are identical. Both spectra have two peaks with visible $^{1}J_{Pt\text{-}P}$ coupling. The singlet resonance at 14.4 ppm ($^{1}J_{Pt\text{-}P}$ 3686 Hz) corresponds to the complex *cis*-$[PtCl_2(TPPMS)_2]K_2$, which is consistent with literature values.[81] The complex responsible for the singlet resonance at 6.7 ppm ($^{1}J_{Pt\text{-}P}$ 3688 Hz) could not be determined. Both peaks have very similar $^{1}J_{Pt\text{-}P}$ coupling values (Table 4.1), indicating that the Pt-P bond in both complexes is nearly identical. The other phosphorus peaks present in the spectra remain mostly unidentifiable, except for that of TPPMS oxide at 28.8ppm.

Table 4.1: Observed resonances in the $^{31}P\{^{1}H\}$ NMR spectra of *cis*-$[PtCl_2(TPPMS)_2]K_2$.

Resonances (ppm)	$^{1}J_{Pt\text{-}P}$ (Hz)	Formula
14.4	3686	*cis*-$[PtCl_2(TPPMS)_2]K_2$
6.7	3688	Unknown
28.8	-	$(TPPMS)O^-$

4.2.1 Attempted Synthesis of $[Pt_2(\mu_2\text{-}S)_2(TPPMS)_4]K_4$

In the synthesis attempts of $[Pt_2(\mu_2\text{-}S)_2(TPPMS)_4]K_4$ from the starting material *cis*-$[PtCl_2(TPPMS)_2]K_2$, several 'one-pot' reactions were attempted to avoid the loss of material that arose when transferring the sticky yellow intermediate complex *cis*-$[PtCl_2(TPPMS)_2]K_2$. The first of two 'one-pot' reactions aiming to achieve the synthesis of $[Pt_2(\mu_2\text{-}S)_2(TPPMS)_4]K_4$ had the fewest alterations to the previous method used to synthesise *cis*-$[PtCl_2(TPPMS)_2]K_2$.[81] At the end of this method the DMF solution containing *cis*-$[PtCl_2(TPPMS)_2]K_2$ had sodium sulfide added directly to the reaction solution, in place of precipitation of *cis*-$[PtCl_2(TPPMS)_2]K_2$ with diethyl ether. After the sodium sulfide addition the reaction mixture was allowed to stir for 24 hours, before the excess diethyl ether was added to force precipitation. This resulted in the formation of an off-white precipitate that behaved in a similar manner to *cis*-$[PtCl_2(TPPMS)_2]K_2$: after the precipitate was removed from solution, the material became an oily residue but was then resolidified in a desiccator, becoming a dark orange solid.

The negative-ion ESI mass spectrum revealed only two anions of any significant intensity: TPPMS oxide and TPPMS sulfide. There were no platinum isotope patterns present in the negative-ion ESI mass spectrum. This was unexpected, if $[Pt_2(\mu_2\text{-}S)_2(TPPMS)_4]K_4$ was produced, it would have readily formed an anion through the SO_3^- group on the phenyl ring.

The positive-ion ESI mass spectrum revealed a large number of cations with charges of 1+ and 2+, all possessing isotope patterns that resemble platinum containing complexes. All of the 1+ cations observed in the spectrum had a mass too low to be the reaction product $[Pt_2(\mu_2\text{-}S)_2(TPPMS)_4]K_4$ or any of its adducts or fragments. The 2+ ions observed in the spectra also remained unidentified as they matched no $[Pt_2(\mu_2\text{-}S)_2(TPPMS)_4]K_4$ adduct or fragment.

To determine if any phosphorus-platinum bonding occurred in the product (as no ions were successfully identified in any mass spectra) the $^{31}P\{^1H\}$ NMR spectrum was obtained. This showed several resonances, all of which lacked platinum coupling, and most of which remained unassignable (Figure 4.5). The resonances present in the $^{31}P\{^1H\}$ NMR spectrum of the starting material *cis*-$[PtCl_2(TPPMS)_2]K_2$ (14.4 ppm and 6.7 ppm) were not present in this spectrum.

The resonance of greatest intensity in the spectrum given in Figure 4.5 was that of TPPMS sulfide, which was observed as a singlet at 44.3 ppm. A small resonance attributed to TPPMS oxide at 28.8 ppm was also present; this value agrees with the literature.[81] It was therefore concluded that the synthesis of $[Pt_2(\mu_2\text{-}S)_2(TPPMS)_4]K_4$ was unsuccessful but the known compound TPPMS sulfide was unintentionally synthesised.[86] No literature value for the $^{31}P\{^1H\}$ NMR of TPPMS sulfide was found, so a sample was prepared through the reaction of $[TPPMS]K\cdot H_2O$ and powdered elemental sulfur. The $^{31}P\{^1H\}$ NMR spectrum was recorded, a single singlet resonance at 44.3 ppm was observed.

There are two small resonances at -2.2 and -17.2 ppm, which are due to PTA oxide and PTA sulfide. The ligand PTA was not used in this reaction, so these signals are a result of small amounts of cross contamination occurring between the $Pt_2(\mu_2\text{-}S)_2(PTA)_4$ synthesis that was undertaken alongside the synthesis of

$[Pt_2(\mu_2\text{-}S)_2(TPPMS)_4]K_4$ and will have occurred in the preparation of the NMR samples.

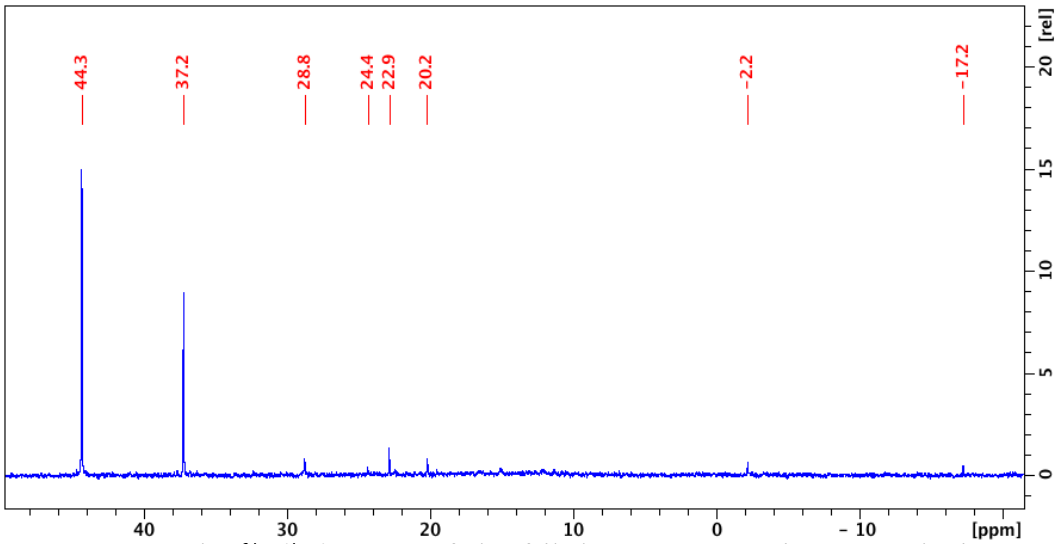

Figure 4.5: The $^{31}P\{^{1}H\}$ NMR of the failed 'one-pot' reaction to synthesise $[Pt_2(\mu_2\text{-}S)_2(TPPMS)_4]K_4$. Assignable peaks are TPPMS sulfide s 44.3 ppm, and TPPMS oxide 28.8 ppm. Recorded at 121.5 MHz on a 300 MHz NMR spectrometer.

As this 'one-pot' reaction had the least amount of change from the *cis*-$[PtCl_2(TPPMS)_2]K_2$ synthesis, before it was undertaken it was necessary to determine if the solvent used, DMF, would readily react with the $\{Pt_2(\mu_2\text{-}S)_2\}$ core. This was determined by a sample of $Pt_2(\mu_2\text{-}S)_2(PPh_3)_4$ being stirred and heated at 60° C for three hours in DMF. The positive-ion ESI mass spectrum of the solution was then recorded to determine if any reaction between the platinum complex and the solvent occurred. The spectrum showed the $\{Pt_2(\mu_2\text{-}S)_2\}$ core unaltered in the ions observed, with both the protonated and oxidised ions $[Pt_2(\mu_2\text{-}S)_2(PPh_3)_4+H]^+$ and $[Pt_2(\mu_2\text{-}S)_2(PPh_3)_4]^{\cdot+}$ both contributing to the isotope pattern at 1503 *m/z*.[12] This ion was the highest intensity in the spectrum, and the only one present of consequence, so it was determined that no reaction had taken place between the $\{Pt_2(\mu_2\text{-}S)_2\}$ core and the solvent.

The second 'one-pot' method undertaken to synthesise $[Pt_2(\mu_2\text{-}S)_2(TPPMS)_4]K_4$ involved the synthesis of *cis*-$[PtCl_2(TPPMS)_2]K_2$ in a benzene suspension, followed by the addition of $Na_2S{\cdot}9H_2O$ to form the desired product. This synthetic method was unsuccessful. The negative-ion ESI mass spectrum of the red solid collected showed no platinum complex ions were present. The ions

whose peaks were present in the spectrum were a result of $[TPPMS]^-$, $[TPPMS=O]^-$, and $[TPPMS=S]^-$. The positive-ion ESI spectrum revealed a considerable number of complexes (Figure 4.6). The cation of the greatest intensity at 693.10 *m/z* surprisingly corresponds to $[Pt_2(\mu_2\text{-}S)_2(cod)_4+Na]^+$, and the ion $[(Pt_2(\mu_2\text{-}S)_2(cod)_4)_2+Na]^+$ was also present, with a peak at 1364.18 *m/z*.

The ligand exchange reaction to form *cis*-$[PtCl_2(TPPMS)_2]K_2$ in solution between $PtCl_2(cod)$ and [TPPMS]K appeared to have been unsuccessful, as cod remained bonded to the platinum. This was unexpected due to cod's increased lability compared to [TPPMS]K. The complex $Pt_2(\mu_2\text{-}S)_2(cod)_2$ observed in the positive-ion ESI mass spectrum has not previously been documented in the literature, although analogues of it have been documented. A complex that bears similarities to the ions observed are $[Pt_2(\mu_3\text{-}S)_2(cod)_2Pt(dppp)]Cl_2$,[87] which differs in that it has a triplatinum sulfur core, with a phosphine ligand dppp bound to the third metal centre.

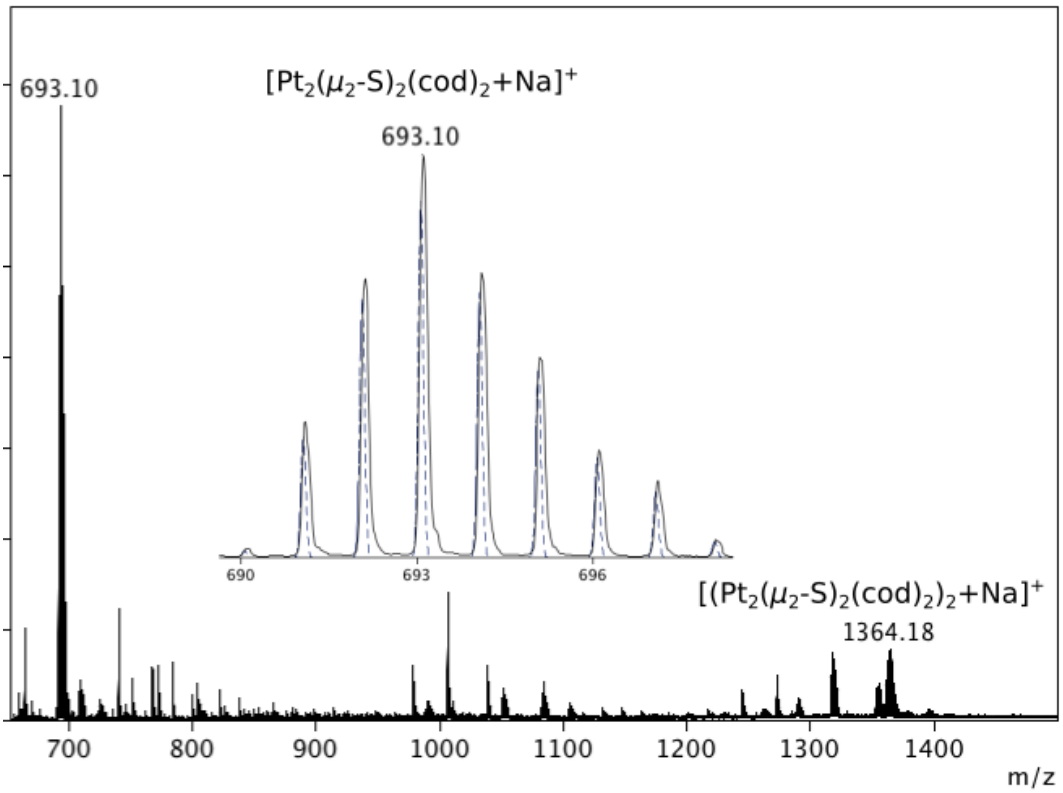

Figure 4.6: The positive-ion ESI mass spectrum from the failed $[Pt_2(\mu_2\text{-}S)_2(TPPMS)_4]K_2$ synthesis. The spectrum shows the presence of $[Pt_2(\mu_2\text{-}S)_2(cod)_2+Na]^+$ and $[Pt_2(\mu_2\text{-}S)_2(cod)_2)_2+Na]^+$. The inset spectrum shows the observed (solid line) and calculated (dashed line) isotope pattern of $[Pt_2(\mu_2\text{-}S)_2(cod)_2+Na]^+$.

Other known analogues are that of $Pt_2(\mu_2\text{-}OH)_2(cod)_2$ which has been used in the reactions of ethylene oxidation and $[Pt_2(\mu_2\text{-}Cl)_2(cod)_2](BF_4)_2$ which is air stable only for hours.[88,89]

4.3 Investigation into the Synthesis of $Pt_2(\mu_2\text{-}S)_2(cod)_2$

The complex $Pt_2(\mu_2\text{-}S)_2(cod)_2$ was serendipitously produced during the attempted synthesis of $[Pt_2(\mu_2\text{-}S)_2(TPPMS)_4]K_4$, (Section 4.2.1). This cod platinum complex had not previously been reported in the literature, so the synthetic method was repeated without the presence of $[TPPMS]K\cdot H_2O$ to check whether the synthesis of $Pt_2(\mu_2\text{-}S)_2(cod)_2$ was reproducible.

The reaction between $PtCl_2(cod)$ and $Na_2S\cdot 9H_2O$ in the absence of $[TPPMS]K\cdot H_2O$ was successful, the reaction suspension during the 48 h stirring period changed from the starting yellow to a red. Both starting materials in benzene individually are colourless; upon addition together in benzene a yellow colouration occurred at the beginning of the stirring. The red solid was collected from the filtration of the reaction suspension, the positive-ion ESI mass spectrum of this solid revealed a single platinum complex ion of $[Pt_2(\mu_2\text{-}S)_2(cod)_2+Na]^+$ 692.84 *m/z*. The product from the first synthesis of $Pt_2(\mu_2\text{-}S)_2(cod)_2$ decomposed during an attempt to remove the sodium salt by-products. Therefore the stability of the second synthesis was assessed. This involved a low temperature thermal decomposition assessment, where a dried sample of $Pt_2(\mu_2\text{-}S)_2(cod)_2$ was stored in a sealed vial for 14 days at 4 °C. The positive-ion ESI mass spectra of this sample was recorded periodically throughout this 2 week period. The mass spectra recorded all showed the same ion for $Pt_2(\mu_2\text{-}S)_2(cod)_2$, indicating that the complex did not decompose at low temperature.

An ambient temperature thermal decomposition assessment was also undertaken, where the $Pt_2(\mu_2\text{-}S)_2(cod)_2$ sample was stored at ambient temperature in a sealed vial over 16 days. This resulted in the decomposition of the complex. The decomposition was first noticed due to the smell of cod coming from the solid, which was accompanied by a colour change as the orange became lighter over

time. Positive-ion ESI mass spectra were recorded periodically over the two weeks, and the intensity of the $[Pt_2(\mu_2\text{-}S)_2(cod)_2+Na]^+$ peak decreased over time. The intensity of the $[Pt_2(\mu_2\text{-}S)_2(cod)_2+Na]^+$ ion peak was negligible after 16 days.

A freshly synthesised amount of $Pt_2(\mu_2\text{-}S)_2(cod)_2$ was prepared and studied extensively *via* NMR spectroscopy. First the ^1H NMR spectrum was recorded (Figure 4.7). Two resonances are not shown in the spectrum but are listed in Table 4.2. These resonances appear at 0.4 ppm (an unidentified resonance showing no $^2J_{Pt\text{-}H}$) and 7.2 ppm (a result of non-deuterated benzene being present).

Table 4.2: Resonances and integration data from the $Pt_2(\mu_2\text{-}S)_2(cod)_2$ ^1H NMR spectrum.

Resonances (ppm), $^2J_{Pt\text{-}H}$ (Hz)	Integration Values	Formula
7.2	-	C_6H_6
4.8, 55	1	CH
1.9	2.4	CH_2
1.5-1.4	3.6	CH_2
0.4	-	-

The resonance at 4.8 ppm ($^2J_{Pt\text{-}H}$ 55 Hz) is a result of the 4 hydrogen atoms of the alkenes in the cod ring bonded to the platinum, which are located on carbon 1 of the diagram within Figure 4.7. In total there are 12 hydrogen atoms in a cod ring, this leaves 8 remaining hydrogen atoms found in the 4 methylene groups, located

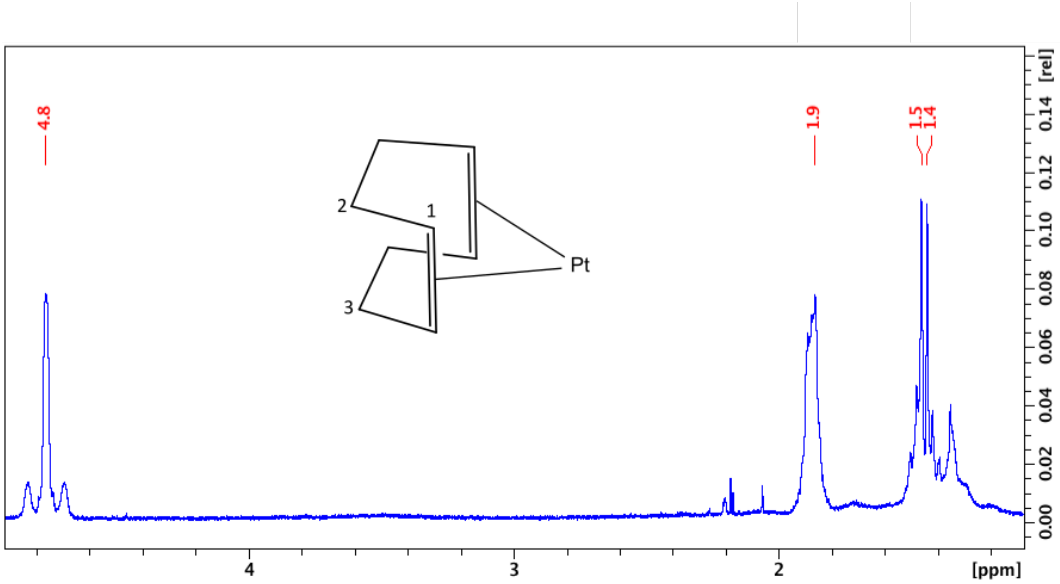

Figure 4.7: The ^1H NMR spectrum of $Pt_2(\mu_2\text{-}S)_2(cod)_2$, recorded on a 400 MHz NMR spectrometer. The inset diagram shows the proposed structure of $Pt_2(\mu_2\text{-}S)_2(cod)_2$, along the mirror plane. Solvent d_6-benzene.

on carbons 2 and 3 of the diagram within Figure 4.7 to provide the last two signals.

The 8 hydrogen atoms are not magnetically equivalent: 4 are in one magnetic environment and 4 are in another slightly different environment, which gives rise to the two resonances at 1.5 and 1.9 ppm. These two peaks are broad, making accurate integration of the peaks difficult.

For comparison, the ^{1}H NMR of the starting material $PtCl_2(cod)$ shows a resonance at 5.6 ppm ($^{2}J_{Pt\text{-}H}$ 68 Hz) which is a result of the alkene hydrogen atoms, and two peaks at 2.73 & 2.28 ppm, a result of the 4-methylene hydrogen atoms.[90] This provides supporting evidence that the two resonances at 1.8 and 1.5-1.4 ppm result from the 4-methylene groups lacking equivalence. It has previously been shown that the *trans*-influence of groups can affect the value of $^{2}J_{Pt\text{-}H}$ coupling.[91] A complex that demonstrates the high *trans*-influence of a sulfur atom on the alkene hydrogen atoms of cod, is the complex $[Pt(SC_6H_4CO_2)(cod)]$, with $^{2}J_{Pt\text{-}H}$ 49.73 Hz.[66] This helps to explain why the platinum-hydrogen coupling of $Pt_2(\mu_2\text{-}S)_2(cod)_2$ is smaller (55 Hz) than that in $PtCl_2(cod)$ (68 Hz).[90]

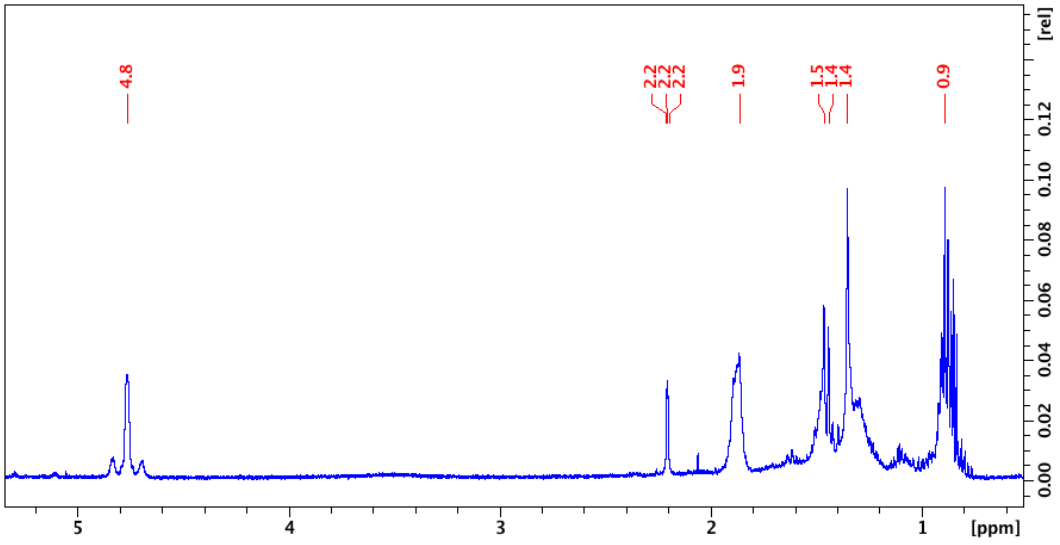

Figure 4.8: ^{1}H NMR spectrum of $Pt_2(\mu_2\text{-}S)_2(cod)_2$ showing the additional peaks from decomposition at 2.3, 1.4, and 0.9 ppm. Recorded on a 400 MHz NMR spectrometer in d_6-benzene.

The ^{1}H-^{1}H COSY spectrum of $Pt_2(\mu_2\text{-}S)_2(cod)_2$ (Figure 4.9) was also obtained. A small amount of time had lapsed between recording the ^{1}H NMR spectrum and recording the ^{1}H-^{1}H COSY, thus a new ^{1}H NMR spectrum was recorded to go along with the ^{1}H-^{1}H COSY in order to account for any decomposition that may have occurred in the time that lapsed. The decomposition of the product can be seen in the differences between the first ^{1}H NMR spectrum and the spectrum alongside the ^{1}H-^{1}H COSY experiment (Figure 4.8). There are several more peaks present as a result of decomposition.

The ^{1}H-^{1}H COSY spectrum (Figure 4.9) clearly shows the $^{3}J_{H\text{-}H}$ coupling interactions between the hydrogen atoms that give rise to the resonance at 4.8 ppm (CH) and 1.9 ppm (CH_2), an also the hydrogen atoms that give rise to the

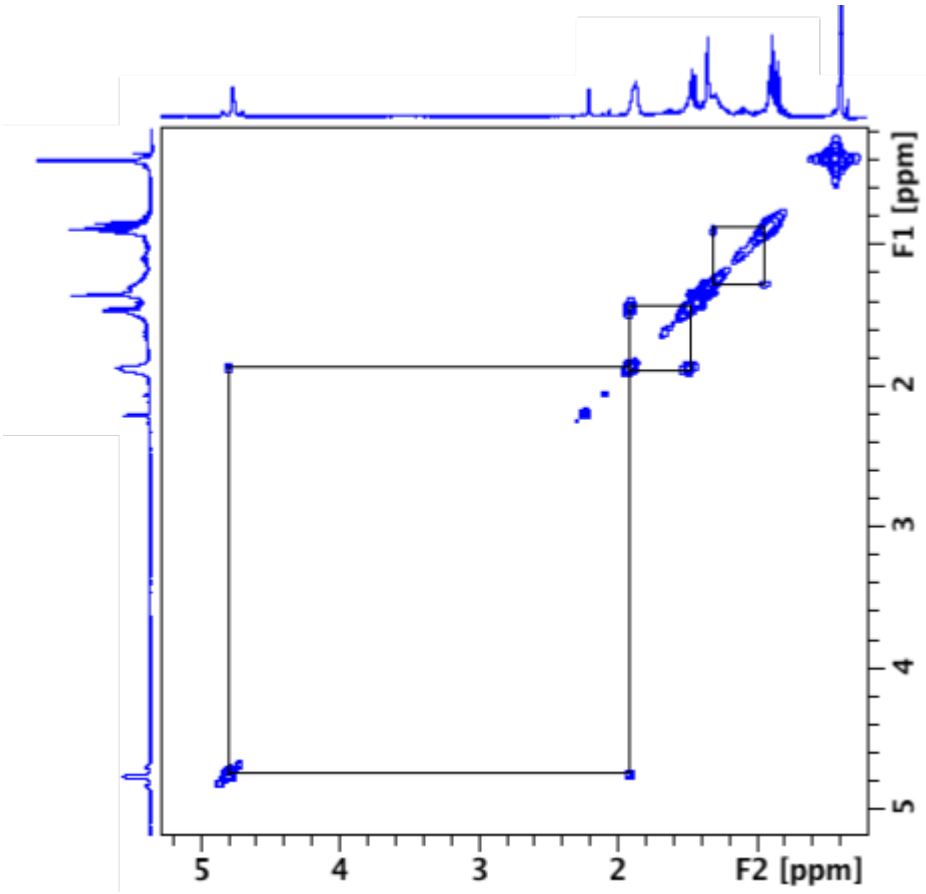

Figure 4.9: The ^{1}H-^{1}H COSY spectrum of $Pt_2(\mu_2\text{-}S)_2(cod)_2$ showing the $^{3}J_{H\text{-}H}$ coupling interactions as correlations between CH-CH_2 and CH_2-CH_2' that are present in the platinum complex, and also the coupling of the decomposition products. Recorded on a 400 MHz NMR spectrometer, in d_6-benzene. (black lines indicate correlations).

resonance at 1.9 ppm (CH_2) and 1.4 ppm (CH_2'). This spectrum supports the original atom assignment of the first ^{1}H NMR spectrum with the $^3J_{H\text{-}H}$ coupling present. It also shows that the unknown resonance present at 0.4 ppm (Table 4.2) has no involvement in the platinum complex, as no $^3J_{H\text{-}H}$ or $^2J_{Pt\text{-}H}$ couplings are observed in either the ^{1}H-^{1}H COSY or ^{1}H NMR spectrum.

The spectrum also shows $^3J_{H\text{-}H}$ coupling between the decomposition products (the resonances of which increased in intensity over time). This coupling indicates that some of the broadness of the 1.5 ppm resonance was contributed to by peaks from other hydrogen atoms overlapping in the spectrum. The coupling interactions between $Pt_2(\mu_2\text{-}S)_2(cod)_2$ and the unknown can be seen to begin from slightly different places on the same broad area, helping to explain why the integrations of this region are larger than suspected.

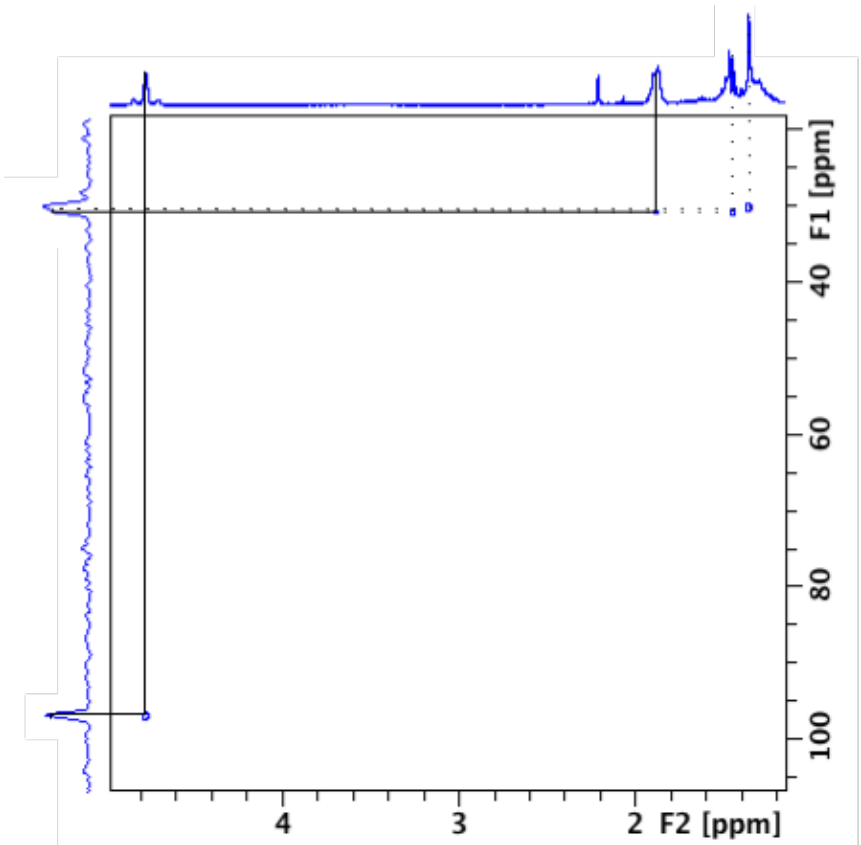

Figure 4.10: The ^{13}C-^{1}H HSQC spectrum of $Pt_2(\mu_2\text{-}S)_2(cod)_2$ showing $^1J_{H\text{-}C}$ correlations between couplings shown as black and dashed lines. Recorded on a 400 MHz NMR spectrometer, in d_6-benzene.

The ^{13}C-^{1}H HSQC spectrum further corroborates this as it shows there are two correlations caused by different carbon atoms within the broad resonances of the 1.5-1.4 ppm range in the ^{1}H NMR spectrum, indicated by the couplings to the carbon (CH_2) resonance at 30.4 ppm in the ^{13}C-^{1}H HSQC spectrum (dashed lines in Figure 4.10) This leaves two more correlations, one for the resonance at 1.9 ppm in the ^{1}H NMR spectrum to the carbon (CH_2) resonance at 30.4 ppm, and the final correlation observed is between the resonance at 4.8 ppm in the ^{1}H NMR spectrum to the carbon (CH) resonance at 96.5 ppm (Figure 4.10).

A synthetic method analogous to that used to produce $Pt_2(\mu_2\text{-}S)_2(cod)_2$ was carried out using the analogue $PtCl_2(bipy)$ (bipy = 2,2'-bipyridine). The $PtCl_2(bipy)$ complex was reacted with $Na_2S{\cdot}9H_2O$ in an attempt to form $Pt_2(\mu_2\text{-}S)_2(bipy)_2$, but this was not successful. The reaction solution became brown then deposited a black solid on the bottom of the flask. The positive- and negative-ion ESI mass spectra of this solid had no peaks with platinum isotope patterns. This provides an interesting contrast between $PtCl_2(cod)$ which forms the $\{Pt_2(\mu_2\text{-}S)_2\}$ core when reacted with $Na_2S{\cdot}9H_2O$, and $PtCl_2(bipy)$ which does not form the same core. Both the cod and bipy ligands are considered labile, but only one goes on to form the $\{Pt_2(\mu_2\text{-}S)_2\}$ core.

4.3.1 Reactions of $Pt_2(\mu_2\text{-}S)_2(cod)_2$ with Phosphine Ligands

The cod ligand is labile, being easily replaced with phosphine ligands. This can be seen in the reaction of $PtCl_2(cod)$ with PPh_3, giving *cis*-$PtCl_2(PPh_3)_2$.[92] Therefore the newly made $Pt_2(\mu_2\text{-}S)_2(cod)_2$ complex had its reactivity with PPh_3 assessed, to determine if the same ligand exchange was possible. $Pt_2(\mu_2\text{-}S)_2(cod)_2$ was synthesised following the method outlined in Sections 4.2.1 - 4.3, after which PPh_3 was added to the benzene suspension so that a molar ratio of 1:4 complex:ligand was reached. This solution was stirred for 24 hours, during which time a notable colour change occurred. The reaction suspension changed from the red of $Pt_2(\mu_2\text{-}S)_2(cod)_2$ to the orange associated with $Pt_2(\mu_2\text{-}S)_2(PPh_3)_4$.

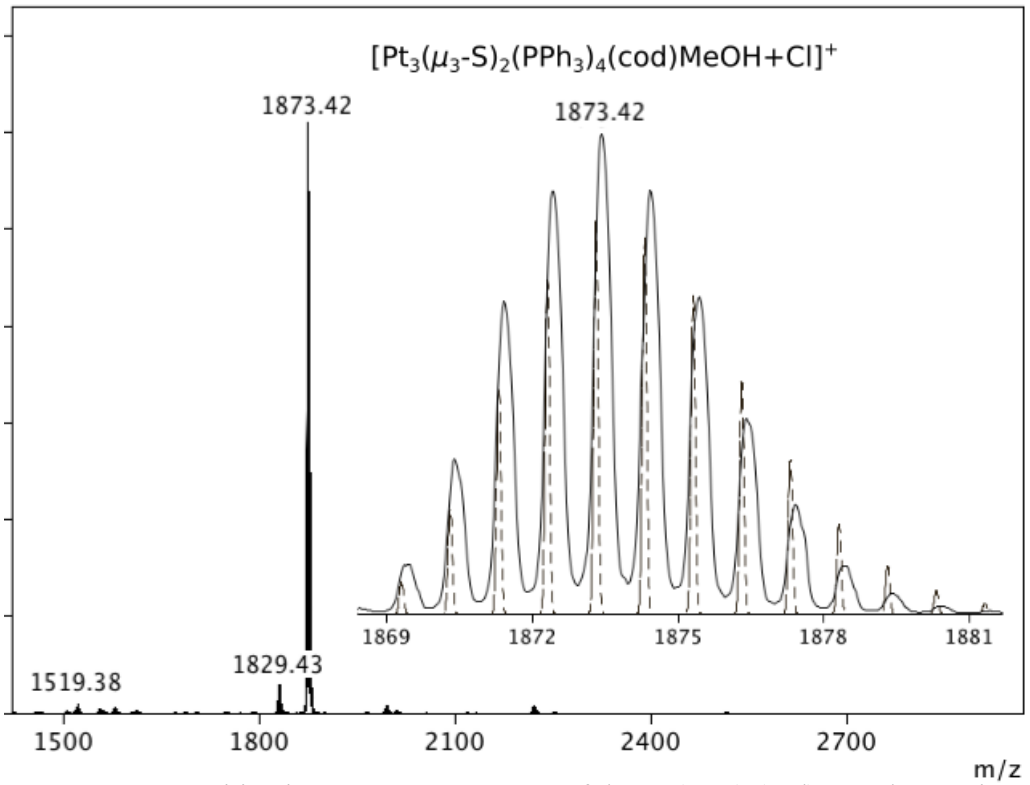

Figure 4.11: Positive-ion ESI mass spectrum of the $Pt_2(\mu_2\text{-}S)_2(cod)_2$ + PPh_3 reaction suspension. The inset spectrum shows both observed (solid line) and calculated (dashed line) isotope patterns of $[Pt_3(\mu_3\text{-}S)_2(PPh_3)_4(cod)MeOH+Cl]^+$. Less intense peaks resulting from the ions $[Pt_3(\mu_3\text{-}S)_2(PPh_3)_4(cod)+Na]^+$ and $[Pt_2(\mu_2\text{-}S)_2(PPh_3)_4O+H]^+$ are also present. CEV 150, MeOh solution.

The positive-ion ESI mass spectrum of the suspension was recorded after only a few hours of mixing. The spectrum showed an intense platinum complex ion peak that resulted from neither the reactant $Pt_2(\mu_2\text{-}S)_2(cod)_2$ nor the desired reaction product $Pt_2(\mu_2\text{-}S)_2(PPh_3)_4$. The peak was attributed to the ion of the triplatinum complex $[Pt_3(\mu_3\text{-}S)_2(PPh_3)_4(cod)MeOH+Cl]^+$ due to the isotope pattern (Figure 4.11), and indeed the formation of $[Pt_3(\mu_3\text{-}S)_2(PPh_3)_4(cod)MeOH+Cl]^+$ in the reaction solution was feasible, as the mass spectrum sample was prepared for analysis in a dilute MeOH solution. This explains the presence of MeOH in the ion as the sample was removed from a benzene suspension, so it would have needed to be introduced during this stage of analysis. This peak was accompanied by much lower intensity peaks attributed to the ions $[Pt_2(\mu_2\text{-}S)_2(PPh_3)_4O+H]^+$ (at 1519.38 *m/z*) and $[Pt_3(\mu_3\text{-}S)_2(PPh_3)_4(cod)+Na]^+$ (at 1829.42 *m/z*) a problem arises with this ion assignment as $[Pt_3(\mu_3\text{-}S)_2(PPh_3)_4(cod)+Na]^+$ although the mass and isotope pattern match. The charge is incorrect, as the ligands are neutral and the

platinum sulfur core is charged $\{Pt_3(\mu_3\text{-}S)_2\}^{2+}$, with the addition of a Na^+ would provide a 3+ complex. This assignment is therefore most likely incorrect even tho the isotope patterns match.

Upon filtration of the suspension, the solid collected had the distinct orange colouration of $Pt_2(\mu_2\text{-}S)_2(PPh_3)_4$. The positive-ion ESI mass spectrum was recorded and clearly showed peaks for the ions $[Pt_2(\mu_2\text{-}S)_2(PPh_3)_4+H]^+$ and $[Pt_2(\mu_2\text{-}S)_2(PPh_3)_4O+H]^+$ at values of 1503.86 and 1518.84 *m/z*, respectively. There were several smaller peaks with discernible platinum isotope patterns that could not be identified, at 1602.71 and 1702.63 *m/z*. There was also what appeared to be a triplatinum complex present at 2280.53 *m/z* (Figure 4.12).

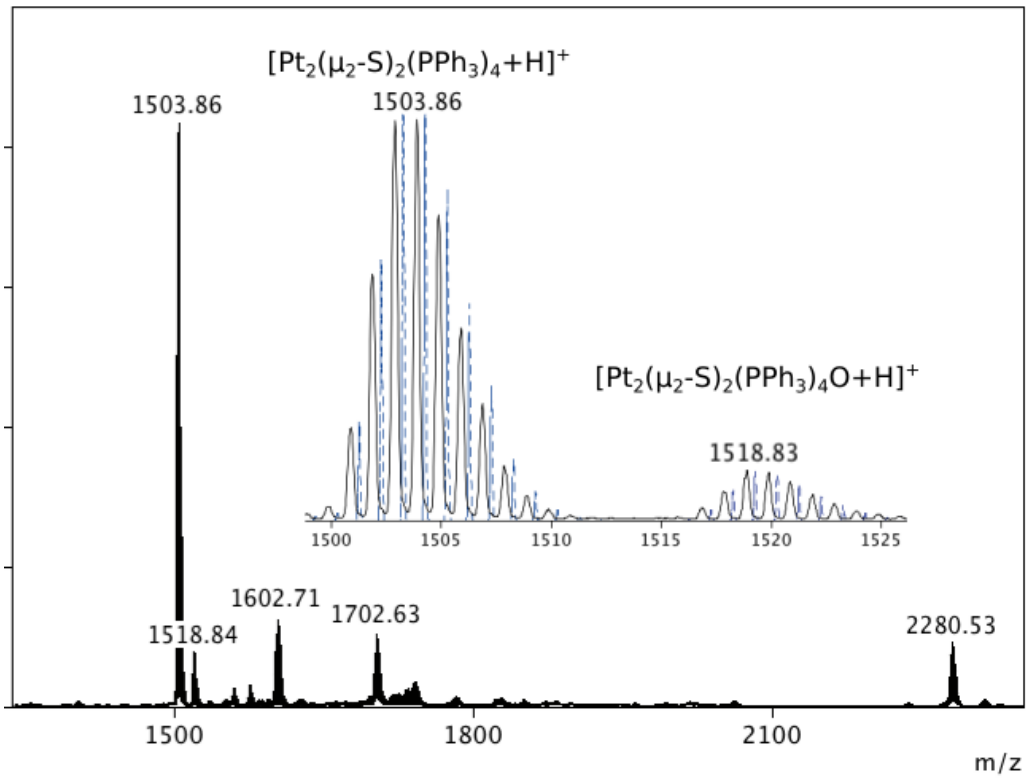

Figure 4.12: Positive-ion ESI mass spectrum of the dried product from the $Pt_2(\mu_2\text{-}S)_2(cod)_2 + PPh_3$ reaction. Relevant platinum ion peaks are shown, while low mass non-platinum ions are excluded. Inset shows the observed (solid line) and calculated (dashed line) isotope patterns of $[Pt_2(\mu_2\text{-}S)_2(PPh_3)_4+H]^+$ and $[Pt_2(\mu_2\text{-}S)_2(PPh_3)_4O+H]^+$. CEV 150 V, MeOH solution.

The filtrate from this reaction was burnt orange in colour and the mass spectrum of it showed high intensity peaks resulting from triplatinum ions. One of these peaks resulted from the $[Pt_3(\mu_3\text{-}S)_2(PPh_3)_4(cod)MeOH+Cl]^+$ ion that was

previously observed in the spectrum of the reaction solution (Figure 4.11.). This indicates that $Pt_3(\mu_3\text{-}S)_2(PPh_3)_4(cod)MeOH$ remained dissolved in solution and was thus separated from the desired product $Pt_2(\mu_2\text{-}S)_2(PPh_3)_4$ during filtration. The second prominent triplatinum ion observed was a peak at 1992 *m/z*, assigned to $[Pt_3(\mu_3\text{-}S)_2(PPh_3)_5S+H]^+$ as it possesses a closely matching isotope pattern and the formation of the complex in the mass spectrometer or as a side product of the reaction is feasible.

The reaction was partially successful, with $Pt_2(\mu_2\text{-}S)_2(PPh_3)_4$ forming as the major product due to ligand exchange occurring between the cod ligand and the unbound PPh_3. As this reaction was successful two other water-soluble phosphines were investigated to see if they are capable of undergoing the same ligand exchange with $Pt_2(\mu_2\text{-}S)_2(cod)_2$.

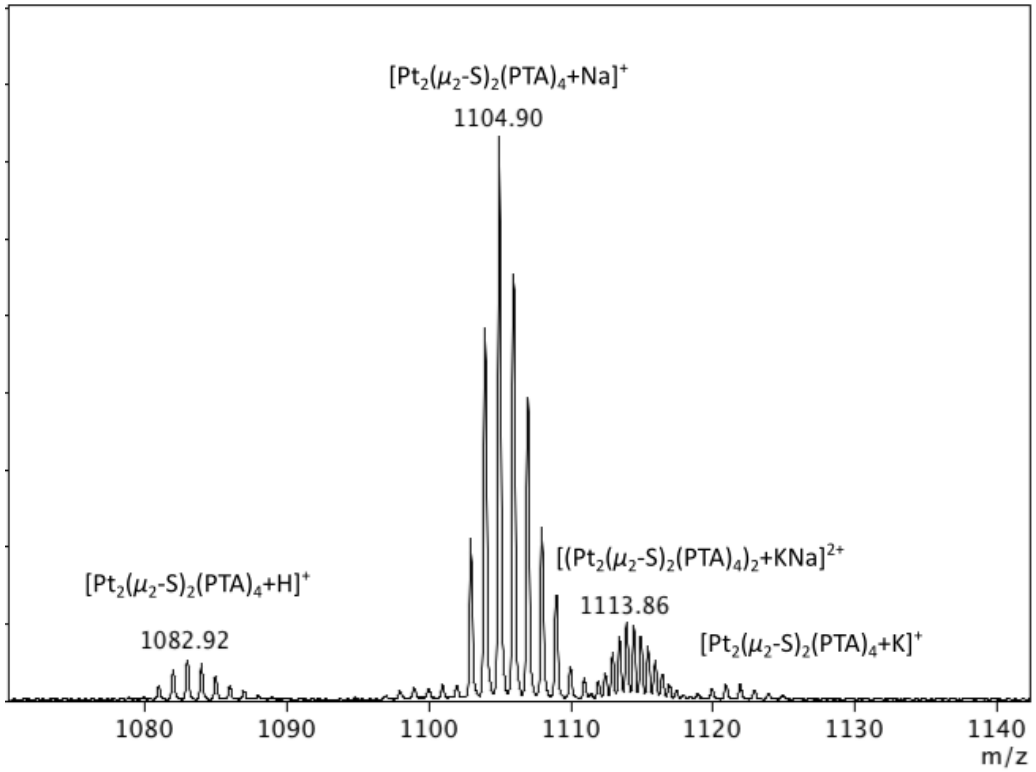

Figure 4.13: Positive-ion ESI mass spectrum of $Pt_2(\mu_2\text{-}S)_2(PTA)_4$ formed v*ia* ligand exchange between $Pt_2(\mu_2\text{-}S)_2(cod)_2$ and PTA. CEV 150V, MeOH/water (2:5) solution.

The two phosphines used were $[TPPMS]^-$ and PTA. As PPh_3 exchanged readily, it is not unreasonable to assume that a similar exchange would happen for its monosulfonated form, $[TPPMS]^-$. However $[TPPMS]^-$ did not appear to react with $Pt_2(\mu_2\text{-}S)_2(cod)_2$ under the same reaction conditions as were used for PPh_3. The positive- and negative-ion ESI mass spectra of the product and reaction solution revealed no peaks with discernible platinum isotope patterns and there was no evidence of any substitution of $[TPPMS]^-$ for cod occurring during the attempted reaction. The starting material $Pt_2(\mu_2\text{-}S)_2(cod)_2$ was no longer visible in the positive-ion ESI mass spectrum either, indicating decomposition during the attempted reaction had occurred. This is supported by the observed colour change of the solid product, which was more yellow than the orange starting material. The $[TPPMS]^-$ ligand itself was fairly prominent within the negative-ion ESI mass spectrum, along with its oxide and sulfide forms.

The next reaction investigated was a ligand exchange reaction between PTA and the $Pt_2(\mu_2\text{-}S)_2(cod)_2$ complex. This reaction was partially successful, with a peak attributed to the ion $[Pt_2(\mu_2\text{-}S)_2(PTA)_4+Na]^+$ strongly visible in the positive-ion ESI mass spectrum. Peaks attributed to the ions $[Pt_2(\mu_2\text{-}S)_2(PTA)_4+H]^+$ and $[(Pt_2(\mu_2\text{-}S)_2(PTA)_4)_2\,H_2O+2Na]^{2+}$ were also observed (Figure 4.13).

Ligand exchange between $Pt_2(\mu_2\text{-}S)_2(cod)_2$ and unbound PTA has been shown to be an alternative route of synthesis for the complex $Pt_2(\mu_2\text{-}S)_2(PTA)_4$. PTA has been discussed in more depth in Chapter 2. However this synthetic method fails to provide a pure product. This is revealed by the $^{31}P\{^1H\}$ NMR spectrum of the product (Figure 4.14), as there are several phosphorus resonances present in the spectrum. One of these was attributed to the desired platinum complex $Pt_2(\mu_2\text{-}S)_2(PTA)_4$ (-54.4 ppm) at an intensity so low the $^1J_{Pt\text{-}P}$ coupling is barely visible. The highest intensity resonances present were attributed to PTA=S (-17.2 ppm) and PTA=O (-2.2 ppm).

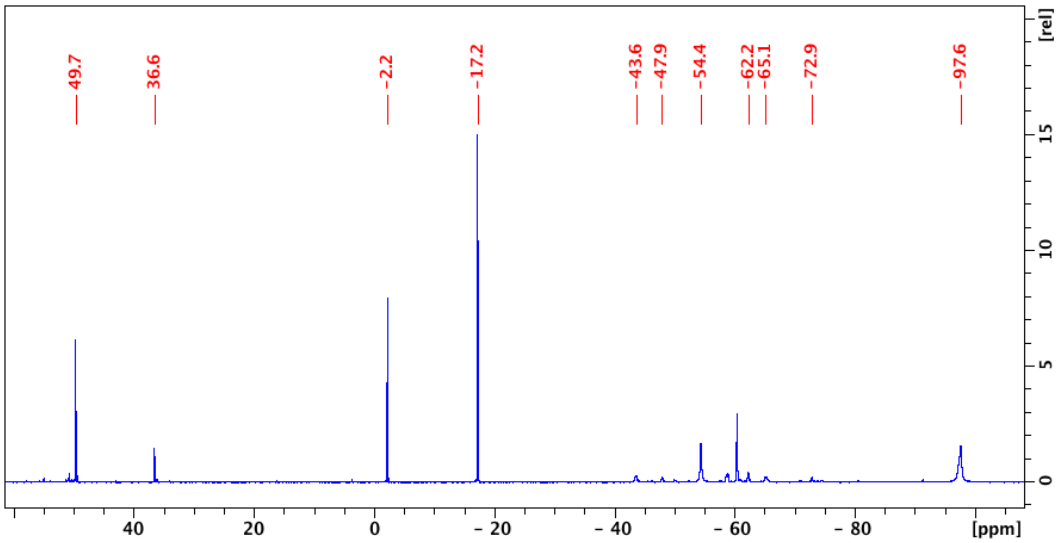

Figure 4.14: $^{31}P\{^{1}H\}$ NMR spectrum of $Pt_2(\mu_2\text{-}S)_2(PTA)_4$, produced from the reaction of $Pt_2(\mu_2\text{-}S_2)(cod)_2$ and PTA. The peak assignments are as follows: PTA oxide at -2.2 ppm, PTA sulfide at -17.2 ppm, $Pt_2(\mu_2\text{-}S)_2(PTA)_4$ at -54.4 ppm. Recorded at 121.5 MHz on a 300 MHz NMR spectrometer in D_2O.

4.4 Attempted Synthesis of $[Pt_2(\mu_2\text{-}S)_2(TPPMS)_4]K_4$ Directly from $Pt_2(\mu_2\text{-}S)_2(PPh_3)_4$

An attempt at a biphasic ligand exchange reaction between the phosphine ligand $[TPPMS]^-$ and the platinum complex $Pt_2(\mu_2\text{-}S)_2(PPh_3)_4$ was undertaken. The reaction replicated the PTA biphasic ligand exchange reaction (Section 2.7), with water and toluene as the solvents used, with ratios of $Pt_2(\mu_2\text{-}S)_2(PPh_3)_4$ to $[TPPMS]K\cdot H_2O$ at 1:1, 1:2, 1:3, 1:4.

The reaction was deemed to be unsuccessful, as the positive- and negative-ion ESI mass spectra failed to show any peaks corresponding to $[TPPMS]^-$ substituted complexes with either the di or triplatinum sulfide core. Both spectra did show peaks indicating the presence of the respective starting materials, $[Pt_2(\mu_2\text{-}S)_2(PPh_3)_4+H]^+$ in the positive-ion spectrum and the ligand $[TPPMS]^-$ and its oxide in the negative-ion spectrum.

In order to rule out the possibility that this ligand exchange reaction and the other synthetic methods attempted in Sections 4.2.1 and 4.3.1 were all unsuccessful due to the quality of the ligand initially prepared, the $^{31}P\{^{1}H\}$ NMR of the (TPPMS)K·H_2O was obtained to ensure the purity, shown in Figure 4.15. The spectrum shows two singlet resonances $[TPPMS]^-$ at 5.5 ppm and TPPMS=O at 26.5 ppm which are both in line with reported literature measurements.[81,83] This provides evidence that the unsuccessful reactions are not due to the quality of the ligand prepared.

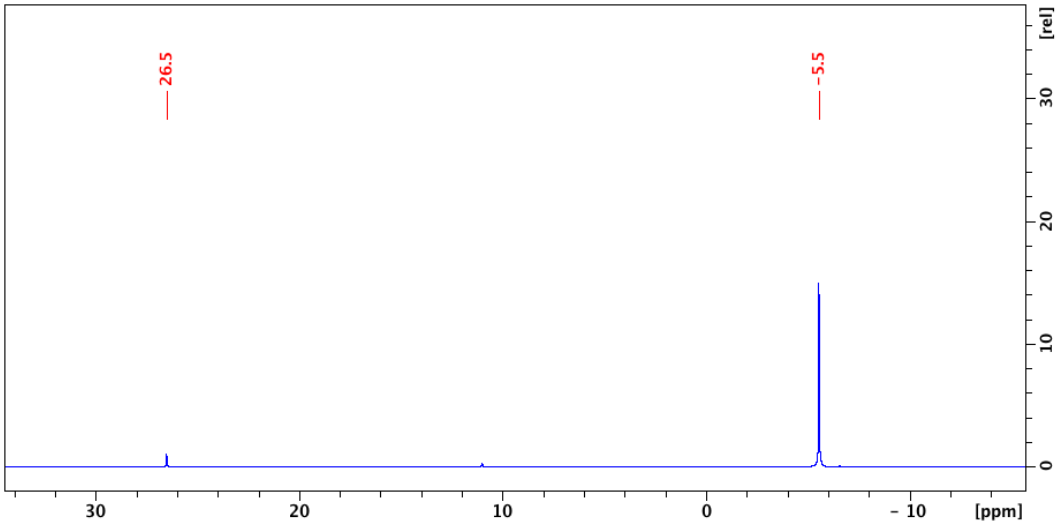

Figure 4.15 $^{31}P\{^{1}H\}$ NMR of (TPPMS)K·H_2O. $[TPPMS]^-$ s 5.5 ppm. TPPMS=O s 26.5 ppm. Recorded at 121.5 MHz on a 300 MHz NMR spectrometer in a solvent of DMSO-d_6.

4.5 Conclusion

Monosulfonated triphenylphosphine in the form (TPPMS)K·H_2O was used during several unsuccessful attempts to synthesise the complex $[Pt_2(\mu_2\text{-}S)_2(TPPMS)_4]K_4$. None of the synthetic attempts revealed the desired reaction product in the negative-ion ESI mass spectra acquired. This phosphine ligand was selected for the attempted synthesis due to its water-solubility and its similarity to PPh_3, along with the fact that its reaction products are easily analysed: all complexes formed would be anions that could be identified through negative-ion ESI mass spectrometry, and this was the primary analytical method used. This method of analysis, alongside $^{31}P\{^{1}H\}$ NMR spectroscopy, demonstrated that $[TPPMS]^-$ was not a suitable ligand for the $\{Pt_2(\mu_2\text{-}S)_2\}$ core.

An attempted synthesis of $[Pt_2(\mu_2\text{-}S)_2(TPPMS)_4]K_4$ did yield the platinum complex $Pt_2(\mu_2\text{-}S)_2(cod)_2$ which is unreported in the literature. Further research in to the successful synthesis and characterisation of this new platinum complex was completed. The complex was prepared *via* the reaction of $PtCl_2(cod)$ and $Na_2S{\cdot}9H_2O$ in a benzene suspension. The characterisation was completed by positive-ion ESI mass spectrometry and NMR spectroscopy. Both 1D NMR spectroscopy (^1H, $^{31}P\{^1H\}$) and 2D NMR spectroscopy (^1H-^1H COSY and ^{13}C-^1H HSQC) were used. The complex $Pt_2(\mu_2\text{-}S)_2(cod)_2$ was found to be thermally unstable, decomposing over 16 days while stored at ambient temperature. Before decomposition occurs the cod ligand can readily be exchanged for the phosphine ligands PPh_3 and PTA producing the respective $Pt_2(\mu_2\text{-}S)_2(L)_4$ (L = PPh_3, PTA) complexes. A possible reason for instability of the cod complex is because S^{2-} has high *trans*-influence, subsequently making the cod more labile, resulting in decomposition.

4.6 Experimental

The general experimental work and chemical suppliers, accompanied by the equipment parameters are detailed in Appendix 1.

4.6.1) Synthesis of cis-[$PtCl_2(TPPMS)_2$]K_2

The literature method was used,[81] with $PtCl_2(cod)$ (0.0534g, 0.14 mmol) and $[TPPMS]K{\cdot}H_2O$ (0.1089 g, 0.27 mmol) being reacted in DMF at 60 °C while being stirred for 4 h. The reaction was performed under a N_2 atmosphere. When at ambient temperature the addition of diethyl ether was made to force precipitation.

Filtration of the white precipitate resulted in it changing to a yellow oil. Drying under vacuum provides a yellow solid. The solid appeared to be hygroscopic, becoming oily after being removed from the desiccator. The reaction to produce *cis*-$[PtCl_2(TPPMS)_2]K_2$ was repeated several times in an effort to understand the change it undergoes from the white precipitate to yellow oil. The resulting ESI-MS and $^{31}P\{^1H\}$ NMR spectra are discussed in Section 4.1. It was determined that no decomposition is occurring when the precipitate undergoes the change.

4.6.2) Monitoring $Pt_2(\mu_2\text{-}S)_2(PPh_3)_4$ Stability in DMF

A sample of $Pt_2(\mu_2\text{-}S)_2(PPh_3)_4$ (small spatula full) was added to DMF (10 mL). This solution was then heated to 60 °C while being continually stirred for 3 h. The reaction solution remained the distinct orange of $Pt_2(\mu_2\text{-}S)_2(PPh_3)_4$. The solution became darker during the midpoint of the reaction time, but had lightened to the original orange by the end of the 3 h. During this it was monitored periodically with positive-ion ESI mass spectra.

The only notable cation in the positive-ion ESI-MS spectrum was $[Pt_2(\mu_2\text{-}S)_2(PPh_3)_4+H]^+$ at 1504.27 *m/z*. This stability assessment was performed to determine if the $\{Pt_2(\mu_2\text{-}S)_2\}$ core was stable in DMF, to determine if DMF was a suitable reaction medium for further experimentation.

4.6.3) Attempted Synthesis of $[Pt_2(\mu_2\text{-}S)_2(TPPMS)_4]K_4$ via a "one-pot" Reaction Method, using a DMF Reaction Solution

cis-$[PtCl_2(TPPMS)_2]K_2$ was synthesised *in situ* according to Section 4.6.1 from $PtCl_2$(cod) (0.0504g, 0.13 mmol) and $[TPPMS]K\cdot H_2O$ (0.104 g, 0.26 mmol).

After cooling, $Na_2S\cdot 9H_2O$ (0.1604 g, 0.66 mmol) was added to the DMF solution. The solution was then stirred continually for 48 h, after this point the solution was a yellow-orange. An excess of diethyl ether (approximately 50 mL) was added forcing precipitation of an off-white slightly yellow solid to occur. The solid was filtered *via* a Büchner funnel, whereupon the precipitate changed to a dark yellow-orange oil, which was then dried under vacuum.

The solid demonstrated the same hygroscopic behaviour as *cis*-$[PtCl_2(TPPMS)_2]K_2$ when removed from solution.

4.6.4) Attempted Synthesis of $[Pt_2(\mu_2\text{-}S)_2(TPPMS)_4]K_4$ via a "one-pot" Reaction Method, using a Benzene Suspension

First *cis*-$[PtCl_2(TPPMS)_2]K_2$ was prepared *in situ* in a benzene (10 mL) suspension heated to 60 °C, under a N_2 atmosphere for 3 h, from $PtCl_2$(cod) (0.056 g 0.15 mmol) and [TPPMS]K·H_2O (0.1075 g, 0.27 mmol).The suspension was a burnt yellow-brown during the heating. The reaction suspension was continually stirred while cooling, followed by addition of $Na_2S·9H_2O$ (0.1571 g, 0.65 mmol), which resulted in the colour becoming more orange. The reaction suspension was then stirred continually for 48 h, after which the orange colouration intensified.

Filtration of the suspension *via* a Büchner funnel and drying under vacuum provided a dark orange solid. Positive-ion ESI mass spectrum reveals 693.10 *m/z* $[Pt_2(\mu_2\text{-}S)_2(cod)_2+Na]^+$ as the major ion present.

Followed by preferentially dissolving the present sodium salts in an attempted purification, the isolated solid was dissolved in the minimum amount of ethanol then filtered followed by evaporation. This led to decomposition of $Pt_2(\mu_2\text{-}S)_2(cod)_2$ while in solution, this is supported by the strong smell of cod that was present coming from the ethanol solution. The positive-ion ESI-MS spectrum that was recorded during the evaporation of the solvent also showed a complete lack of the $[Pt_2(\mu_2\text{-}S)_2(cod)_2+Na]^+$ ion accompanied by several unidentified non-platinum peaks. The colour of the solution did not change much in this time, the orange solid collected after evaporation resulted in a similar positive-ion ESI-MS spectrum with negligible amounts of $[Pt_2(\mu_2\text{-}S)_2(cod)_2+Na]^+$.

4.6.5) Synthesis of $Pt_2(\mu_2\text{-}S)_2(cod)_2$

$PtCl_2$(cod) (0.05 g, 0.13 mmol) and $Na_2S·9H_2O$ (0.16 g, 0.66 mmol) in a benzene suspension (10 mL) were continually stirred for 48 h. The suspension started the stirring with a yellow colouration and after the 24 h the solution was red, and after the 48 h, a red solid had been deposited on the bottom of the flask.

The solid was collected *via* a Büchner funnel, washed with benzene (5 mL) and dried under vacuum. No further purification attempts were made. The positive-ion ESI-MS spectrum showed $[Pt_2(\mu_2\text{-}S)_2(cod)_2+Na]^+$ 693.10 *m/z* as the major ion product. This method was used to produce the sample that was used for the thermal decomposition assessments, along with the NMR study of $Pt_2(\mu_2\text{-}S)_2(cod)_2$. It was shown that after a period of time no greater than two weeks, that $Pt_2(\mu_2\text{-}S)_2(cod)_2$ decomposes at ambient temperature, discussed in Section 4.3.

4.6.7) Attempted Reaction Between $PtCl_2(bipy)$ and $Na_2S{\cdot}9H_2O$

An identical synthetic method for the production of $Pt_2(\mu_2\text{-}S)_2(cod)_2$ (Section 4.6.5) was used. $PtCl_2(bipy)$ (0.0492 g, 0.12 mmol) was used in place of the $PtCl_2(cod)$ along with $Na_2S{\cdot}9H_2O$ (0.056 g, 0.23 mmol).

Four to five hours into the 24 h mixing period the solution deposited a black precipitate along the bottom of the reaction vessel. The positive- and negative-ion ESI mass spectra of the reaction suspension and final solid collected revealed a lack of platinum complexes.

4.6.8) Synthesis of $Pt_2(\mu_2\text{-}S)_2(PPh_3)_4$ from $Pt_2(\mu_2\text{-}S)_2(cod)_2$

The synthetic method for $Pt_2(\mu_2\text{-}S)_2(cod)_2$ followed Section 4.6.5 using $PtCl_2(cod)$ (0.10 g, 0.26 mmol) and $Na_2S{\cdot}9H_2O$ (0.32 g, 1.33 mmol). After the 48 h mixing period PPh_3 (0.1407 g, 0.53 mmol) was added to the reaction suspension. Mixing continued for another 24 h. The now orange suspension was filtered *via* a Büchner funnel and dried under vacuum. Yield 0.1274 g, 0.085 mmol (63.4 %).

The positive-ion ESI mass spectrum showed a strong presence of $[Pt_2(\mu_2\text{-}S)_2(PPh_3)_4+H]^+$, the reaction filtrate remained yellow in colouration. The results of the positive-ion ESI-MS characterisation of this are discussed in Section 4.3.1.

4.6.9) Synthesis of $Pt_2(\mu_2\text{-}S)_2(PTA)_4$ from $Pt_2(\mu_2\text{-}S)_2(cod)_2$

A sample of $Pt_2(\mu_2\text{-}S)_2(cod)_2$ (0.053 g, 0.086 mmol) synthesised with the method in Section 4.6.5 was added to benzene (10 mL) followed by 4 mole equivalents of PTA (0.0577 g, 0.37 mmol). The suspension was stirred for 24 h. The $Pt_2(\mu_2\text{-}S)_2(cod)_2$ red solid clumped at the bottom of the flask and over the 24 h duration changed to the yellow-green of $Pt_2(\mu_2\text{-}S)_2(PTA)_4$. The suspension was filtered *via* a Büchner funnel, washed with benzene (10 mL), and dried under vacuum.

The resulting positive-ion ESI mass spectrum showed a strong presence of $[Pt_2(\mu_2\text{-}S)_2(PTA)_4+H]^+$ (1083.88 *m/z*) and the related sodium adduct. The $^{31}P\{^1H\}$ NMR showed the resonance of -54.3 ppm, $^1J_{(Pt\text{-}P)}$ 2616 Hz (D_2O) 300 MHz, at far lower intensity then is expected for a pure product. Significant resonances for PTA=S (-17.2) ppm and PTA=O (-2.2) ppm were observed.

4.6.10) Attempted Synthesis of $[Pt_2(\mu_2\text{-}S)_2(TPPMS)_4]K_4$ from $Pt_2(\mu_2\text{-}S)_2(cod)_2$

A sample of $Pt_2(\mu_2\text{-}S)_2(cod)_2$ (0.167 g, 0.24 mmol) was added to benzene (10 mL) followed by TPPMS (0.403 g, 1 mmol), and the suspension stirred for 24 h. The orange-red suspension was filtered *via* a Büchner funnle and the orange-red solid was washed with benzene (5 mL), and dried under vacuum.

The resulting negative-ion ESI mass spectrum showed the strong presence of $[TPPMS]^-$ along with its oxide and sulfide. The positive-ion ESI mass spectrum revealed a lack of platinum complex ions.

4.6.11) Attempted Synthesis of $[Pt_2(\mu_2\text{-}S)_2(TPPMS)_4]K_4$ Through a Biphasic Ligand Exchange

This reaction was prepared using a suitable sealable sample vial containing the biphasic reaction solvents of distilled water (20 mL) and toluene (20 mL). Added to the vial was $Pt_2(\mu_2\text{-}S)_2(PPh_3)_4$ (0.04 g, 0.026 mmol) and $[TPPMS]K\cdot H_2O$ (0.36, 0.106 mmol) with 4 mole equivalents. The sealed vial was stirred continuously for 7 days. During this the $Pt_2(\mu_2\text{-}S)_2(PPh_3)_4$ as an orange mass floated in the aqueous

phase and around the phase boundary the solvents were allowed to settle before samples of the aqueous phase were taken for negative-ion ESI mass analysis. No ligand-exchanged complexes were observed. This was simultaneously repeated with ratios of $Pt_2(\mu_2\text{-}S)_2(PPh_3)_4$ to $[TPPMS]K\cdot H_2O$ at 1:1, 1:2, 1:3.

4.6.12) Synthesis of TPPMS Sulfide

A sample of $[TPPMS]K\cdot H_2O$ (small spatula full) and powdered elemental sulfur (small spatula full) was stirred continually in a solution of distilled water at 60 °C over 3 h. The phosphine sulfide was obtained from evaporation of the solvent after undissolved and unreacted solids were removed by gravity filtration.

The negative-ion ESI mass spectrum showed the ion of TPPMS sulfide 373 *m/z* $^{31}P\{^1H\}$ NMR s, 44.3 ppm (D_2O) recorded at 121.5 MHz on a 300 MHz NMR spectrometer.

Chapter 5: Synthesis of Tris(2-carboxyethyl)phosphine (TCEP) Complexes

5.1 Synthesis and Characteristics of TCEP·HCl

Tris(2-carboxyethyl)phosphine (TCEP, Figure 5), which can be synthesised as its hydrochloride, is another phosphine ligand that was investigated for its coordination to the $\{Pt_2(\mu_2\text{-}S)_2\}$ core to produce a water-soluble complex of the general form $Pt_2(\mu_2\text{-}S)_2(L)_4$. This phosphine has previously been documented as a co-ordinating ligand in monoplatinum complexes. An example of this is *cis*-$PtCl_2(TCEP)_2$,[93] which was used as starting material in later synthetic attempts.

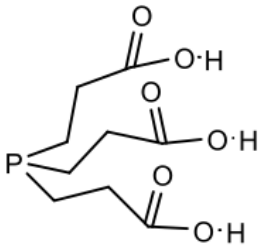

Figure 5: Diagram of TCEP.

TCEP·HCl was synthesised *via* the hydrolysis of tris(2-cyanoethyl)phosphine with concentrated aqueous HCl under reflux in a N_2 atmosphere. This was followed by cooling, filtration of the precipitate and recrystallisation in water.[94]

5.2 Synthesis of *cis*-$PtCl_2(TCEP)_2$

Cis-$PtCl_2(TCEP)_2$ was the starting material used in the first attempt to make the $Pt_2(\mu_2\text{-}S)_2(TCEP)_4$ complex. The monoplatinum complex was first synthesised using a literature method with one slight alteration.[93] The literature method started with *cis*-$PtCl_2(CH_3CN)_2$ as the initial platinum complex, while $PtCl_2$(cod) was used here, due to its availability. This reaction took place in water with a 1:2 molar ratio of $PtCl_2$(cod) and TCEP·HCl, this reaction solution was stirred at ambient temperature for 24 hours before filtration and evaporation of the solution allowed for the collection of solid *cis*-$PtCl_2(TCEP)_2$.

The positive-ion ESI mass spectrum for the white solid produced from this reaction is given in Figure 5.1 before recrystallisation from water, the peak with the greatest intensity was at 694 *m/z*. After recrystallisation this changed, with the most intense peak observed at 716 *m/z*. The desired product, *cis*-$PtCl_2(TCEP)_2$,

was not observed in the spectrum. The *cis*-$PtCl_2(TCEP)_2$ appeared to have readily lost the chloride ligands, giving the ions $[Pt(TCEP)_2\text{-}2H+Na]^+$ and $[Pt(TCEP)_2\text{-}H]^+$. Both ions appeared to have at least one deprotonated carboxylic acid group, however which group(s) was/were deprotonated was not known with certainty. This deprotonation may have led to cyclisation within the ion (Figure 5.2), where the now O^- group bonds to the platinum forming a six-membered ring, resulting in a three-coordinated platinum complex with a 1+ charge. The cyclisation of TCEP while acting as a ligand has been documented in the literature,[93,95,96] and the X-ray crystal structure of $[PdCl\{P\{RCOO\text{-}\kappa O\text{-}\mu\text{-}O)(RCOOD)_2\text{-}\kappa P\}]$ has been reported.[96]

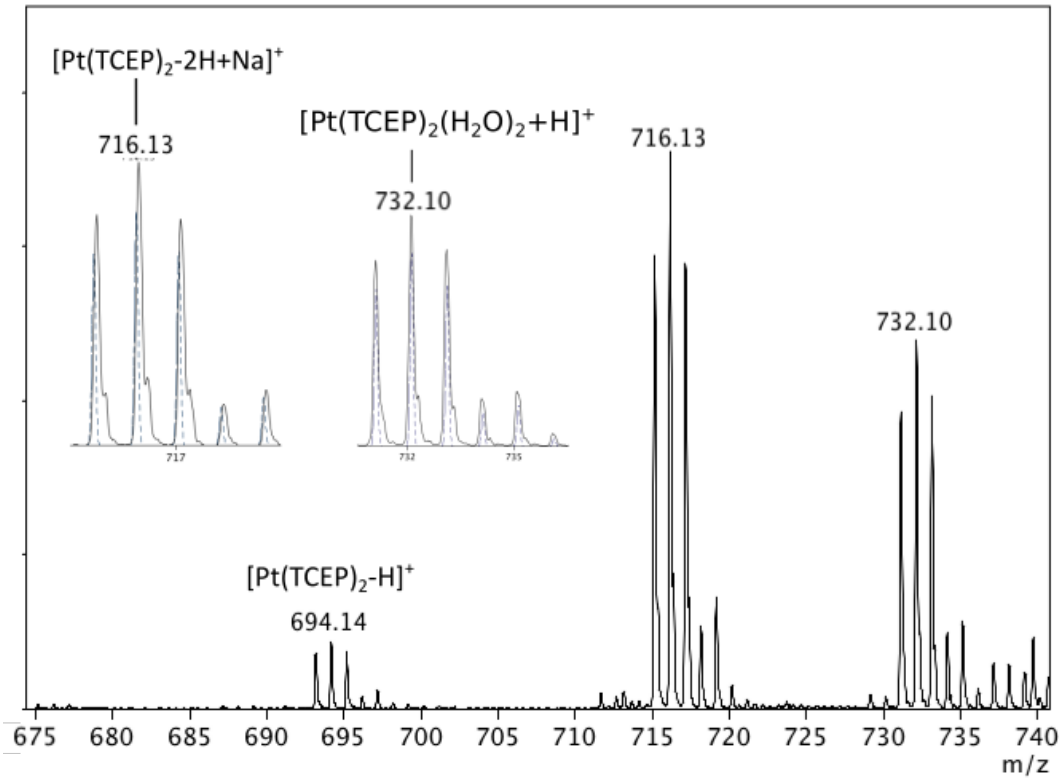

Figure 5.1: Positive-ion ESI mass spectrum of recrystallised *cis*-$PtCl_2(TCEP)_2$, showing the major platinum-containing ions. The inset spectra show the observed (solid line) and calculated (dashed line) isotope patterns for $[Pt(TCEP)_2\text{-}2H+Na]^+$ and $[Pt(TCEP)_2(H_2O)_2+H]^+$. The exact carboxylic acid groups that were deprotonated is subject to speculation. CEV 150 V, MeOH solution.

The peak at 732 *m/z* was initially thought to be a result of the ion $[PtCl(TCEP)_2]^+$, however this was ruled out due to the lack of a contribution from a chlorine atom to the isotope pattern. The ion $[Pt(TCEP)_2(H_2O)_2]^{2+}$ has been mentioned in the literature with the synthetic method,[93] but not observed here. The isotope pattern and mass for the ion $[Pt(TCEP)_2(H_2O)_2+H]^+$ ion at 732 *m/z* does match (Figure

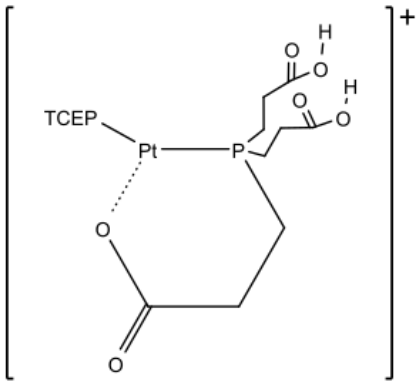

Figure 5.2: Diagram showing a suggested mode of cyclisation in the $[Pt(TPEP)_2\text{-}H]^+$ ion.

5.1), but the ligands of TCEP and H_2O are neutral. Therefore for this ion to be correct the addition of the hydrogen atom would have to have been to the Pt^{2+} centre as a hydride (H^-), resulting in a five-coordinated platinum centre which is rare as platinum prefers to form four-coordinated complexes.[1] There is the significant possibility the assignment of $[Pt(TCEP)_2(H_2O)_2 +H]^+$ to the ion at 732 *m/z* is incorrect, but at time of writing an ion assignment with more compelling evidence was not found.

The $^{31}P\{^1H\}$ NMR of *cis*-$PtCl_2(TCEP)_2$ was recorded in D_2O on a 300 MHz spectrometer. The ^{31}P resonances observed in the spectrum 5.9 ppm $^1J_{Pt\text{-}P} \approx 3500$ Hz are consistent with reported literature values.[93]

5.2.1 Attempted Synthesis of $Pt_2(\mu_2\text{-}S)_2(TCEP)_4$ from *cis*-$PtCl_2(TCEP)_2$

The reaction between *cis*-$PtCl_2(TCEP)_2$ and $Na_2S{\cdot}9H_2O$ was carried out using the literature method to attempt to obtain the $\{Pt_2(\mu_2\text{-}S)_2\}$ core.[2] Within five minutes of the addition of $Na_2S{\cdot}9H_2O$ to the suspension of *cis*-$PtCl_2(TCEP)_2$ in benzene, a small amount of black oily solid began to form. The black solid continued to form upon mixing and became what resembled a black oily pool in the bottom of the flask.

There was no further visible change after two hours of mixing. The positive- and negative-ion ESI mass spectra of this black oil were recorded. The spectra revealed no visible platinum complex ions. No peaks were observed for the ions of the starting material or unbound ligands either. The $^{31}P\{^1H\}$ NMR of the dried black oil was recorded and this showed a complex set of low intensity phosphorus resonances that all lacked platinum satellites, the only strong resonance present was at 53.4 ppm. No resonance of *cis*-$PtCl_2(TCEP)_2$ was present at 5.9 ppm. A sample of TCEP·HCl with an equal molar amount of base (triethylamine) was reacted with an excess of powdered elemental sulfur, to prepare TCEP sulfide.

The $^{31}P\{^{1}H\}$ NMR obtained in D_2O on the same 300 MHz NMR spectrometer, revealed two resonances a strong signal at 53.6 ppm and a less intense resonance at 57.5 ppm. This provides evidence that the reaction between *cis*-$PtCl_2(TCEP)_2$ and $Na_2S{\cdot}9H_2O$ resulted in the TCEP sulfide as one of the complexes in the black oil, as the resonance at 57 ppm was present in both spectra. No further studies were carried out with direct synthetic methods.

5.3 Attempted Synthesis of $Pt_2(\mu_2\text{-}S)_2(TCEP)_4$ by Ligand Substitution from $Pt_2(\mu_2\text{-}S)_2(PPh_3)_4$

The biphasic ligand exchange reaction between the platinum complex $Pt_2(\mu_2\text{-}S)_2(PPh_3)_4$ and free TCEP·HCl was undertaken using a solvent mixture of water and toluene as the reaction medium, with the ratios of platinum complex to ligand of 1:1, 1:2, 1:3, 1:4. Vigorous continuous stirring took place over a week. The reactions were deemed unsuccessful, with the positive- and negative-ion ESI mass spectra of the homogenous mixture showing only the starting materials $[Pt_2(\mu_2\text{-}S)_2(PPh_3)_4+H]^+$and $[TCEP\text{-}H]^-$ after seven days of mixing at ambient temperature.

The pH of the reaction solution was unadjusted during the first attempt at the ligand exchange reaction. After no reaction occurred with an unadjusted pH, one drop of a mild base (triethylamine) was added to the reaction solution. This was intended to deprotonate the TCEP·HCl in order to promote the ligand exchange to proceed. The reaction was also gently heated at this time. After these alterations to the procedure the positive- and negative-ion ESI mass spectra of the homogenous mixture showed no successful ligand substitution had occurred. The positive-ion ESI mass spectrum revealed the ions $[Pt_2(\mu_2\text{-}S)_2(PPh_3)_4]^{\cdot+}$ (1502.61 *m/z*) and $[Pt_2(\mu_2\text{-}S)_2(PPh_3)_4+Cl]^+$ (1537.7 *m/z*), an ion from the protonated or oxidised ligand was not observed in any of the positive-ion ESI mass spectra samples analysed.

5.4 Conclusion

Through the studies completed here, TCEP·HCl was shown to not be a suitable phosphine ligand for the $\{Pt_2(\mu_2\text{-}S)_2\}$ core in either a direct synthetic method or biphasic ligand exchange reaction with $Pt_2(\mu_2\text{-}S)_2(PPh_3)_4$.

5.5 Experimental

The general experimental work and chemical suppliers, accompanied by the equipment parameters are detailed in Appendix 1.

5.5.1) Synthesis of cis-$PtCl_2(TCEP)_2$

The literature method for the synthesis of *cis*-$PtCl_2(TCEP)_2$ used,[93] with the alteration that $PtCl_2(cod)$ (0.0506 g, 0.13 mmol) was used as the starting platinum complex in place of *cis*-$[PtCl_2(CH_3CN)_2]$, with TCEP·HCl (0.076 g, 0.3 mmol) yield 0.0959 g (97%).

5.5.2) Attempted Synthesis of $Pt_2(\mu_2\text{-}S)_2(TCEP)_4$

cis-$PtCl_2(TCEP)_2$ (0.05 g, 0.068 mmol) and $Na_2S{\cdot}9H_2O$ (0.0787 g, 0.32 mmol) in a benzene suspension (10 mL) was continually stirred for 48 h. A black solid formed from the suspension after 2 minutes, and the solution remained clear and colourless. The positive- and negative-ion ESI-MS spectra of the black solid showed no platinum complexes.

5.5.3) Attempted Synthesis of $Pt_2(\mu_2\text{-}S)_2(TCEP)_4$ Through a Biphasic Ligand Exchange Reaction

This reaction was prepared using a suitable sealable sample vial containing the biphasic reaction solvents of distilled water (20 mL) and toluene (20 mL). Added to the vial was $Pt_2(\mu_2\text{-}S)_2(PPh_3)_4$ (0.04 g, 0.026 mmol) and TCEP·HCl (0.04, 0.01 mmol) in a 1:4 molar ratio. The sealed vial was stirred continuously for 7 days. The solvents were allowed to settle before samples of the aqueous phase were

taken for negative-ion ESI mass analysis. No ligand-exchanged complexes were observed. This reaction was repeated simultaneously with ratios of 1:1, 1:2, 1:3.

5.4.3) Synthesis of TCEP Sulfide

Distilled water (20 mL) was deoxygenated by bubbling N_2 through for 1 h. Then a sample of TCEP·HCl (0.05 g, 0.2 mmol) with one equivalent of base (triethylamine 0.02 g, 0.2 mmol), along with an excess of powdered elemental sulfur (small spatula full) were added to the deoxygenated water. The reaction solution was stirred continually for 3 h. The solution was gravity filtered to remove all undissolved and unreacted solids, before the TCEP=S was isolated by evaporation of the solvent.

TCEP=S: $^{31}P\{^{1}H\}$ NMR m, 5.9 ppm, (D_2O) recorded at 121.5 MHz on a 300 MHz NMR spectrometer.

Chapter 6: Recommendations for Further Study

A synthetic method that yielded a pure product for the water-soluble platinum complex $Pt_2(\mu_2\text{-}S)_2(PTA)_4$ was not developed during the course of this research. Further study to devise a viable synthetic method could be undertaken.

The X-ray crystal structures of the three complexes synthesised during this work; namely $Pt_2(\mu_2\text{-}S)_2(PTA)_4$, $[Pt_3(\mu_3\text{-}S)_2(PTA)_6]^{2+}$, $[Pt(CH_3C(S)NH)(PPh_3)_2](BPh_4)$, were not obtained as no suitable crystals were able to be grown. Further recrystallisation attempts could be undertaken, using different solvents and under various conditions.

A computational study on the ion $[PtCl_3(PTA)_2]^-$ could be carried out in order to help determine where the third chloride was located in the structure. This may give information about whether the third chloride was coordinating to the platinum centre, resulting in a five-coordinate platinum complex being observed in the negative-ion ESI mass spectrum. Alternatively the third chloride could be bound through a hydrogen-bonding interaction on a PTA ligand.

The X-ray crystal structure of a side product, *trans*-$Pt(PPh_3)_2(SC(O)CH_3)_2$, was obtained during the course of this research. Further characterisation by NMR spectroscopy and ESI-MS was not completed as a synthetic method to form solely *trans*-$Pt(PPh_3)_2(SC(O)CH_3)_2$ was not undertaken due to time constrains. Further experimental work can be done to complete this characterisation. The synthesis of *trans*-$Pt(PPh_3)_2(SC(O)CH_3)_2$ could be achieved through an alteration of the synthetic method used to prepare the palladium analogue,[79] where a solution of *cis*-$PtCl_2(PPh_3)_2$ and thioacetic acid in methanol would be reacted in the presence of a mild base (triethylamine).

Reference:

(1) Cotton, F. A.; Wilkinson, G.; Murillo, C. A.; Bochmann, M. *Advanced Inorgamic Chemistry*, 6th ed.; John Wiley & Sons, inc, 1999.
(2) La Monica, G.; Ugo, R.; Cenini, S. *J. Chem. Soc.(A)* **1971**, 522–528.
(3) González-Duarte, P.; Lledós, A.; Mas-Ballesté, R. *Eur. J. Inorg. Chem.* **2004**, 3585–3599.
(4) Fong, S.-W. A.; Hor, T. S. A. *J. Chem. Soc., Dalt. Trans.* **1999**, 639–651.
(5) Henderson, W.; Hor, T. S. A. *Inorg. Chim. Acta* **2014**, *411*, 199–211.
(6) Aullón, G.; Ujaque, G.; Lledós, A.; Alvarez, S.; Alemany, P. *Inorg. Chem.* **1998**, *37*, 804–813.
(7) Fong, S.-W. A.; Hor, T. S. A.; Henderson, W.; Nicholson, B. K.; Gardyne, S.; Devoy, S. M. *J. Organomet. Chem.* **2003**, *679*, 24–31.
(8) Webb, J. R.; Burgess, S. A.; Cundari, T. R.; Gunnoe, T. B. *Dalt. Trans.* **2013**, *42*, 16646–16665.
(9) Liu, H.; Tan, A. L.; Cheng, C. R.; Mok, K. F.; Hor, T. S. A. *Inorg. Chem.* **1997**, *36*, 2916–2918.
(10) Fong, S.-W. A.; Yap, W. T.; Vittal, J. J.; Hor, T. S. A.; Henderson, W.; Oliver, A. G.; Rickard, C. E. F. *J. Chem. Soc., Dalt. Trans.* **2001**, 1986–2002.
(11) Henderson, W.; Oliver, A. G.; Turnbull, M. M. *Inorg. Chem. Comm.* **2013**, *27*, 142–145.
(12) Clarke, H. M.; Henderson, W.; Nicholson, B. K. *Inorg. Chim. Acta* **2011**, *376*, 446–455.
(13) Ujam, O. T.; Devoy, S. M.; Henderson, W.; Wilkins, A. L.; Nicholson, B. K. *J. Coord. Chem.* **2011**, *64*, 2782–2790.
(14) Chong, S. H.; Henderson, W.; Hor, T. S. A. *Dalt. Trans.* **2007**, 4008–4016.
(15) Ujam, O. T.; Devoy, S. M.; Henderson, W.; Nicholson, B. K.; Hor, T. S. A. *Inorg. Chim. Acta* **2010**, *363*, 3558–3568.
(16) Deadman, B. J.; Henderson, W.; Nicholson, B. K.; Petchell, L. E.; Rose, S. L.; Hor, T. S. A. *Inorg. Chim. Acta* **2010**, *363*, 637–644.
(17) Ujam, O. T.; Henderson, W.; Nicholson, B. K.; Hor, T. S. A. *Inorg. Chim. Acta* **2011**, *376*, 255–263.
(18) Chong, S. H.; Koh, L. L.; Henderson, W.; Hor, T. S. A. *Chem. Asian J.* **2006**, 264–272.
(19) Henderson, W.; Chong, S. H.; Hor, T. S. A. *Inorg. Chim. Acta* **2006**, *359*, 3440–3450.
(20) Chong, S. H.; Young, D. J.; Hor, T. S. A. *J. Organomet. Chem.* **2006**, *691*, 349–355.
(21) Chong, S. H.; Tjindrawan, A.; Hor, T. S. A. *J. Mol. Catal. A Chem.* **2003**, *204–205*, 267–277.
(22) Henderson, W.; Nicholson, B. K.; Ujam, O. T. *J. Coord. Chem.* **2011**, *64*, 2771–2781.
(23) Henderson, W.; Nicholson, B. K.; Devoy, S. M.; Hor, T. S. A. *Inorg. Chim. Acta* **2008**, *361*, 1908–1914.
(24) Fong, S.-W. A.; Hor, T. S. A.; Devoy, S. M.; Waugh, B. A.; Nicholson, B. K.; Henderson, W. *Inorg. Chim. Acta* **2004**, *357*, 2081–2090.
(25) White, B. C.; Harrison, D.; Henderson, W.; Nicholson, B. K.; Hor, T. S. A. *Inorg. Chim. Acta* **2010**, *363*, 2387–2393.
(26) Unkown. Triphenyl Phosphine (TPP) Product Information

https://pmcorganometallix.com/wp-content/uploads/2014/04/Triphenyl-Phosphine-TPP.pdf.
(27) Stewart, B.; Harriman, A.; Higham, L. J. *Organometallics* **2011**, *30*, 5338–5343.
(28) Briant, C. E.; Gardner, C. J.; Hor, T. S. A.; Howells, N. D.; Mingos, D. M. P. *J. Chem. Soc., Dalt. Trans.* **1984**, 2645–2651.
(29) Yam, V. W.-W.; Kok-Yan, P.; Cheung, Y.; Cheung, K.-K. *J. Chem. Soc. Chem. Commun.* **1995**, 267–269.
(30) Mas-Ballesté, R.; Capdevila, M.; Champkin, P. A.; Clegg, W.; Coxall, R. A.; Lledós, A.; Mégret, C.; González-Duarte, P. *Inorg. Chem.* **2002**, *41*, 3218–3229.
(31) Capdevila, M.; Carrasco, Y.; Clegg, W.; Coxall, R. A.; González-Duarte, P.; Lledós, A.; Sola, J.; Ujaque, G. *Chem. Commun.* **1998**, 597–598.
(32) Zhou, M.; Lam, C. F.; Mok, K. F.; Leung, P.-H.; Hor, T. S. A. *J. Organomet. Chem.* **1994**, *476*, c32–c34.
(33) Agbossou, F.; Carpentier, J.; Mortreux, A. *Chem. Rev.* **1995**, *95*, 2485–2506.
(34) Capdevila, M.; Clegg, W.; González-Duarte, P.; Jarid, A.; Lledós, A. *Inorg. Chem.* **1996**, *35*, 490–497.
(35) Dierkes, P.; van Leeuwen, P. W. N. M. *J. Chem. Soc., Dalt. Trans.* **1999**, 1519–1530.
(36) Jain, V. K.; Kannan, S.; Butcher, R. J.; Jasinski, J. P. *J. Chem. Soc., Dalt. Trans.* **1993**, 1509–1513.
(37) Matsumoto, K.; Takahashi, K.; Ikuzawa, M.; Kimoto, H.; Okeya, S. *Inorg. Chim. Acta* **1998**, *281*, 174–180.
(38) Neve, F.; Cesco; Crispini, A.; Ghedini, M.; De Munno, G. *Inorg. Chim. Acta* **1990**, *176*, 23–25.
(39) Manojlovic-Muir, L.; Muir, K. W.; Solomun, T. *Acta Cryst.* **1979**, *B35*, 1237–1239.
(40) Grossel, M. C.; Batson, J. R.; Moulding, R. P.; Seddon, K. R. *J. Organomet. Chem.* **1986**, *304*, 391–423.
(41) Yam, V. W. W.; Yu, K. L.; Cheng, E. C. C.; Yeung, P. K. Y.; Cheung, K. K.; Zhu, N. *Chem. Eur. J.* **2002**, *8*, 4121–4128.
(42) Yam, V. W.-W.; Yeung, P. K.-Y.; Cheung, K.-K. *Angew. Chem. Int. Ed. Engl.* **1996**, *35*, 739–740.
(43) Ford, P. C.; Vogler, A. *Acc. Chem. Res.* **1993**, *26*, 220–226.
(44) Li, J.; Hor, T. S. A. *Dalt. Trans.* **2008**, *4*, 6619–6623.
(45) Murahashi, T.; Fujimoto, M.; Kawabata, Y.; Inoue, R.; Ogoshi, S.; Kurosawa, H. *Angew. Chem. Int. Ed.* **2007**, *46*, 5440–5443.
(46) Chatt, J.; Mingos, D. M. P. *Inorg. Phys. Theor.* **1970**, 1243–1245.
(47) Ruiz, J.; Rodríguez, V.; Pérez, A.; López, G.; Bautista, D. *J. Organomet. Chem.* **2004**, *689*, 2080–2086.
(48) Brunner, H.; Weber, M.; Zabel, M. *J. Organomet. Chem.* **2003**, *684*, 6–12.
(49) *Ferrocenes-Homogeneous Catalysis, Organic Synthesis, Materials Science*; Togni, A., Hayashi, T., Eds.; VCH, Weinheim, Germany, 1995.
(50) Miller, T. M.; Ahmed, K. J.; Wrighton, M. S. *Inorg. Chem.* **1989**, *28*, 2347–2355.
(51) Neo, S. P.; Zhou, Z.-Y.; Mark, T. C. W.; Hor, T. S. A. *J. Chem. Soc., Dalt. Trans.* **1994**, 3451–3458.
(52) Zhou, M.; Xu, Y.; Tan, A.-M.; Leung, P.-H.; Mok, K. F.; Koh, L.-L.; Hor,

T. S. A. *Inorg. Chem.* **1995**, *34*, 6425–6429.
(53) Balch, A. L.; Rowley, S. P. *J. Am. Chem. Soc.* **1990**, *112*, 6139–6140.
(54) Jeram, S.; Henderson, W.; Nicholson, B. K.; Hor, T. S. A. *J. Organomet. Chem.* **2006**, *691*, 2827–2838.
(55) González-Duarte, P.; Lledos, A.; Novio, F.; Gallardo, I.; Vila, N.; Mas-Balleste, R. *Dalt. Trans.* **2005**, 2742–2753.
(56) Coughlan, N. J. A.; Henderson, W. *J. Coord. Chem.* **2014**, *67*, 3987–4002.
(57) Darensbourg, D. J.; Decuir, T. J.; Stafford, N. W.; Robertson, J. B.; Draper, J. D.; Reibenspies, J. H.; Katho, A.; Joó, F. *Inorg. Chem.* **1997**, *36*, 4218–4226.
(58) Alyea, E. C.; Ferguson, G.; Kannan, S. *Polyhedron* **1998**, *17*, 2727–2732.
(59) Darensbourg, D. J.; Stafford, N. W.; Joó, F.; Reibenspies, J. H. *J. Organomet. Chem.* **1995**, *488*, 99–108.
(60) Krogstad, D. A.; Owens, S. B.; Halfen, J. A.; Young, V. G. *Inorg. Chem. Comm.* **2005**, *8*, 65–69.
(61) Daigle, D. J.; Decuir, T. J.; Robertson, J. B.; Darensbourg, D. J. In *Inorg. Synth.*; Wiley, 1998; Vol. 32, pp 40–45.
(62) Demakova, M. Y.; Luzyanin, K. V.; Starova, G. L.; Kukushkin, V. Y. *Inorg. Chem. Comm.* **2014**, *50*, 17–18.
(63) Cotton, F. A.; Wilkinson, G. *Advanced Inorganic Chemistry: A Comprehensive Text*, 3nd ed.; John Wiley & Sons, inc, 1972.
(64) Otto, S.; Roodt, A. *Inorg. Chem. Comm.* **2001**, *4*, 49–52.
(65) Forward, J. M.; Bohmann, D.; Fackler, J. P. *Z. Krist.* **1996**, *211* (485), 1996.
(66) McCaffrey, L. J.; Henderson, W.; Nicholson, B. K.; Mackay, J. E.; Dinger, M. B. *J. Chem. Soc., Dalt. Trans.* **1997**, 2577–2586.
(67) Li, J.; Koh, L. L.; Hor, T. S. A. *Chem. Commun.* **2009**, 3416–3418.
(68) Smoleński, P.; Kochel, A. *Polyhedron* **2010**, *29*, 1561–1566.
(69) Trovo, G.; Bandoli, G.; Casellato, U.; Corain, B.; Nicolini, M.; Longato, B. *Inorg. Chem.* **1990**, *29*, 4616–4621.
(70) Briant, C. E.; Gilmour, D. I.; Luke, M. A.; Mingos, D. M. P. *J. Chem. Soc., Dalt. Trans.* **1985**, 851–855.
(71) Chanda, M.; Rempel, G. L. *React. Polym.* **1995**, *24*, 203–212.
(72) Bushnell, W. G.; Dixon, K. R.; Ono, R.; Pidcock, A. *Can. J. Chem.* **1984**, *62*, 696–702.
(73) Ujam, O. T.; Devey, K.; Henderson, W.; Nicholson, B. K.; Mucalo, M. R.; Decker, C.; Hor, T. S. A. *Phosphorus, Sulfur Silicon Relat. Elem.* **2013**, *188*, 1508–1525.
(74) Butler, E. A.; Peters, D. G.; Swift, E. H. *Anal. Chem.* **1958**, *30*, 1379–1383.
(75) Sugimoto, T.; Chen, S.; Muramatsu, A. *Colloids Surf. A* **1998**, *135*, 207–226.
(76) Desai, J. D.; Lokhande, C. D. *Mater. Chem. Phys.* **1995**, *41*, 98–103.
(77) Trindade, T.; De Jesus, J. D. P.; O'Brienn, P. *J. Mater. Chem.* **1994**, *4*, 1611–1617.
(78) Ösz, K.; Espenson, J. H. *Inorg. Chem.* **2003**, *42*, 8122–8124.
(79) Neo, Y. C.; Vittal, J. J.; Hor, T. S. A. *J. Organomet. Chem.* **2001**, *639*, 757–761.
(80) Calligaris, M. *Coord. Chem. Rev.* **2004**, *248*, 351–375.
(81) Shim, Y. J.; Lee, H. J.; Park, S. *J. Organomet. Chem.* **2012**, *696*, 4173–4178.

(82) Janusson, E.; Zijlstra, H. S.; Nguyen, P. P. T.; Macgillivray, L.; Martelino, J.; McIndoe, J. S. *Chem. Commun.* **2017**, *53*, 854–856.
(83) Roman, P. J.; Paterniti, D. P.; See, R. F.; Churchill, M. R.; Atwood, J. D. *Organometallics* **1997**, *2*, 1484–1490.
(84) Francisco, L. W.; Moreno, D. A.; Atwood, J. D. *Organometallics* **2001**, *20*, 4237–4245.
(85) Pinault, N.; Bruse, D. W. *Coord. Chem. Rev.* **2003**, *241*, 1–15.
(86) Burrows, A. D.; Harrington, R. W.; Mahon, M. F.; Teat, S. J. *Eur. J. Inorg. Chem.* **2003**, 1433–1439.
(87) Mas-Ballesté, R.; Champkin, P. A.; Clegg, W.; González-Duarte, P.; Lledós, A.; Ujaque, G. *Organometallics* **2004**, *23*, 2522–2532.
(88) Weliange, N. M.; Szuromi, E.; Sharp, P. R. *J. Am. Chem. Soc.* **2009**, *131*, 8736–8737.
(89) Weliange, N. M.; Sharp, P. R. *Organometallics* **2012**, *31*, 6823–6833.
(90) Dell'Amico, D. B.; Labella, L.; Marchetti, F.; Samaritani, S. *J. Organomet. Chem.* **2011**, *696*, 1349–1354.
(91) Clark, H. C.; Manzer, L. E. *J. Organomet. Chem.* **1973**, *59*, 411–428.
(92) McDermott, J. X.; White, J. F.; Whitesides, G. M. *J. Am. Chem. Soc.* **1976**, *98*, 6521–6528.
(93) Pruchnik, H.; Lis, T.; Pruchnik, F. P. *J. Organomet. Chem.* **2015**, *791*, 124–129.
(94) Burns, J. A.; Butler, J. C.; Moran, J.; Whitesides, G. M. *J. Org. Chem.* **1991**, *56*, 2648–2650.
(95) Knight, D. A.; Deschamps, J. R.; Butcher, R. J.; Simmers, C.; Chang, E. L. *Polyhedron* **2008**, *27*, 1795–1801.
(96) Pruchnik, H.; Lis, T.; Latocha, M.; Zielińska, A.; Pruchnik, F. P. *J. Inorg. Biochem.* **2016**, *156*, 14–21.
(97) Parshall, G. W.; Curtis, M. D.; Job, R. C. In *Inorg. Synth.*; Parry, R. W., Ed.; Wiley, 1970; Vol. 12, pp 26–33.
(98) Morgan, G. T.; Burstall, F. H. *J. Chem. Soc.* **1934**, 965–971.
(99) Giordano, G.; Crabtree, R. H. In *Inorg. Synth.*; Wiley, 1977; Vol. 19, pp 218–220.

Appendix I: General Experimental Details

Materials: The following section details the origins of all chemicals used throughout this work. All chemicals were used as obtained, without purification. All deuterated solvents were purchased from Aldrich. Tris(2-ethylhexyl)amine, sodium sulfide nonahydrate (Aldrich); hydrated lead nitrate, Dowex 1-X8, laboratory reagent, thioacetamide (BDH Chemicals Ltd); toluene, benzene, chloroform, dimethylformamide, methanol, diethyl ether, dichloromethane, drum grade (Merck); tetrakis(hydroxymethyl)phosphonium chloride (Albright & Wilson UK Ltd); hexamine laboratory reagent, formaldehyde solution analytical reagent and powdered sulfur (APS Ajax Finechem).

The phosphine ligands PTA[61] and TCEP·HCl[94] were synthesised with the methods outlined in the literature. [TPPMS]K·H_2O was synthesised using a literature method,[83] with minor alterations; tris(2-ethylhexyl)amine was used in place of tri-n-octylamine. $Pt_2(\mu_2\text{-}S)_2(PPh_3)_4$ was synthesised with an established literature procedure.[2] The platinum complexes $PtCl_2(cod)$[92] and *cis*-$PtCl_2(PMe_3)_2$,[97] $PtCl_2(bipy)$[98] $[RhCl(cod)]_2$[99] were synthesised *via* established literature methods. The complexes *cis*-$PtCl_2(PPh_3)_2$, *cis*-$PtCl_2(DMSO)_2$, *cis*-$PdCl_2(PTA)_2$ were prepared through the use of the generalised method, the reaction between the appropriate $[MCl_2(cod)]$ (M = Pt, Pd) complex and a stoichiometric quantity of the desired ligand in a dichloromethane solution, and the product precipitated by addition of petroleum spirits. These complexes were used as obtained.

Instrumentation: All ^{1}H,^{13}C, and $^{31}P\{^{1}H\}$ NMR spectra were recorded on a Bruker Avance DRX 400 MHz spectrometer along with $^{31}P\{^{1}H\}$ NMR spectra on a Bruker Avance DRX 300. The specific figure description describes which instrument was used. All NMR figures were generated with the use of topspin 5.5 pl 7. All positive- and negative-ion ESI spectra were recorded on Bruker MicrOTOF with the skimmer cone voltage a third that of the capillary exit voltage (CEV). The CEV and solvent used are stated in figure descriptions, commonly 150 V and a MeOH solution with a flow rate of 180 μL/h. Mass spectra data

processing software used to generate figures and calculated isotope patterns was mMass version 5.5.0. The UV/Visible spectrum was recorded using a Dynamica Halo VIS-20 visible spectrophotometer.

Appendix II: Additional X-ray Crystal Structure Data

Table I: Refinement and crystallographic Information.

Complex	*trans*-$Pt(SC(O)CH_3)_2(PPh_3)_2$
Empirical formula	$C_{40}H_{36}O_2P_2PtS_2$
Formula weight	869.89
Temperature/K	99.99(10)
Crystal system	triclinic
Space group	P-1
a/Å	7.9782(3)
b/Å	10.8295(3)
c/Å	11.0763(4)
α/°	114.711(3)
β/°	95.558(3)
γ/°	95.996(3)
Volume/$Å^3$	854.08(6)
Z	1
$\rho_{calc}g/cm^3$	1.6912
μ/mm^{-1}	9.99
F(000)	429.8
Crystal size/mm^3	0.124 × 0.099 × 0.081
Radiation	Cu Kα (λ = 1.54184 Å)
2Θ range for data collection/°	8.9 to 147.64
Index ranges	$-9 \leq h \leq 9$, $-13 \leq k \leq 13$, $-13 \leq l \leq 13$
Reflections collected	16356
Independent reflections	3395 [R_{int} = 0.0682, R_{sigma} = 0.0519]
Data/restraints/parameters	3395/0/215
Goodness-of-fit on F^2	1.035
Final R indexes [I>=2σ (I)]	R_1 = 0.0380, wR_2 = 0.1012
Final R indexes [all data]	R_1 = 0.0433, wR_2 = 0.1028
Largest diff. peak/hole / e $Å^{-3}$	3.28/-2.40

Table II: Fractional atomic coordinates ($\times 10^4$) and equivalent isotropic displacement parameters ($Å^2 \times 10^3$) for *trans*-$Pt(SC(O)CH_3)_2(PPh_3)_2$. U_{eq} is defined as 1/3 of the trace of the orthogonalised U_{IJ} tensor.

Atom	***x***	***y***	***z***	**U(eq)**
Pt1	5000	10000	10000	17.15(12)
P1	3089.7(15)	8862.3(11)	8020.3(11)	15.7(2)
S1	6361.3(15)	11239.5(11)	8985.3(11)	19.0(2)
C22	3925(7)	8521(5)	5482(5)	20.9(10)
C35	-1117(7)	6557(5)	8326(5)	24.1(10)
O1	5228(5)	13349(4)	10815(4)	25.4(8)
C21	4215(6)	8209(5)	6572(5)	17.5(9)
C11	1674(7)	9924(5)	7657(5)	19.2(9)
C33	253(7)	4989(5)	6622(5)	25.1(11)
C14	-404(7)	11537(5)	7003(5)	24.5(10)
C31	1516(6)	7382(5)	7790(5)	17.5(9)
C34	-1094(8)	5238(5)	7337(5)	26.4(11)
C32	1551(7)	6053(5)	6832(5)	23.9(10)
C1	6141(7)	12966(5)	9952(5)	22.5(10)
C25	6266(7)	6783(5)	5479(5)	22.1(10)
C24	5945(7)	7077(5)	4377(5)	25.7(11)
C12	2031(7)	11357(5)	8336(5)	24.4(10)
C16	229(7)	9314(5)	6670(5)	22.4(10)
C15	-820(7)	10107(5)	6347(5)	24.3(10)
C13	976(8)	12148(5)	7981(6)	29.9(12)
C36	185(7)	7629(5)	8552(5)	21.6(10)
C23	4795(7)	7955(5)	4379(5)	23.7(10)
C26	5423(7)	7361(5)	6586(5)	21.8(10)
C2	7206(8)	13984(5)	9610(6)	30.9(12)

Table III: Anisotropic displacement parameters ($Å^2 \times 10^3$) for *trans*-$Pt(SC(O)CH_3)_2(PPh_3)_2$. The anisotropic displacement factor exponent takes the form: $-2\pi^2[h^2a^{*2}U_{11}+2hka^*b^*U_{12}+\ldots]$.

Atom	U_{11}	U_{22}	U_{33}	U_{12}	U_{13}	U_{23}
Pt1	18.60(18)	16.43(15)	15.50(16)	-1.7(1)	3.40(11)	6.88(11)
P1	16.7(6)	15.1(5)	13.3(5)	-0.6(4)	2.2(4)	5.1(4)
S1	21.7(6)	18.3(5)	17.1(5)	-2.8(4)	4.6(4)	8.7(4)
C22	23(3)	22(2)	17(2)	1.7(19)	1.6(19)	8.4(18)
C35	18(3)	30(2)	25(2)	-3(2)	2(2)	15(2)
O1	29(2)	24.1(16)	22.4(17)	0.9(15)	6.1(15)	9.1(14)
C21	17(2)	18(2)	16(2)	-1.6(18)	2.7(18)	6.9(16)
C11	21(3)	18(2)	18(2)	1.2(18)	5.2(19)	6.9(17)
C33	30(3)	17(2)	26(2)	-2(2)	3(2)	8.7(19)
C14	27(3)	23(2)	28(2)	7(2)	7(2)	13.7(19)
C31	15(2)	19(2)	17(2)	-1.1(18)	0.7(18)	8.6(17)
C34	31(3)	23(2)	27(3)	-6(2)	0(2)	15(2)
C32	24(3)	23(2)	24(2)	3(2)	9(2)	8.9(19)
C1	25(3)	19(2)	22(2)	0(2)	0(2)	9.1(18)
C25	20(3)	21(2)	22(2)	0.9(19)	3.6(19)	6.2(18)
C24	25(3)	26(2)	23(2)	2(2)	11(2)	7.1(19)
C12	20(3)	18(2)	25(2)	-1(2)	-3(2)	2.7(19)
C16	24(3)	20(2)	22(2)	0.9(19)	3(2)	8.1(18)
C15	19(3)	26(2)	26(2)	1(2)	0(2)	11(2)
C13	26(3)	21(2)	38(3)	7(2)	4(2)	9(2)
C36	21(3)	21(2)	21(2)	-2.6(19)	1.5(19)	8.5(18)
C23	20(3)	29(2)	19(2)	-2(2)	0.1(19)	9.4(19)
C26	25(3)	22(2)	20(2)	2(2)	4(2)	10.0(18)
C2	39(3)	20(2)	34(3)	-5(2)	10(2)	13(2)

Table IV: Hydrogen atom coordinates ($Å \times 10^4$) and isotropic displacement parameters ($Å^2 \times 10^3$) for *trans*-$Pt(SC(O)CH_3)_2(PPh_3)_2$.

Atom	*x*	*y*	*z*	U(eq)
H22	3153(7)	9108(5)	5482(5)	25.0(11)
H35	-2001(7)	6723(5)	8834(5)	28.9(12)
H33	295(7)	4099(5)	5993(5)	30.1(13)
H14	-1078(7)	12077(5)	6768(5)	29.4(12)
H34	-1984(8)	4529(5)	7160(5)	31.6(13)
H32	2442(7)	5876(5)	6332(5)	28.7(12)
H25	7044(7)	6200(5)	5478(5)	26.6(12)
H24	6502(7)	6686(5)	3639(5)	30.9(13)
H12	2962(7)	11785(5)	9019(5)	29.3(12)
H16	-32(7)	8359(5)	6223(5)	26.9(12)
H15	-1791(7)	9691(5)	5701(5)	29.2(12)
H13	1225(8)	13104(5)	8421(6)	35.9(14)
H36	169(7)	8509(5)	9212(5)	25.9(12)
H23	4599(7)	8168(5)	3651(5)	28.5(12)
H26	5663(7)	7184(5)	7332(5)	26.2(12)
H2a	8150(40)	14480(40)	10320(20)	46.4(18)
H2b	7620(50)	13498(7)	8780(30)	46.4(18)
H2c	6518(19)	14620(30)	9520(50)	46.4(18)